A general dynamic model of a complete milk pasteurizer unit subject to fouling

Mengjia Zhu (CID: 01611294)

9th September 2019

Supervised by Cav. Prof. Sandro Macchietto
Professor of Process Systems Engineering, Imperial College London

Co-supervised by Federico Lozano Santamaria
PhD Student, Imperial College London

A thesis presented to Imperial College London in partial fulfilment of the requirements for the degree of *Master of Science in Advanced Chemical Engineering (with Process Systems Engineering)* and for the *Diploma of Imperial College*

Department of Chemical Engineering

Imperial College London

Abstract

Milk fouling in the pasteurization process reduces heat transfer efficiency. Periodic cleanings generate downtime and large amounts of waste water requiring treatment. System performance of a pasteurizer unit is dictated by the overall configurations, including not just the milk heater, a plate heat exchanger (PHE) (previously studied), but also a holding tube, a cooler and a “regeneration” preheater for energy recovery, all tightly integrated. A model of the whole pasteurization process can be used as a virtual unit to test different operational strategies and therefore optimize the system performance. However, none of the models that currently available considers heating-cleaning cycles for the overall pasteurizer unit.

In this research, a 2D dynamic thermal model was developed for a complete milk pasteurizer unit using first principle modelling approach. The thermal model is then coupled with a semi-mechanistic fouling model and an empirical cleaning in place (CIP) model so that it can be used to test various heating-cleaning cycles. This unit model consists of three PHEs (heating, regeneration, and cooling), a non-isothermal holding tube, and two non-isothermal tubular connections. The thermal, fouling and CIP models of individual PHEs extended and modified the 2D distributed model developed previously[1,2]. For the tubes, the distributed thermal model of Coletti[3], Diaz-Bejarano and Macchietto[4] was adapted and modified to account for deposition in the tubes and CIP. The entire unit was modelled by joining the component models via suitable boundary conditions. The dynamics of the system were also studied, and the model was coupled with two PI controllers to ensure that the required pasteurization temperature and the specified storage/outlet temperature are met.

The generality and flexibility of the model were demonstrated in two common pasteurization processes: high temperature short time (HTST) and ultra-high temperature (UHT) treatments. The thermal model of the whole pasteurizer unit was first validated against experimental data for a HTST process, with excellent agreement. The evolution, extent and location of fouling, and its impact on the process was then assessed for both processes. For the HTST process, deposition mass was not significant for the first 2.1 days. For the UHT process, a realistic case was simulated, and the results indicate a much more severe fouling in the main PHE heater, but also in the regeneration section as well as the tubes. It is noted that experimental validation is still needed to confirm the prediction of deposition mass for both cases. A heating-CIP cycle was also simulated for the UHT case to study the amount of cleaning agent and rinsing water required as well as the cleaning time needed within an operation cycle. This modelling approach gives a wholistic view of the operations of the unit. It can capture the main features of different pasteurization processes and provide valuable insights, which can be useful for optimization of cleaning strategies and schedules, and therefore reduce cleaning cost and shorten the operational downtime.

Note: a modified version of this Abstract has been submitted to ESCAPE-30

Acknowledgements

Firstly, I would like to express my deep gratitude to my supervisor, Prof. Sandro Macchietto for his continuous guidance and support along the journey. He is extremely knowledgeable in the field of the research and could always provide feedbacks with valuable insights and suggestions to guide me in the right direction. Also, he is open for discussions and I can always reach him via email and in-person meetings. Moreover, he helped me to develop good research habits and be more organized regarding the research process. Additionally, he has often challenged me to think more thoroughly and independently. Under his supervision, my research journey has been continuously inspiring and rewarding.

I am also extremely grateful for the assistance given by Federico Lozano Santamaria. He is knowledgeable about the research topic and has arranged several seminars to help us get familiar with the software. Whenever I faced a tough problem, he would always be available and provide me with valuable feedbacks. Also, he has often challenged me to think more critically and broadly regarding the research topics, which inspired me to explore more interesting areas. His help along the journey is greatly appreciated.

This thesis is based on the work by many great researchers and I would like to extend my appreciation to Abhishek Sharma, Justin Guan, Prof. Michael Georgiadis, Dr. Francesco Coletti and Dr Emilio Diaz Bejarano. Also, I wish to acknowledge the help provided by the Chemical Engineering Department and Process Systems Enterprise.

Finally, I would like to thank my parents for their generous and continuous support along my personal and study journey all these years. Nothing would be possible without them.

Table of Contents

List of Figures

List of Tables

Nomenclature

Abbreviations

CFD	Computational Fluid Dynamic
PHE	Plate Heat Exchanger
HE	Heat Exchanger
P	Plate
STHE	Shell-and-Tube Heat Exchanger
UHT	Ultra-High Temperature
β-lg	Beta-lactoglobulin
PDAE	Partial Differential Algebraic Equation
PDE	Partial Differential Equation
DAE	Differential Algebraic Equation
BFDM	Backward Finite Difference Method
FFDM	Forward Finite Difference Method
CFDM	Central Finite Difference Method

Notations

A_{flow}	[m^2]	Flow cross-sectional area in the PHE
A_j	[m^2]	Plate heat transfer area
A_x	[m^2]	Channel cross-sectional area w/o fouling
A_{TB}	[m^2]	Flow cross-sectional area in the holding tube
Bi	[-]	Biot number (dimensionless) for fouling resistance
BT_w	[m]	Thickness of the wall within the conservation boundary
C	[kg/m^3]	Bulk protein concentration in channel
C^*	[kg/m^3]	Protein concentration in thermal boundary layer
C_p	[J/kg.K]	Specific heat capacity
d	[m]	Particle diameter for protein species
dir	[-]	Flow direction in each channel (+1 or -1)
D	[m^2/s]	Diffusivity for protein species
D_h	[m]	Hydraulic/Equivalent diameter
e_j	[m]	Gap between adjoint plate (clean)
e_x	[m]	Actual gap between adjoint plate (with fouling)
E	[J/mol]	Activation energy
h	[$W/m^2.K$]	Local convective heat transfer coefficient

H	[J/kg]	Specific mass enthalpy
h_f^o	[W/m^2.K]	Local convective heat transfer coefficient (clean)
k_m	[m/s]	Mass transfer coefficient of protein species
k_o	[s^{-1}]	Reaction pre-exponential factor
k_τ	[s^{-1}]	Pre-exponential factor for entrainment
k_w	[m/s]	Mass transfer coefficient of the deposition
L	[m]	Length of the plate
Nu	[-]	Nusselt number (dimensionless)
Pr	[-]	Prandtl number (dimensionless)
q	[W/m^2]	Heat flux
$Q_{channel}$	[m^3/mol]	Volumetric flowrate in each channel
R	[m]	Radius
R_g	[J/K.mol]	Ideal gas constant
Re	[-]	Reynolds number (dimensionless)
Sc	[-]	Schmidt number (dimensionless)
Sh	[-]	Sherwood number (dimensionless)
PT	[m]	Thickness of the plate
t	[s]	Time
T	[K]	Temperature
u_x	[m/s]	Average fluid velocity in each channel
U	[W/m^2.K]	Overall heat transfer coefficient
U_o	[W/m^2.K]	Overall heat transfer coefficient (clean)
V	[m^3/mol]	Molecular volume of protein particle
v	[m/s]	Velocity of the bulk fluid in the holding tube
W	[m]	Width of the plate
x	[m]	Axial coordinate (along flow direction) of PHE
y	[m]	Horizontal coordinate (normal to flow direction) of PHE
$\tilde{y}$	[-]	Normalized horizontal coordinate of PHE
r	[m]	Radial coordinate (from center of the holding tube)
z	[m]	Axial coordinate of the holding tube
$\tilde{r}$	[-]	Normalized radial coordinate of the holding tube
β	[m^2/kg]	Proportionality constant used to quantify fouling effects
δ	[m]	Deposit thickness (boundary layer)
$\dot{\delta}$	[m/s]	Rate of change for deposit thickness
λ	[W/m.K]	Thermal conductivity

μ	[Pa.s]	Dynamic viscosity
ρ	[kg/m^3]	Density

Subscripts

$P\ (p)$	Plate
W	Wall domain
$L\ (l)$	Layer domain
F	Flow domain
j	Channel number
N	Native protein
U	Unfolded protein
A	Aggregated protein
d	Deposit
T	Thermal boundary layer
M	Mass boundary layer
TB	Tube
I	Condition at inner radius of the holding tube
O	Condition at outer radius of the holding tube

Superscripts

L	Left plate in the channel
R	Right plate in the channel

1 Introduction

Milk pasteurization is a heat treatment commonly used to eliminate pathogenic microorganisms in raw milk to ensure food safety and extend shelf life. A pasteurizer unit (Figure 1.1) includes a preheater (energy regenerator), a main heater, a holding tube, and a cooler. Firstly, the unprocessed milk is pre-heated in the regeneration section. Then, the pre-treated milk is further heated to the required pasteurization temperature in the heating section. After which, the holding tube is utilized to keep the heated milk for a fixed duration at the pasteurization temperature to kill microorganisms. Then, the outgoing hot milk flows back to the regenerator to heat the incoming cold milk[5,6]. By heat integration, less heating and cooling energy is consumed[5]. Lastly, the milk is cooled to the specified storage/outlet temperature in the cooling section.

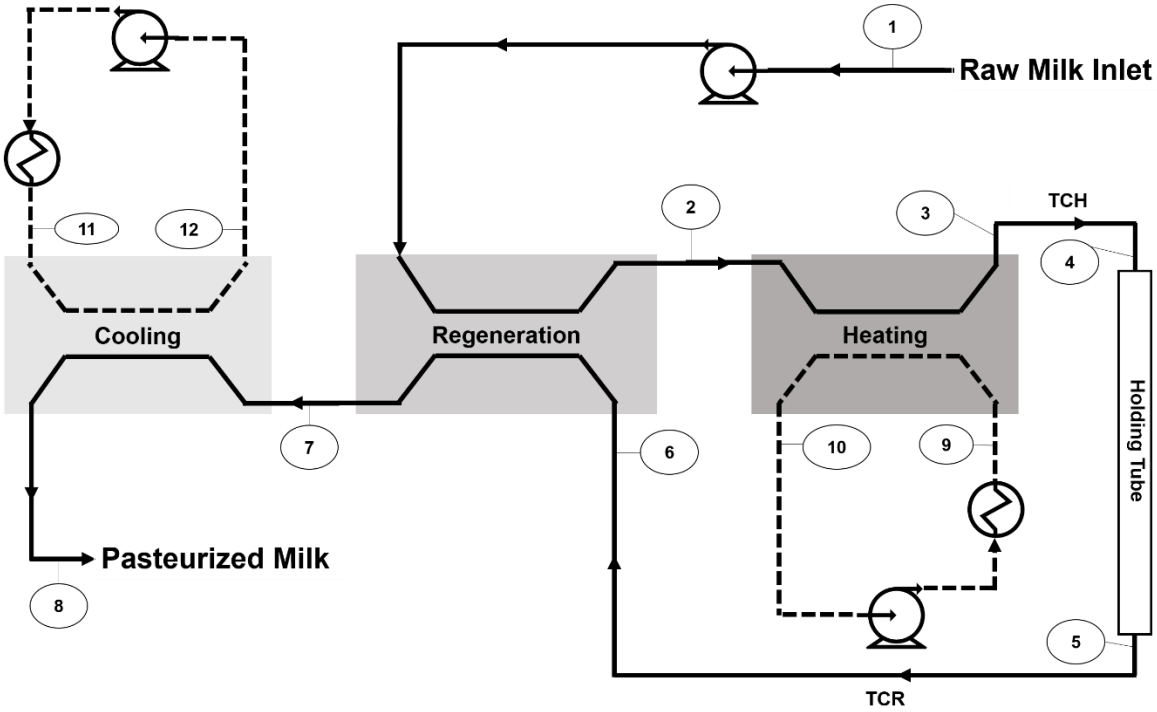

Figure 1.1. Schematic diagram of a pasteurizer unit (reproduced from Gutierrez et al[7]).

Plate heat exchangers (PHEs) (Figure 1.2) are extensively used for heating, regeneration and cooling sections of the pasteurizer unit. In a PHE, cold and hot fluid streams flow through alternating channels and exchange heat across the plate wall, which prevents direct contact between streams and reduce contamination. The PHE is featured with high compactness, flexible, easy operation, and enhanced thermal and hydraulic performance, which make it suitable for milk processing[5]. During operations, certain amounts of materials within milk stream can deposit and grow on the surface of the plate wall, leading to extensive economic losses (e.g. consume more energy, use more heat exchangers) and environmental problems (e.g. use more cleaning water, generate more waste). Multiple fouling mitigation treatment

techniques are developed but most of the works focus on the qualitative analysis and there is lack of a quantitative assessment of anti-fouling strategies. Experimentation and validation of these anti-fouling methods can be both time-consuming and costly. Also, experiments could reflect conditions tested but are often difficult to extrapolate to other conditions. Therefore, developing more accurate and reliable model is a more suitable and resource-saving approach. The model should: (1) capture the main thermal and hydraulic behaviours of fluids within the heat exchangers (HE); (2) reflect the interactions among different sections of the pasteurizer unit; (3) predict fouling severity and locations; (4) optimize the operation and cleaning of HEs. Currently, none of the models available includes all four features. The objective of this research is to fill this gap and develop a model for the whole pasteurizer unit with these features.

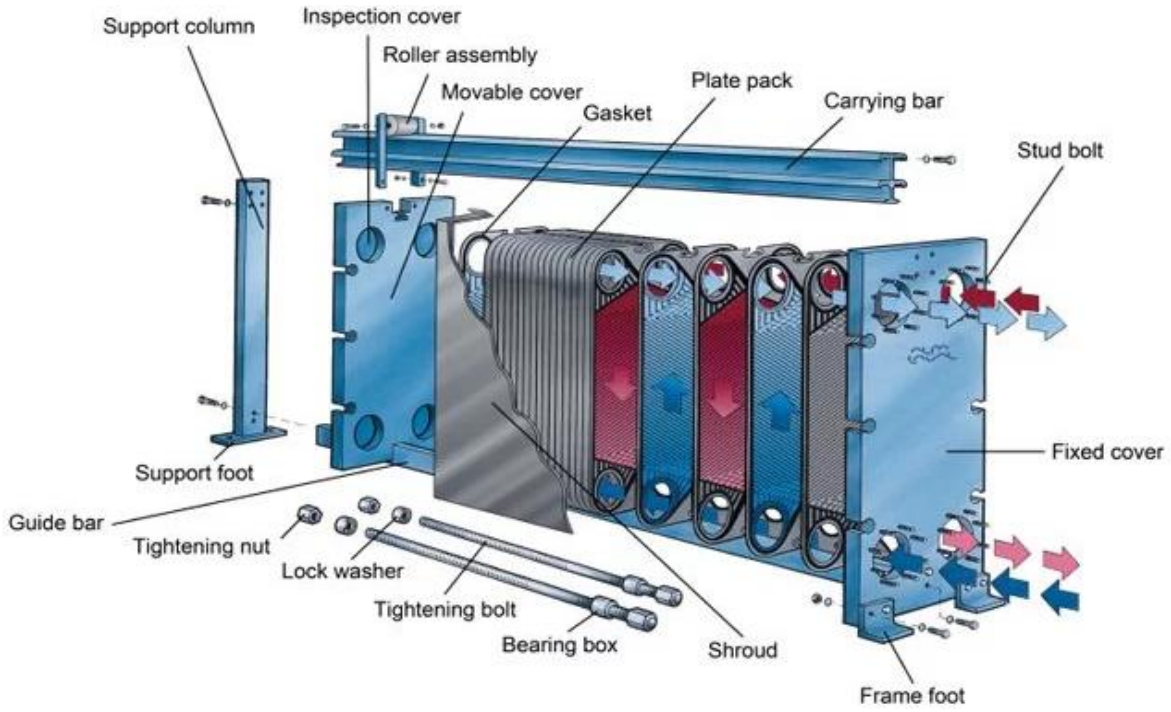

Figure 1.2. Schematic diagram of a PHE[8]*.*

2 Literature review

In this chapter, a literature review is conducted for the milk pasteurization process and the operations involved. The review comprises four main parts. In section 2.1, milk processing system is introduced with milk fouling analysis and milk fouling models. In section 2.2, PHE fouling monitoring and cleaning methods (cleaning in place, CIP, in particular) are discussed. Based on the analysis of current models, the need for this work is identified and the research objectives are listed in section 2.3. Lastly, the thesis structure is presented in section 2.4. It is noted that this review focus on the models (PHE, fouling and CIP models) involved in dairy processing and the ones developed for other industries are either excluded or briefly covered in this review.

2.1 Dairy Processing system and models

Heat treatment is widely used for milk processing to eliminate bacteria and ensure food safety. The results of the treatment depend on the temperature and duration of the heating process, since the heat resistance varies with bacteria. The lethal effect curves of common bacteria presented in milk are shown in Figure B.1 in Appendix B. In general, higher temperature could eliminate pathogenic micro-organism faster and therefore leads to shorter holding time, but higher intensity of heat could lead to flavour change. Therefore, the choice of heat treatment method needs to consider the trade-offs among quality preservation, bacterial elimination, recontamination prevention and energy efficiency[5,6]. This project focus on two commonly used: high temperature short time (HTST) and ultra-high temperature (UHT) processes. HTST pasteurization is a process used to heat milk at a medium high temperature (usually between 72 and 80^{o}C) for at least 15 seconds[5,9,10], while UHT process heat milk at elevated temperature (usually between 135-140℃) for 2 to 5 seconds[10]. Some other milk treatment processes are also summarized in Table C. 1 in Appendix C.

A pasteurization system (Figure 1.1) often consists three PHEs and a holding tube. PHEs are suitable for milk pasteurization over other types of heat exchangers (e.g. shell-and-tube heat exchangers (STHEs)) because: (1) ease for cleaning and maintenance of hygienic requirements; (2) high heat transfer coefficients which ensure close operating temperature difference (as low as 1 ^{o}C comparing to 5-10 ^{o}C for STHEs); (3) compact structure which allows different treatment sections to be mounted onto a single frame and thus reduces installation space and capital cost dramatically[5,6,11]. PHEs are commonly used for milk pasteurization since 1880s when PHEs were originated and rapidly developed due to public awareness of untreated milk safety[5,6].

Design of PHEs, their configurations, choice of pattern on plates (corrugations) and number of plates, affect heat transfer performance as well as capital and operational costs of the

process. Different flow arrangements can be used during operation, for which different configurations of PHEs might be required. To increase driving force for heat transfer and thus enhance PHE performance, counter-current arrangement is normally more desirable over co-current arrangement. Also, narrow channels are often better for heat transfer but could elevate flow velocity and pressure drop especially when the flowrate is high[6]. To minimize these effects, the inlet streams of PHE can be divided into several parallel flows and each flow then interact with the other fluid counter-currently in different channels[6]. An example of two-inlet and four-pass configuration is illustrated in Figure 2.1.

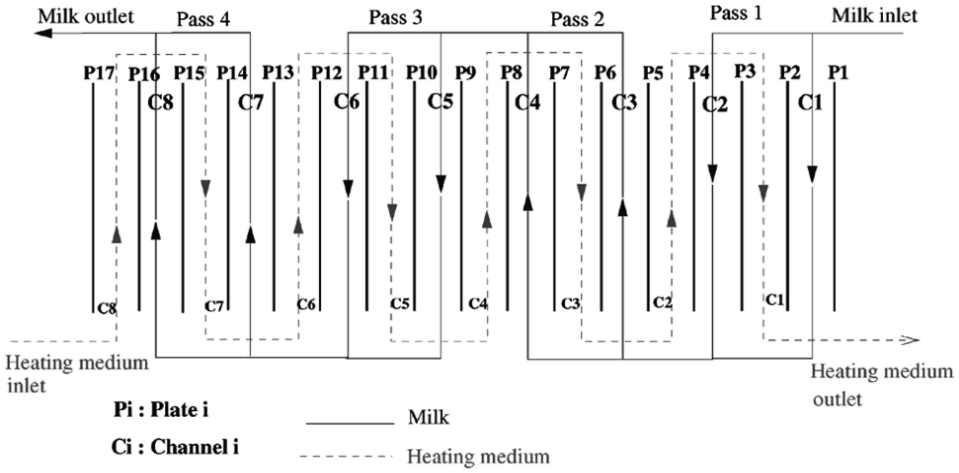

Figure 2.1. Example of multi-pass PHE configuration[12].

Some efforts have been made to optimize the overall milk pasteurization system. For instance, De Jong *et al*[13] developed a model to optimize the process operation based on the desired product safety and quality, which is unique among the models developed. Three predictive models are involved in this method: the kinetic model for components transformation predictions, the process model for the overall production chain and the predictive model for cost estimation. A flowsheet with the general approach of this method is shown in Figure B.3 (Appendix B). However, in this method, model reactors were used in the simulation to simply the PHE configurations and therefore only limited information of the heat transfers within the PHEs are available from the simulated results. Gutierrez, Diniz and Gut[7] developed a dynamic model for the continuous pasteurization process, which can be used as a virtual unit to compare different operational policies and control strategies. Thus, better product quality could be achieved with less energy consumption. However, water (instead of milk) was used as the working fluid in this model and to better represent the pasteurization process, fouling models need to be integrated[7]. Bon *et al.*[9] developed and bulit flowsheets and database for milk pasteurization using process simulator tool (ProSimPlus), which are used to simulate and optimize the process. They first solved the design optimization case, whose results was then used to solve the operating optimization. This approach was used to simulate and study

alternative designs by changing the exchanger capacity or mass flowrate of the fluid. In this way, it can be used to understand the interactions between different parameters[9]. Nevertheless, this approach relies heavily on databases and semi-empirical equations to achieve reliable simulation results[9]. Additionally, a fixed PHE configuration is used in this method and detailed heat transfer information is not availabe through this method since only the inlet and outlet temperatures of the whole PHE is included in the model[9].

2.1.1 Fouling in dairy processing

Milk fouling has been studied extensively during past decades from different approaches (through both experimentation and modelling)[14]. This section covers milk fouling analysis, including fouling types, compositions, mechanism and existing models. Fouling causes many operational problems. Particularly in dairy processing, heat exchangers are cleaned every 5-10 hours depending on the production capacity[6,15]. It is also noted that fouling and cleaning accounts for about 80% of the total production costs, which leads to significant economic loss[16,17]. Thus, finding effective methods to reduce fouling or reduce operational cost associated with fouling and cleaning is critical and essential.

The composition of fouling deposit varies widely due to different milk types, pH, operating temperature, equipment, etc[18,19]. The effects of these factors on milk fouling are discussed and summarized in detail by Alharthi[20]. Among these factors, temperature is the most important one and is often used to distinguish the type of fouling. For milk fouling, it is often classified into two types (type A & B) based on the deposit composition and the temperature that the fouling appears. Type A (protein fouling) occurs at temperature between 75 and 110^{o}C and type B (mineral fouling) happens at temperature above 110^{o}C[17,21]. Figure 2.2 shows the amount of deposit formed for both type A and B at different temperatures and locations within the heater. For type A fouling, initially the amount of protein deposit increases as temperature rises and the maximum is reached around 95-110 ^{o}C, after which the amount decreases as the fluid moves along the heater where temperature continue to increase[22]. It is widely agreed that type A fouling is majorly affected by the β-Lactoglobulin (β-Lg) reaction. However, the full mechanism of β-Lg reaction and its interaction with the heating surface (bulk or thermal layer reaction) remains unclear or unsettled[15,23]. A commonly used protein reaction scheme for modelling is show in Figure 2.3. Descriptions of the mechanism is summarized in detail by many

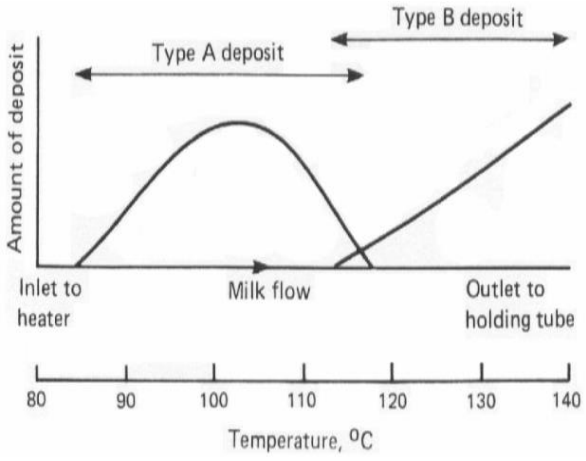

Figure 2.2. Type A and B milk fouling distribution in an indirect heat exchanger[22].

authors[12,18,24,25]. Tolkach and Kulozik[26] also summarized a more detailed molecular level description for the multistage β-Lg thermal denaturation mechanism. Additionally, Bansal and Chen[17] conducted a comprehensive summary of different type A fouling mechanisms presented in the literature (Table C. 2 in Appendix C). Therefore, the reason for the formation of bell-shaped curve in Figure 2.2 could due to different β-Lg fouling reactions involved at different temperature ranges. Different from type A fouling, the deposits involved in type B fouling increase continuously with temperature (Figure 2.2) because the solubility of minerals decreases as temperature increases[17,22]. For HTST pasteurization, only type A fouling is considered since type B fouling is negligible during the process of interest; while for UHT pasteurization, both type A and type B fouling need to be considered.

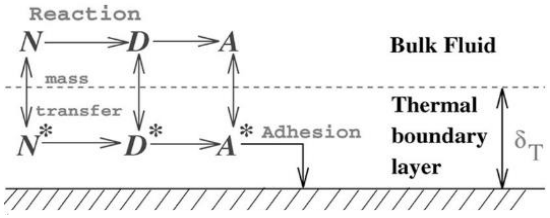

Figure 2.3. Protein reaction scheme on heat exchanger surface[12].

Different PHE models have been developed to better understand the thermal and hydraulic behaviours of the processing fluid. For milk, several models that consider the kinetics of fouling have also been developed. Extensive summaries for these existing models have been done by multiple authors[7,12,18,24,27–29]. Summary tables for the main PHE and milk fouling models as well as their advantages and limitations are also presented in Table A.1 and Table A.3 (Appendix A). Overall, most of the existing fouling models integrate β-Lg reaction scheme with a simplified 1D or 2D representations of PHE (Table A.3 in Appendix A). Among these models, many of them used Biot number to describe fouling layer, and the deposition growth was not considered[12,27]. To account for the deposit layer growth, Guan[24] proposed a more detailed 2D distributed model with moving boundary for a single channel of a PHE. The deposition model is adapted from the model developed by Coletti and Macchietto[3] and Diaz-Bejarano *et al.*[4] for crudie oil fouling in STHE. Sharma[18] extended this distributed model to a full PHE system and simulated two arrangments, considering deposit re-entrainment and two types of depostion mechanism (aggregation and denaturation of protein). It was noted that different Biot number values need to be used to describe and predict these tested conditions. Although detailed 2D models are more accurate comparing to 1D models, plate topology such as corrugation are not considered, which could lead to discrepancies between simulated results and experimental data. As noted by Jun[30], hydrodynamic characteristics of fluid within PHE could be strongly affected by corrugation parameters (angle, depth and pitch); therefore, to describe PHE plate topology in a detailed way, multiple computational fluid dynamics (CFD) models have been developed[30–34]. Due to high complexity of the models, CFD models are often computationally intensive, which leads to longer simulation time (often days)[1]. Moreover, only a small section of the PHE (e.g. a channel or a plate) can be simulated and it is impossible to

study the whole PHE or the whole pasteurizer unit through this method. Thus, CFD models are often not suitable for process control and optimization purposes. Nevertheless, the simulated results of CFD models could potentially be used to find correction factors that could be integrated in simplified 2D models and therefore enhance 2D model accuracy. In addition to the models developed for milk processing, models built for other fluids such as oil and water could be refined and adapted to improve milk fouling models. Examples of these models are also shown in Table A.2 (Appendix A).

2.2 Plate heat exchanger cleaning methods and models

Dairy industry operations have been shifted from manually to mechanization in past decades. Cleaning of PHEs, which used to be a labour-intensive task is now replaced by CIP methods. CIP methods use machinery coupled with detergent solutions that can be circulated through the PHE channels based on a set cleaning program[6,35]. Consequently, to fully integrate the cleaning program with the operation procedures, a more advanced and accurate model that can not only predict the severity and location of the fouling, but also predict and monitor the CIP operation would be beneficial and necessary. This type of model can be used to help allocate resources more efficient and reduce waste, therefore enhance the overall production/operation efficiency. This section covers CIP methods and several models developed in the literature. Some fouling monitoring techniques are also discussed.

2.2.1 CIP methods and models

Overall, the choice of cleaning agent and method for PHEs varies with types of deposit, surface material, configuration, and the economic and environmental factors[36]. CIP is a favoured method comparing to off-line cleaning since it does not require dismantle of the PHE and therefore reduces operational downtime. For milk processing, CIP is often done in a two-stage process using alkali and acid solutions[37]. This process involves five-steps: pre-rinse, alkali-clean, water-rinse, acid-rinse and final-rinse[38].

Mathematically models of CIP that are capable accurately predicting operational parameters (e.g. duration, amount of cleaning agent used, mechanical flowrate and thermal energy) [39] can be utilized to test and optimize the cleaning procedures and thus reduce the cost and waste. Only a few models of CIP have been proposed and developed in literature (Table A.4 in Appendix A). Bird and Fryer[40] proposed a simplified empirical model to assess the effects that temperature and velocity have on cleaning of milk deposit. It was developed specifically for cleaning with 1 wt% $NaOH$ solution[40]. The thickness of the deposit was divided into two layers and for each layer, a differential equation was used to quantify the rate of change of thickness. The model was verified against experimental data and relatively good fit was obtained. Nevertheless, the complex mechanism and chemistry involved in cleaning (reactions between

cleaning agent and deposit) were not considered and several oversimplified assumptions were made for the model[40]. Xin *et al.*[41] proposed a more detailed chemical cleaning model based on polymer dissolution, which accounts for several different processes involved through boundary layers (e.g. reputation, disengagement and mass transfer). This model was also extensively verified with experimental data. One limitation for the model is that deposits removed by shear force was not considered. A more general functional form of conditional-based cleaning model for crude oil fouling was proposed by Lanchas-Fuentes *et al.*[42]. This model considered deposit conditions, effectiveness of the chemical cleaning agent and duration. Parameters used in the model still need to be adjusted or verified against experimental data. On the other hand, this general functional form could be adopted for other fluid such as milk. To the best of the author's knowledge, for milk processing, only Sharma[18] has tried to integrate the CIP model with the fouling model and simulated heating-CIP cycles. However, experimental validation is still required to confirm the simulation results (deposit mass, heating and CIP durations).

2.2.2 Heating-CIP cycles and fouling monitoring

Heating and CIP are performed in cycles during pasteurization process. A simplified schematic for the main stages of heating-CIP cycles is shown in Figure 2.4. A more detailed representation for the heating-CIP cycles with monitoring is also illustrated in Figure B.2 (Appendix B). Initially, the process starts with a clean heat transfer surface. Then initial conditioning occurs (precursors like β-Lg deposit in milk process) and allows further fouling to start. Once the HE performance decays significantly, or the hygienic requirements are not met due to deposition, CIP starts followed with disinfection or pretreatment[14]. The process restarts after cleaning is done. Though cleaning is performed, degradation or change of the surface is unavoidable (stainless steel that often used in PHEs for milk pasteurization is relatively robust towards these changes), which leads to cross-contamination and aged deposition and therefore reduces the performance of the PHEs[14]. If a model was used to predict the heating-CIP operations, its accuracy would be affected because of the changes in fouling composition, PHE surface energy and characteristics at different stages of heating-CIP cycles[14]. Thus, to confirm the model adequacy, the performance of PHE needs to be frequently tested. This can be done by fouling monitoring

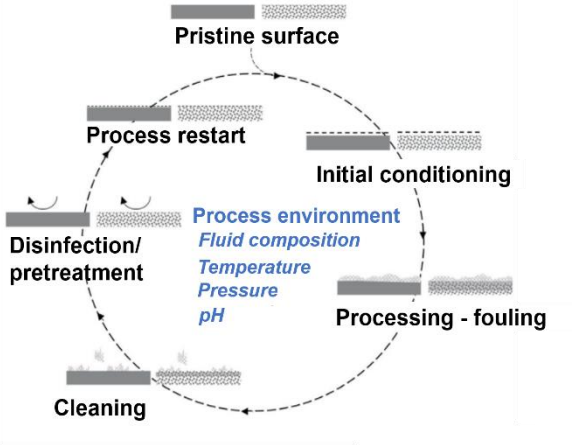

Figure 2.4. Stages for heating-CIP cycles (solid bar refers to a heat transfer surface, dotted bar refers to membrane)[14].

since it detects the needs for cleaning and can be used to validate the effectiveness of cleaning, which provide basis for adjustments of cleaning parameters in the model[39].

Six major methods (Table 2.1) are used as fouling monitoring and detection techniques. Detailed information of these methods are also reported by Wallhäußer, Hussein and Becker[43]. In general, these methods use different types of sensors (e.g. pressure/temperature sensors, acceleration sensor, acoustic sensor, comb sensor) to measure certain parameter, for which an upper- and a lower- bound are set. Once the measured value exceeds the upper-bound or becomes lower than the lower-bound, cleaning action would be triggered or stopped. For instance, Piepiórka-Stepuk *et al*[44] proposed the use of nephelometers to measure the turbidity of the cleaning solution. The turbidity is then used as a cleanliness guideline to determine and control the cleaning time. Overall, the use of monitoring techniques could improve fouling detection and enhance quality control, but it still has several limitations: (1) sensitivity and adaptability of the methods could be low[43]; (2) localized sensor/detector information could be misleading; (3) additional costs are involved in installing and maintaining all the sensors as well as associated equipment. Therefore, there is a need for developing advanced heating-CIP models that are capable predicting the location and severity of the deposit. If the model is coupled with real-time monitoring and adaptive control strategies, not only the limitations of these monitoring techniques can be minimized, but also the model can be constantly validated and adapted. Thus, the cleaning cycles can be scheduled more effectively and the process can be optimized.

Table 2.1. Different fouling detection methods[43].

Method	Short description	Advantages	Limitations
Pressure drop	Pressure between inlet and outlet measured	- No extra equipment - Usually measured - Caution of excessive pressures	- Not very sensitive - More sensitive for PHE - Fouling place unknown
Temperature	Product outlet/heating medium temperature measured	- No extra equipment - Usually measured	- Not very sensitive - Thin layers not monitored - Fouling place unknown
Heat transfer parameters	Heat flux, heat transfer coefficient, thermal resistance measured	- No extra equipment (despite heat flux) - Flow/temperature usually measured	- Certain thickness necessary - Heat flux sensors not usable at high temperatures
Electrical parameters	Electrical resistance, conductivity measured Electrical behaviour of heater monitored	- Very sensitive to thin layers - Fouling thickness determinable	- Invasive - Electrical heating not popular
Acoustic/ Ultrasound/ QCM/QCM-D	Acoustic parameters measured Frequency change and energy dissipation monitored	- Non-invasive - Very sensitive to material changes, thin fouling - Fouling and cleaning monitored - Movable clamp-on sensor	- Scattering can occur - Parameters temperature dependent - One transducer: only one point monitored - QCM/QCM-D invasive
Numerical methods/ANN	Clean/fouled heat exchangers modelled Parameters combined in ANN	- No extra equipment - Very sensitive when appropriate parameters and models used	- Due to parameters errors may occur - First, validation with other methods necessary

In conclusion, a summary of the models in literature related to milk pasteurization process is shown in Table 2.2. According to the literatures reviewed by the author, most of the researches focus on the modelling of the PHE heater only and for the ones that consideres the whole

pasteurizer unit (three PHEs and holding tubes), none of them considers or integrates fouling and CIP models together. However, to better understand heat transfers within the pasteurization process, it is necessary to account the interactions between different parts of the pasteurizer unit in the thermal model. Also, including fouling and CIP models with the thermal model allows testing and optimization of different operational policies. The objective of this research is to develop a model with aforementioned features.

Table 2.2. Summary table for models related to milk pasteurization process.

References	Model characteristics			
	PHE Heater	**Fouling**	**Whole unit**	**CIP**
Georgiadis Rotstein & Macchietto (1998)[15]; Georgiadis & Macchietto (2000)[12]; Jun & Puri (2005, 2006)[27,30]; De Bonis & Ruocco (2009)[34]; Mahdi Mouheb & Oufer (2009)[45]; Boloorchi & Jafari Nasr (2012)[46]; Bouvier *et al* (2014)[33]; Aouanouk, Mouheb & Absi (2018)[29]; Guan & Macchietto (2018)[1]	√	√		
Grijspeerdt *et al* (2004)[47]; Aguiar and Gut (2014)[48]		√	√	
Bird & Fryer (1992)[40]; Xin, Chen, & Özkan (2003)[41]				√
Bon, Clemente, Vaquiro, & Mulet (2010)[9]; Gutierrez, Diniz, & Gut (2014)[7]			√	
Sharma & Macchietto (2018)[2]	√	√		√

2.3 Research objectives

The aim of this research is to develop a high-fidelity model of the whole pasteurization process under fouling (heating, holding, regeneration and cooling). Then, the validated model is used for identification of cleaning strategies as well as tuning and implementation of controllers. Specific research objectives are listed below:

Model development

1. Extend and modify the 2D distributed thermal model of the milk heater (PHE) developed previously[1,2] to all three sections of the pasteurizer unit (heating, cooling and regeneration).
2. Integrate fouling model to the PHEs.
3. Adopt and modify the 2D distributed thermal model of the tube developed previously[3,4] to account for deposition in the tubes (holding and connecting tubes).
4. Integrate fouling model to the tubes.
5. Model the entire pasteurizer unit by joining the component PHE and tube models via suitable boundary conditions.

Model applications

1. Heating-CIP cycle operations: integrate a CIP model to all section models of the pasteurizer unit. Then, perform heating-CIP cycle tests for different configurations

and provide suggestions for cleaning strategies and schedules.

2. Controller implementations: integrate PI controller models to the pasteurizer unit model. Then, tune and assess the controller performance based on a case study. Also, analyse the dynamic behaviour of the model.

2.4 Thesis structure

The thesis is structure as follows: firstly, an overview of the model for the full milk pasteurizer unit is presented (Chapter 3). Then, the segments of the complete pasteurizer unit are introduced one at a time, which includes: the model for a single PHE channel (Chapter 0), a combined PHE section (Chapter 5) and a tube (Chapter 0). Once all the segment models are introduced, the entire unit is modelled by joining the component models via suitable boundary conditions (Chapter 7). For PHE and tube section models as well as the full pasteurizer unit model, simulations were performed to validate and assess the model adequacy in the corresponding chapter. With the developed model of the pasteurizer unit, two model applications (heating-CIP cycle operations and controller implementations) are discussed and case studies were simulated and analysed (Chapter 8 and 9). Lastly, main conclusions and future works are reviewed in Chapter 10.

In addition to the main content, seven appendixes are included at the end of the thesis with information that is useful to refer to but can distract the flow if included in the main body. Appendix A presents the summary tables for models developed in literature with their main advantages and limitations. Appendix B and C show some complementary tables and figures for the main text. Appendix D and E list out the mass balance equations for fouling models of PHEs and tubes, respectively. Appendix F includes a briefly sensitivity analysis of fluid physical properties to support an assumption made in the model. Lastly, Appendix G describes the process for the estimation of PI controller transfer function.

3 Overview of the model for milk pasteurizer unit

The structure of the overall pasteurizer unit model as well as the sub-models involved in the main model are presented in Figure 3.1 and Figure 3.2. The main pasteurizer unit model consists of three PHEs (heating, regeneration and cooling), a non-isothermal holding tube, and two non-isothermal tubular connections (TCH & TCR). Firstly, the initial conditions, equipment specifications and equipment configurations are specified in the main unit model. Then, this information is passed onto the section models for PHEs and tubes. Also, as illustrated in Figure 3.1, the fluid and temperature continuities among section models are established in the main pasteurizer unit model. For each section model (PHE/tube), a thermal model is coupled with a fouling and a CIP models (Figure 3.2). For the PHE section model, a single channel model is defined. Then, multiple channels are connected in the section model based on configurations (e.g. co-current or counter-current) and proper boundary conditions. The tube section model consists of multiple domains: working fluid, deposit layer, and tube wall, which are connected using proper boundary conditions. Detailed illustrations, analysis and validations of the models involved are discussed in the following chapters.

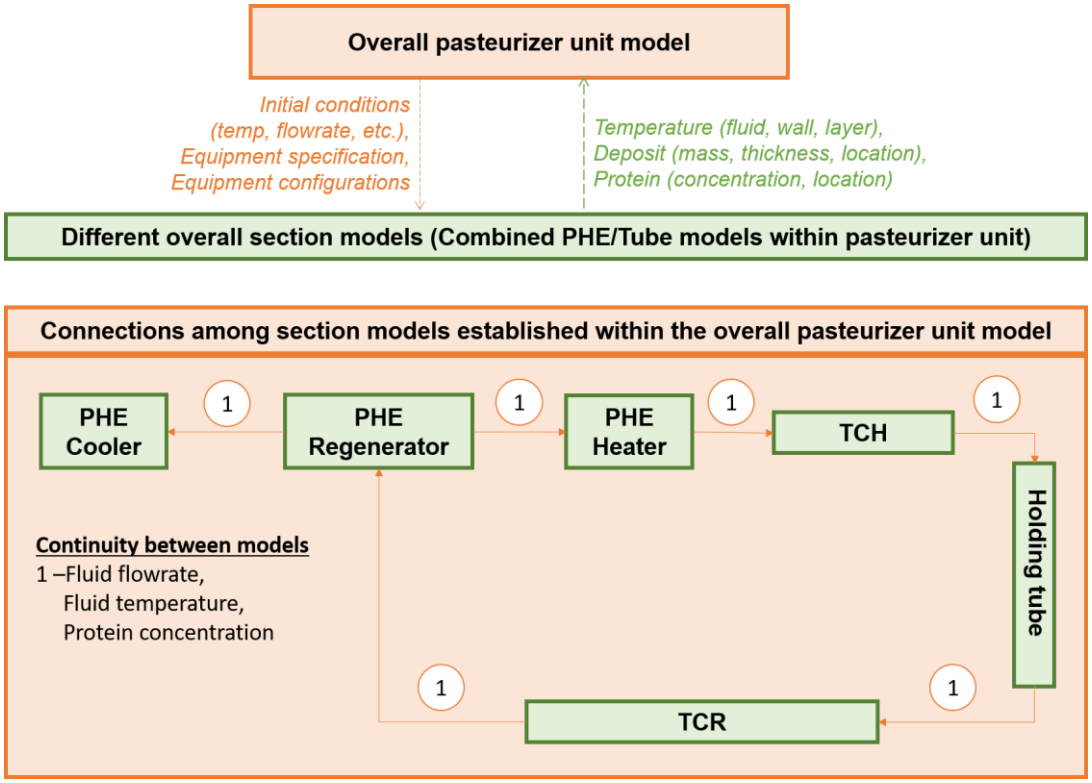

Figure 3.1. Overall pasteurizer unit model.

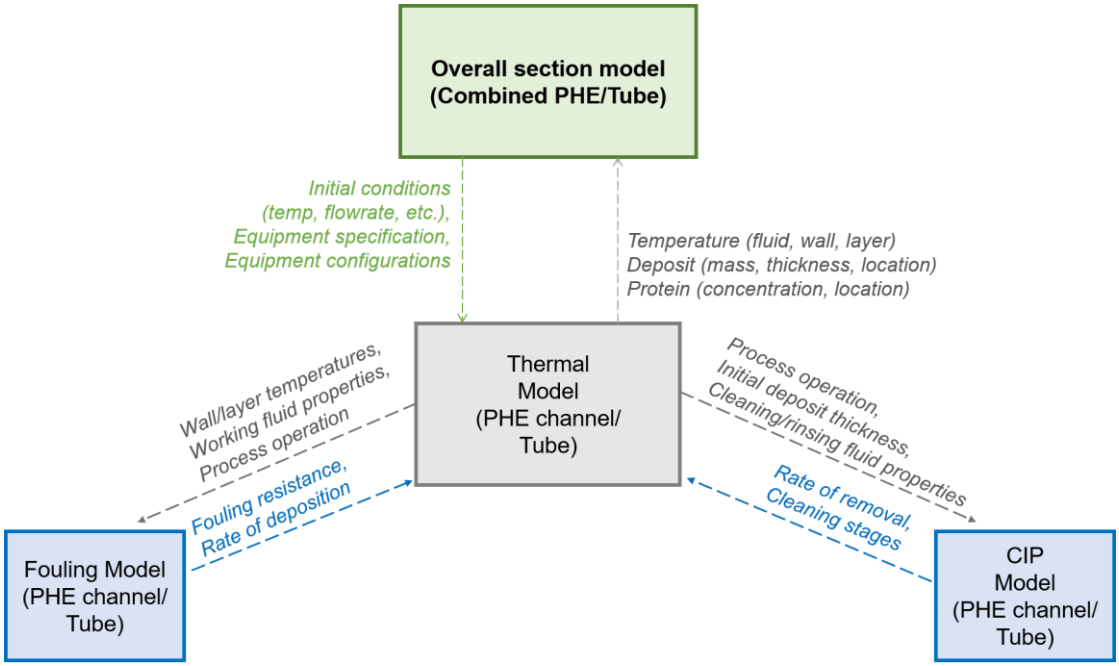

Figure 3.2. Overall section model for combined PHE/Tube.

4 Model for a single PHE channel

This chapter focus on the dynamic and distributed model of a single PHE channel undergoing milk fouling in the pasteurization process. Skimmed milk is chosen as the working fluid in this case. To better describe and represent the boundary conditions and thermal continuities, each internal channel of a PHE is modelled as if it is composed by two half plates. For the two end channels of the PHE, they are modelled as if they are composed by a half plate and a full plate. A schematic representation is shown in Figure 4.1. In this chapter, the governing equations used for each region (flow, wall and deposit layer) within a single channel along with their boundary conditions are discussed.

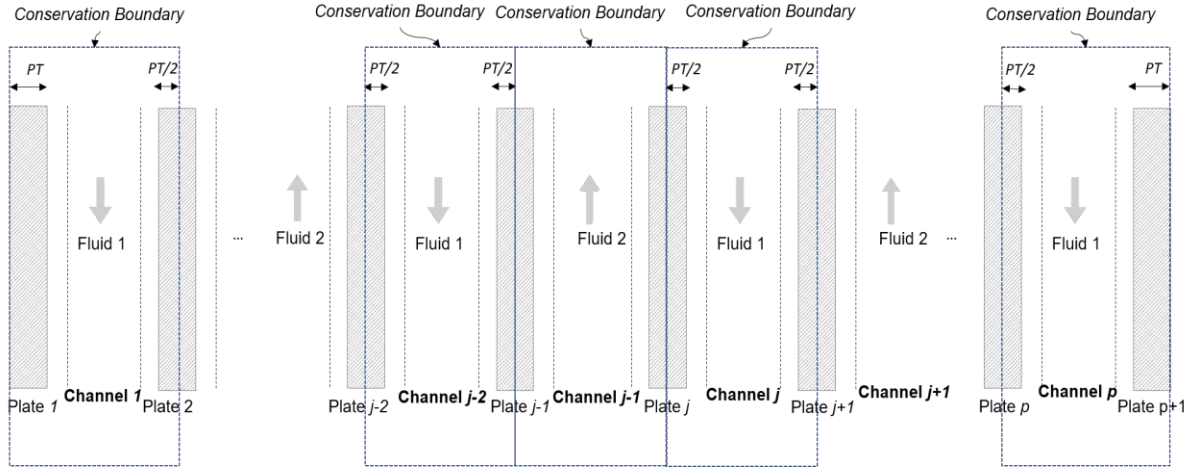

Figure 4.1. Schematic illustration for PHE channel modelling.

4.1 Overview of the moving boundary model

PHE models developed previously for milk processing either exclude fouling effects or only include some parameter (e.g. Biot number) to describe fouling layer but the deposit layer growth within the PHEs and its effects on the heater transfer are not analysed. Therefore, an advanced moving boundary model was proposed and developed by Guan[24], Sharma and Macchietto[2] to account for the deposit layer growth and better represent PHE channels under milk fouling. In this work, the moving boundary model was used with additional modifications (discussed later). A schematic diagram for the model is shown in Figure 4.2. Descriptions of the model and its corresponding assumptions are discussed and analysed in detail by Guan[24], Sharma and Macchietto[2]. For each channel, three domains (plate wall (Ω_w), deposit layer (Ω_l) and processing fluid flow (Ω_f)) are considered. The wall and layer domains are also further classified into left (L) and right (R) parts to account for different dynamic behaviours on each side of the plate. As for the coordinates, $y = 0$ is defined at the centre of the channel and $x = 0$ is defined at the top of the channel as shown in Figure 4.2. All three domains are distributed along the x-axis throughout the channel length $[0, L]$. The wall domains (Ω_w^L & Ω_w^R) are also

distributed along the y-axis to account for the heat transfer across the wall thickness. These domains are defined from y_w^L to y_l^L for Ω_w^L and y_l^R to y_w^R for Ω_w^R, where y_w^L, y_l^L, y_l^R and y_w^R can be calculated using the following equations:

$$y_w^i = -n^i\left(\frac{e_j}{2} + BT_w\right) \qquad \forall\, i \in \{L, R\} \qquad (4.1)$$

$$y_l^i = -\frac{n^i e_j}{2} \qquad \forall\, i \in \{L, R\} \qquad (4.2)$$

$$BT_w = \begin{cases} PT/2 & for\ internal\ plates \\ PT & for\ two\ end\ plates \end{cases} \qquad (4.3)$$

Here, e_j is the channel gap between two clean plates and PT is the thickness of a whole plate. BT_w is defined as the thickness of the plate within the conservation boundary (Figure 4.1). And n^i is used to indicate the direction of the y-coordinate, which equals to +1 for the left-side plate and -1 for the right-side plate.

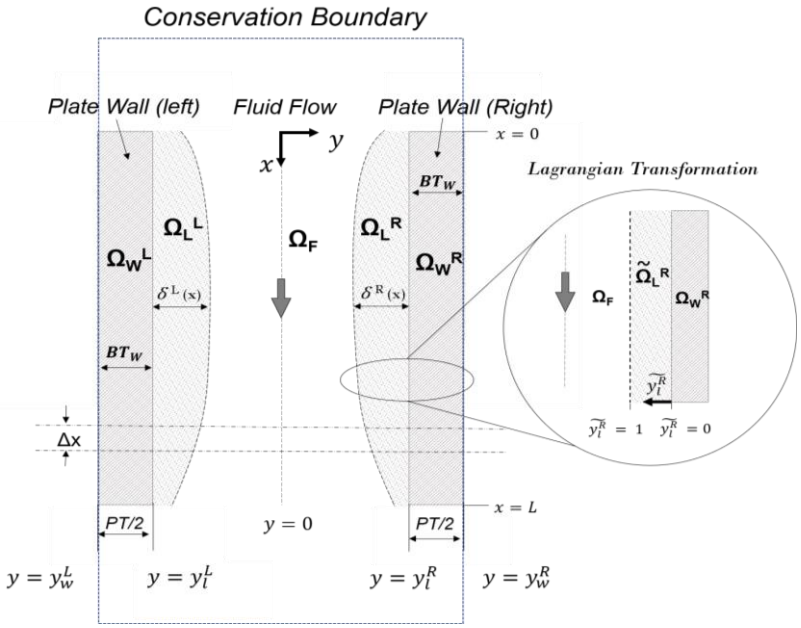

Figure 4.2. Schematic diagram of the moving boundary model for a single heating channel with Lagrangian transformation (Figure is adapted from Guan[24] with minor modifications).

Similarly, the deposit domains (Ω_l^L & Ω_l^R) are also distributed along the y-axis to account for different fouling deposit thickness at different locations along x-axis. The physical domain that describe the deposit thickness at spatial coordinate (x, y) varies, which makes it hard to solve the distributed system. A Lagrangian transformation[24] is used to scale down the y-coordinate of the layer domain to a dimensionless coordinate, $\tilde{y}_l$, which is defined between 0 and 1 (Figure 4.2). When $\tilde{y}_l$ equals to 0, it represents the interface between wall and deposit layer; when $\tilde{y}_l$ equals to 1, it represents the interface between bulk flow and deposit layer. It

transforms the moving boundary into a static boundary in a different coordinate domain. The conservation equations for the deposit domain are also modified accordingly, which are discussed later in this chapter.

4.2 Overall thermal model description

A detailed overall illustration of heat flux between two fluids in the three regions of a PHE channel are shown in Figure 4.3 (internal channels) and Figure 4.4 (end channels). Both hot and cold fluids could flow through the channel upwards or downwards (blue or red arrow is used to indicate cold or hot fluid, respectively). The directions of heat flux across the channels are also indicated by arrows in the figures. For general demonstration, fouling is considered for both fluids and the moving boundary model is used. However, in many cases, fouling on the cold fluid side can be negligible and may not be considered in the model calculation.

The following assumptions are used for the overall thermal model[2]:

- The plates of the PHE are assumed to be flat and smooth: corrugation is not considered.
- The processing fluid flow is assumed to be plug flow: uniform flow profiles across x-axis.
- No heat or mass transfer along channel length direction (x-axis) for both wall and deposit regions.
- Heat loss to the surrounding environment is neglected.
- No heat generation/supply within the channel.

Further assumptions used for different regions (flow, wall and deposit layer) in the channel are discussed with the corresponding equations/models in the following part of the chapter.

4.2.1 Wall region

For the wall region, heat transfer is described through the following equation:

$$\frac{\rho_w C_{pw}}{\lambda_w}\frac{\partial T_w^i(x,\mathrm{y})}{\partial t} = \frac{\partial^2 T_w^i(x,y)}{\partial (y)^2} \qquad \forall\, i \in \{L,R\} \qquad (4.4)$$

And the heat flux through the wall is described by Fourier's law:

$$q_w^i(x,y) = -\lambda_w \frac{\partial T_w^i(x,y)}{\partial y} \qquad \forall\, i \in \{L,R\} \qquad (4.5)$$

Here, the physical properties of the plate (ρ_w, C_{pw} and λ_w) are assumed to be constant throughout the PHE channel. And T_w^i is the local temperature of the left/right wall at spatial coordinates (x, y). Also, there is no heat production within the wall.

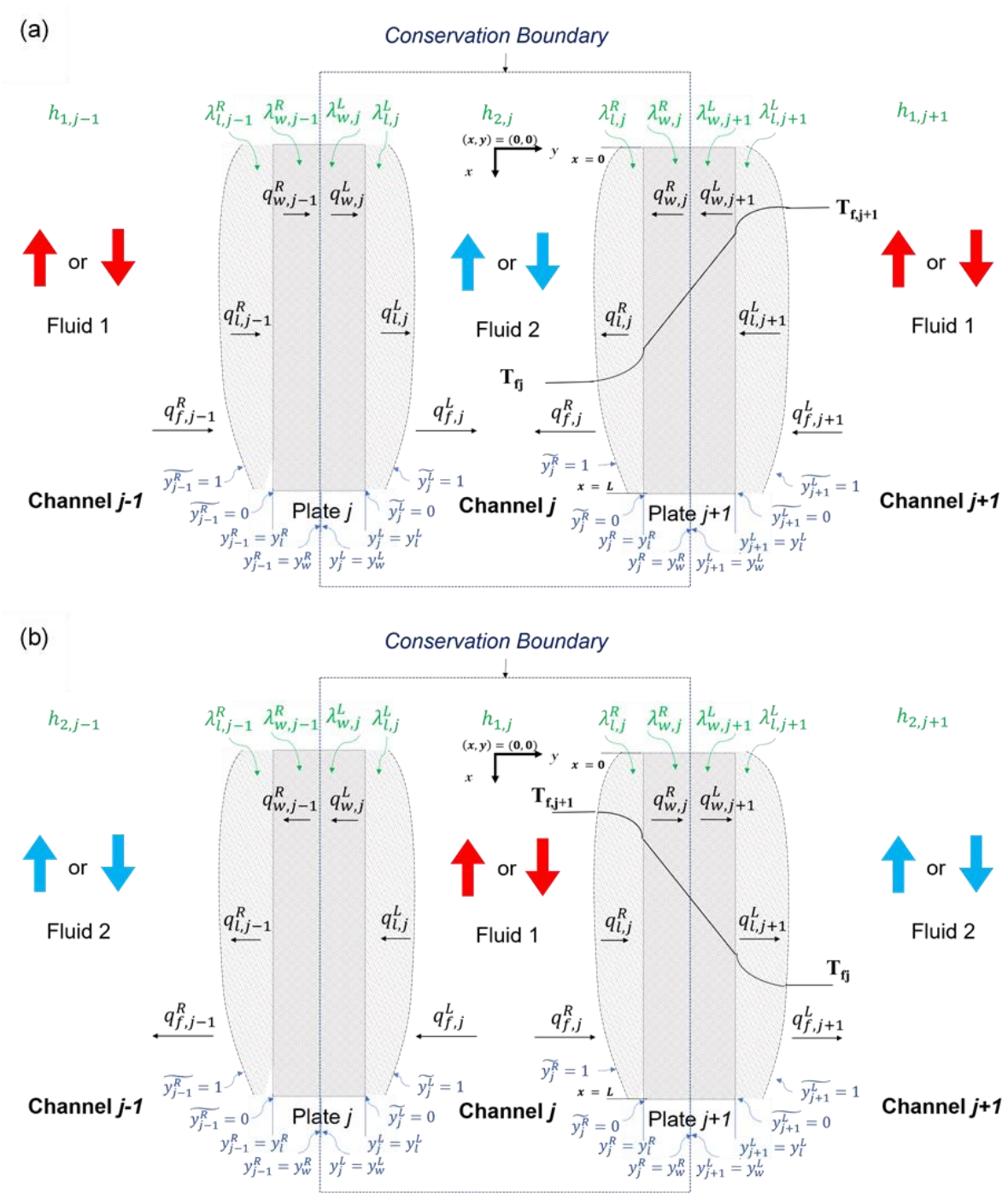

Figure 4.3. Schematic illustration of the heat transfer across different regions for a single internal channel (a): hot-cold-hot arrangement; (b): cold-hot-cold arrangement.

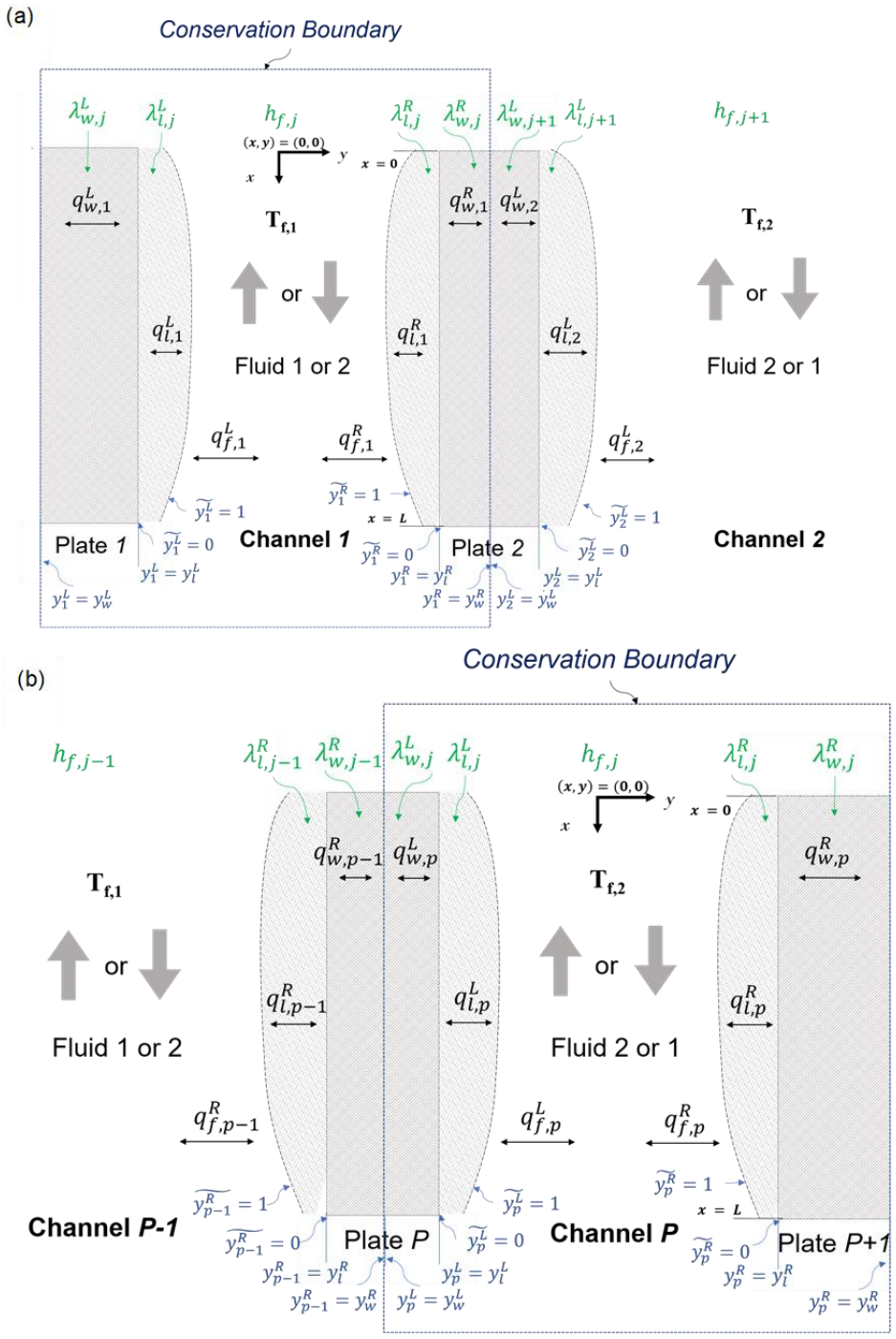

Figure 4.4. Schematic illustration of the heat transfer across different regions for a single end channel (a): left end channel; (b): right end channel.

4.2.2 Milk deposit layer region

For the deposit layer region, same conservation law as that of the wall region is applied. Then, the standard heat transfer and heat flux equations are modified using Lagrangian transformation[24], which result in the following equations:

$$\frac{\rho_l C_{pl}}{\lambda_l}\left(\frac{\partial T_l^i(x,\tilde{y})}{\partial t}-\frac{\tilde{y}_l}{\delta^i(x)}\frac{\partial \delta^i(x)}{\partial t}\frac{\partial T_l^i(x,\tilde{y})}{\partial t}\right)=\frac{1}{(\delta^i(x))^2}\frac{\partial^2 T_l^i(x,\tilde{y})}{\partial \tilde{y}^2} \qquad \forall\, i \in \{L,R\} \quad (4.6)$$

$$q_l^i(x,\tilde{y}) = -n^i \frac{\lambda_l}{\delta^i(x)} \frac{\partial T_l^i(x,\tilde{y})}{\partial \tilde{y}} \qquad \forall\, i \in \{L,R\} \quad (4.7)$$

Here, ρ_l, C_{pl} and λ_l are the physical properties of the deposit layer. These physical properties are assumed to be constant across the PHE channel, and deposit ageing or other changes in its structure are neglected. T_l^i is the deposit layer temperature at the transformed spatial coordinate $(x,\tilde{y})$. $\delta^i(x)$ is the deposit thickness at left or right plate of the channel. And q_l^i is the heat flux through the left or right deposit layer at $(x,\tilde{y})$. Additionally, n^i is used to correct the sign for the heat flux (q_l^i) due to the introduction of dimensionless $\tilde{y}$, where n^i equals to +1 for the left-side plate and -1 for the right-side plate. As illustrated in Figure 4.2, for the main dimensional y-coordinate, the increasing direction is always from left to right; while, for the dimensionless $\tilde{y}$-coordinate, the increasing direction is defined from the wall-layer interface ($\tilde{y}=0$) to layer-fluid interface ($\tilde{y}=1$), whose direction varies with left and right plates. The two coordinates are consistent for the left plate, but they are opposite for the right plate. Thus, the correction of the sign after Lagrangian transformation is necessary to ensure proper interactions among the transformed deposit layer region and other regions (wall/flow) in the channel model.

4.2.3 Flow region

For the flow region, constant mass flow rate is assumed, and a shell energy balance is used to develop the following heat transfer equation:

$$\begin{aligned}\frac{\partial}{\partial t}\left(\rho_f C_{pf} T_f(x) A_{flow}(x)\right) = & -dir\frac{\partial}{\partial x}\left(\rho_f C_{pf} T_f(x) u_f A_{flow}(x)\right) \\ & + \frac{\partial}{\partial x}\left(\lambda_f A_{flow}(x)\frac{\partial T_f(x)}{\partial x}\right) - W(q_f^L + q_f^R)\end{aligned} \quad (4.8)$$

Where q_f^L and q_f^R are convective heat transfer between deposit layer and processing fluid, which are defined as following:

$$q_f^i = h\left(T_f - T_l^i|_{\tilde{y}=1}\right) \qquad \forall\, i \in \{L,R\} \quad (4.9)$$

Here, dir is used to indicate the direction of the flow along x-axis, which equals to +1 for fluid flows from top of the channel to the bottom and equals to -1 if it flows from bottom to top. W is the plate width and u_f is the magnitude of the velocity for the processing fluid, which can be calculated by the following equation:

$$u_f(x) = \frac{Q_{channel}}{A_{flow}(x)} \quad (4.10)$$

The cross-sectional area of flow (A_{flow}) changes at different x locations as the actual gap of channels (e_x) varies when fouling occurs:

$$e_x(x) = e_j - \delta^L(x) - \delta^R(x) \tag{4.11}$$

$$A_{flow}(x) = W\, e_x(x) \tag{4.12}$$

Here, e_j is the channel gap under clean condition; δ^L and δ^R are deposit thickness on left and right plates of the channel.

The convective heat transfer coefficient (h) can be approximated through the empirical correlations based on different dimensionless numbers (Nu, Re and Pr)[2]:

$$Nu(x) = 0.0902\, Re(x)^{0.663}\, Pr(x)^{0.333} \tag{4.13}$$

$$Re(x) = \frac{D_h(x)\rho_f(x)u_f(x)}{\mu_f(x)} \tag{4.14}$$

$$Pr(x) = \frac{C_{pf}(x)\mu_f(x)}{\lambda_f(x)} \tag{4.15}$$

$$Nu(x) = \frac{h(x)D_h(x)}{\lambda_f(x)} \tag{4.16}$$

$$D_h(x) = 2e_x(x) \tag{4.17}$$

Here, D_h is the hydraulic/equivalent diameter which is approximated as twice the value of e_x to account for the deposit layer thickness. The Nusselt number (Nu) correlation is valid for Reynolds number between 90 and 2000[18]. A brief sensitivity analysis (Appendix F) is performed for the physical properties of the processing fluid (ρ_f, C_{pf}, λ_w and μ_f). It shows that using constant physical properties for a specific PHE is a valid assumption and it can simplify calculations and reduces model complexity. Therefore, in this project, the physical properties of the fluid are estimated at the average fluid temperature within the PHE. Correlations used to estimate the physical properties are shown in next section.

4.2.3.1 Physical properties of processing fluid

Different correlations for physical properties are used in the current model. It is noted that the physical properties of milk vary with milk types (whole, skimmed and concentrated)[49–52]. For skimmed milk, it is noted that heat capacity (C_p) remains constant for temperature above 60°C. It is because that the latent heat effect is negligible after most solid milk fats dissolved in the solution[52]. The correlations for density (ρ), thermal conductivity (λ) and dynamic viscosity (μ) of skimmed milk are taken from Kessler[49], Minim et al[50] and Fernández-Martín[51], respectively, and are shown below:

$$C_{pf}(x) = 4022.6 \tag{4.18}$$

$$\rho_f(x) = 1040.6 - 0.2675\, T_{fc}(x) - (2.295 \times 10^{-3})\, T_{fc}^2(x) \tag{4.19}$$

$$\lambda_f(x) = 0.528 + (2.13 \times 10^{-3})\, T_{fc}(x) \tag{4.20}$$

$$\log_{10}(\mu_f(x) \times 1000) = 0.5181 - 0.0147\, T_{fc}(x) + (5.90 \times 10^{-5})\, T_{fc}^2(x) \tag{4.21}$$

As for water, the correlations for Cp, ρ and μ are fitted into similar polynomial form as those equations for milk. The thermodynamic data is taken from NIST[53] at 1 atm. And the correlation for λ is adopted from Choi and Okos[54].

$$C_{pf}(x) = 4188.8 - 0.6286\, T_{fc}(x) + (8.782 \times 10^{-3})\, T_{fc}^2(x) \tag{4.22}$$

$$\rho_f(x) = 1002.9 - 0.1394\, T_{fc}(x) - (3.043 \times 10^{-3})\, T_{fc}^2(x) \tag{4.23}$$

$$\lambda_f(x) = 0.57109 + (1.7625 \times 10^{-3})\, T_{fc}(x) - (6.7306 \times 10^{-6})\, T_{fc}^2(x) \tag{4.24}$$

$$\log_{10}(\mu_f(x) \times 1000) = 0.1994 - 0.01094\, T_{fc}(x) + (3.495 \times 10^{-5})\, T_{fc}^2(x) \tag{4.25}$$

It is noted that temperature (T_{fc}) used in these correlations is in degree C. Therefore, in the future, if these equations are integrated with other model equations, unit conversion is required.

4.2.4 Boundary conditions

Boundary conditions are specified to ensure thermal continuity at both wall-layer and layer-flow interfaces (internal channels).

- For the wall-layer interface, equal temperature and equal heat flux conditions need to be satisfied (Figure 4.3).

$$T_w^i\left(x, y_l^i\right) = T_l^i(x, 0) \qquad \forall\, i \in \{L, R\} \tag{4.26}$$

$$q_w^i\left(x, y_l^i\right) = q_l^i(x, 0) \qquad \forall\, i \in \{L, R\} \tag{4.27}$$

- For the layer-flow interface, conductive heat flux from layer to flow has same magnitude as convective heat flux from flow to layer. And n^i is used to correct the direction, which equals to +1 for the left-side plate and -1 for the right-side plate

$$q_l^i(x, 1) = -n^i q_f^i(x) \qquad \forall\, i \in \{L, R\} \tag{4.28}$$

4.3 Fouling model and material balance for the PHEs

As illustrated in Figure 3.2, a fouling model is coupled with the thermal model of a PHE channel. The combined model is constructed as follows: the thermal model transfers the wall and layer temperatures, fluid properties (e.g. temperature, flowrate, physical properties) and process operations to the fouling model; based on this information, fouling resistance and rate of deposition are determined in the fouling model; these values are then updated to the thermal

model for further calculation. When implement the combined model, all the equations in both thermal and fouling models are solved simultaneously.

For HTST process, protein fouling (type A) is the dominate fouling type; while for UHT process, both protein and mineral fouling occurs at different temperature ranges. However, for the scope of this project, only type A fouling is studied and modelled. Therefore, for UHT process, the fouling deposition mass estimated from the current model would be lower than the experimental values. For this project, the fouling model implemented by Sharma and Macchietto[2] has been adopted with minor modifications (discussed later). Two β-lg reaction schemes have been used: (1) fouling due to aggregated protein (Dep_A) (Figure 4.5); (2) fouling due to unfolded protein (Dep_U) (Figure 4.6). Here, N, U and A represent the native, unfolded and aggregated β-lg protein, respectively. Reactions of $N \rightarrow U$ and $U \rightarrow A$ occur in both bulk fluid as well as the thermal boundary layer. For Dep_A fouling, only aggregated protein is deposit onto the plate surface; while for Dep_U fouling, only unfolded protein can deposit onto the surface.

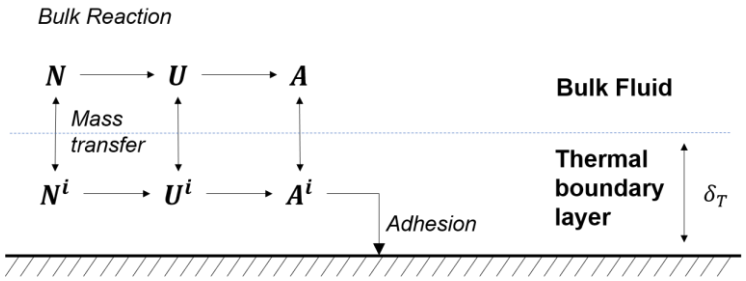

Figure 4.5. β-lg reaction schemes with fouling due to aggregated protein (Dep_A)[12].

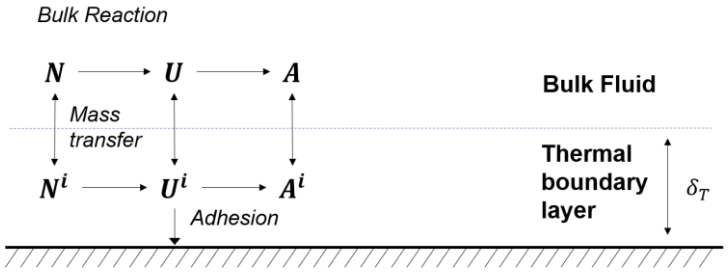

Figure 4.6. β-lg reaction schemes with fouling due to unfolded protein (Dep_U) (adapted from Georgiadis and Macchietto[12].

4.3.1 Kinetic model

The rate of reactions ($r_{protein}$) that is used in the kinetic model to represent the bulk and thermal boundary layer are defined as follows:

$$r_{f_{protein}} = k_{f_{protein}} C_{f_{protein}}^{n_{protein}} \tag{4.29}$$

$$r^i_{T_{protein}} = k^i_{T_{protein}} \left(C^i_{T_{protein}}\right)^{n_{protein}} \qquad \forall\, i \in \{L, R\} \quad (4.30)$$

Here, $C_{protein}$ is the concentration of the protein in bulk flow or thermal boundary layer. And $n_{protein}$ is the order of the reaction. Subscription f and T are used to denote the bulk flow and thermal boundary layer, respectively. And the rate constant (pre-exponential factor) ($k_{protein}$) are calculated from the Arrhenius equation:

$$k_{f_{protein}} = k_{0_{protein}} e^{-\frac{E_{a_{protein}}}{R_g T_f}} \quad (4.31)$$

$$k^i_{T_{protein}} = k_{0_{protein}} e^{-\frac{E_{a_{protein}}}{R_g T^i_T}} \qquad \forall\, i \in \{L, R\} \quad (4.32)$$

Here, $k_{0_{protein}}$ is the reference rate constant; $E_{a_{protein}}$ is the activation energy; R_g is the ideal gas constant; T_f is the bulk fluid temperature and T^i_T is the thermal boundary layer temperature. The heat transfer in the thermal boundary layer is not included in the thermal model, therefore T^i_T is set to be the average of the bulk fluid temperature and the deposit layer temperature:

$$T^i_T = \frac{T_f + T^i_l|_{\tilde{y}=1}}{2} \qquad \forall\, i \in \{L, R\} \quad (4.33)$$

The values of the constants used in the kinetic model as well as their applicable temperature range are shown in Table 4.1[55].

Table 4.1. Constants used in the kinetic model as well as their applicable temperature range[55].

Reaction	**Temperature range (℃)** T	$\ln(pre-exponential\ factor)$ $\ln k_{0_{protein}}$	**Activation energy (kJ/mol)** $E_{a_{protein}}$	**Order of reaction** $n_{protein}$
Unfolding (N → U)	70~90	86.41	261.4	1
Aggregation (U → A)	70~90	91.32	288.5	2
	90~150	13.99	54.7	2

4.3.2 Deposition model

An empirical model based on the Biot number and a proportionality constant (β) is used to account for milk deposition rate[12]. It is noted that β is an adjustable parameter, which is used to fit experimental data for deposition mass. Therefore, its value would change depend on the PHE arrangement and fouling types.

$$\frac{\partial Bi}{\partial t} = \beta k_w C^{n_{protein}}_{protein} \quad (4.34)$$

Here, k_w is the mass transfer coefficient of the protein from the bulk to the deposit. Ans Bi is the Biot number, which is a dimensionless index that compare the convective and conductive heat transfer effects. It can be calculated as following:

$$Bi = \frac{\delta(x) h_f^o}{\lambda_d} \tag{4.35}$$

Here, $\delta(x)$ is the deposit thickness; h_f^o is the local convective heat transfer coefficient under clean condition and λ_d is the thermal conductivity of the deposit. By substituting equation (4.35) into equation (4.34), the change of deposit thickness can be expressed as following:

$$\frac{d\delta(x)}{dt} = \beta \frac{\lambda_d}{h_f^o} k_{w_{protein}} C_{protein}^{n_{protein}} \tag{4.36}$$

For fouling due to aggregated protein (Dep_A), the corresponding k_{wA}, C_A and n_A can be used and the expression becomes:

$$\frac{d\delta_{dA}^i(x)}{dt} = \beta \frac{\lambda_d}{h_f^o} k_{wA} \left(C_A^i\right)^{n_A} \qquad \forall\, i \in \{L, R\} \tag{4.37}$$

Here, based on the model fitting to experimental data, k_{wA} is assumed to be constant[12] and set to be 10^{-7} and n_A is found to be 1.

Similarly, fouling due to unfolded protein can be expressed as:

$$\frac{d\delta_{dU}^i(x)}{dt} = \beta \frac{\lambda_d}{h_f^o} k_{wU}^i \left(C_U^i\right)^{n_U} \qquad \forall\, i \in \{L, R\} \tag{4.38}$$

Here, k_{wD} can be calculated from the Arrhenius equation:

$$k_{wU}^i = k_{wU0} e^{-\frac{E_{aU}}{RT_l^i|_{\tilde{y}=1}}} \qquad \forall\, i \in \{L, R\} \tag{4.39}$$

The values for the constants used in the equation are determined experimentally and shown in Table 4.2[55].

Table 4.2. Constants used in the deposit model due to unfolded protein[55].

$\ln(pre-exponential\ factor)$ $\ln k_{wU0}$	Activation energy (kJ/mol) E_{aU}	Order of reaction n_U
-0.82	45.1	1

It is noted by De Jong[55] that the value for $\ln k_{wU0}$ has large uncertainties (± 1.45) and this deposition model show good agreement for PHE that has surface temperature between 86 and 115 ℃.

4.3.3 Material balance

Concentrations of different β-lg protein (N, U and A) in bulk and thermal boundary layer are determined from the mass balance, which are listed in Appendix D[2,12]. In the material balance, steady state is assumed. Some other simplified assumptions are also used[12]. For instance,

the velocity in the thermal boundary layer is assumed to be same as that of the bulk fluid (Eqn. (D.4)-(D.6)), which could overestimate the mass transfer due to convection. In the model, four deposition mechanisms are included so that it could be used to test different β-Lg reaction schemes proposed in the literature: (1) fouling due to aggregated protein; (2) fouling due to aggregated protein with entrainment due to shear stress; (3) fouling due to unfolded protein; (4) fouling due to unfolded protein with entrainment due to shear stress. Logic parameters are integrated in the mass balance equations to reflect the fouling type selected (Appendix D).

Overall, the fouling model discussed in this section is a semi-mechanistic model. Regardless of the limitations, this model still demonstrates an advance over other purely empirical models in the literature, since it accounts for β-Lg reactions and analyse the protein concentration profile in both bulk and thermal boundary layers.

5 Model for a combined PHE

This chapter focus on the dynamic and distributed model of a combined PHE under milk fouling. Firstly, the general description of the model is discussed. Then, the thermal model is validated against experimental data and simulated results in the literature. Following that, the proportionality constant (β) in the fouling model is estimated for different PHE configurations. Lastly, the simulated deposit mass is compared against literature reference values.

5.1 Channel connections

The model of a single PHE channel consists a thermal model coupled with a milk fouling model. The combined PHE is modelled as a collection of individual channels (Figure 4.1) using a hierarchal model building design[2]. In this way, the single channel model developed can be used repeated for both fluids within the combined PHE (working fluid and heating/cooling medium), which reduces the model complexity. However, proper connections need to be established in order to use the model more effectively. As illustrated in Figure 3.2 and Figure 5.1, the overall section model of the combined PHE defines initial conditions (e.g. temperature of the wall/deposit layer), PHE specifications and PHE configurations of individual channels. Then the overall model passes on this information to all channels within the combined PHE. Depend on the PHE configuration (single- or multiple- inlet), the information of the inlet fluid (inlet temperature, flowrate, protein concentrations) would either pass on to one or multiple channels. Connections between different channels are also constructed in the overall section model. An example of PHE channel connection for a single-inlet and multiple-pass configuration is shown in Figure 5.1. Between sequential channels, fluid mass flowrate, fluid temperature and different β-lg protein concentrations within the fluid are linked with proper continuity equations.

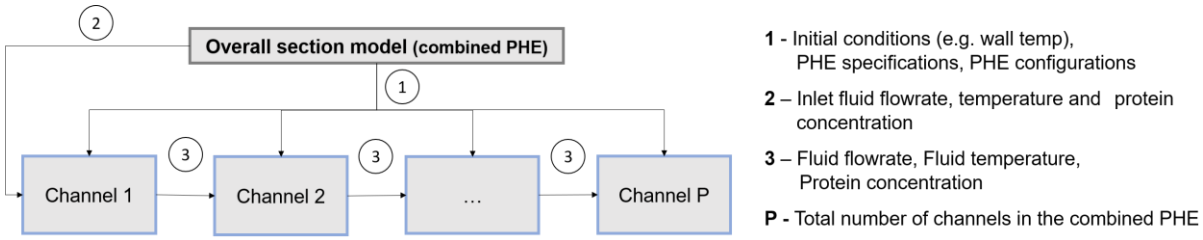

Figure 5.1. PHE channel connection (single inlet & multiple passes).

Thermal model

- Temperature continuity between internal channel walls (Figure 4.1 and Figure 4.3):

$$T^{R}_{w,j}(x, y^{R}_{w}) = T^{L}_{w,j+1}(x, y^{L}_{w}) \qquad \forall\, j \in [1, P-1] \qquad (5.1)$$

  Here P is the total number of channels within the PHE.

- Heat flux continuity between internal channel walls (Figure 4.1 and Figure 4.3):

$$q^{R}_{w,j}(x, y^{R}_{w}) = q^{L}_{w,j+1}(x, y^{L}_{w}) \qquad \forall\, j \in [1, P-1] \qquad (5.2)$$

- Two cases (multiple-passes and single-pass PHEs) are considered for the temperature continuity of the processing fluid:

  Multiple-pass PHEs:

$$T_{f,j}(out) = T_{f,j+n_j a}(in) \qquad \forall\, j \in [1, P] \qquad (5.3)$$

  Here, a is a positive integer, whose value depends on the number of pass and the number of total channels (P) within the PHE.

  Also, based on different configurations, $T_{f,j}(out)$ and $T_{f,j+n_j a}(in)$ are determined through the following equations:

  If $dir > 0$, i.e. fluid flows from the top ($x = 0$) of the channel to the bottom ($x = L$):

  $T_{f,j}(out) = T_{f,j}(L)$; $T_{f,j+n_j a}(in) = T_{f,j+n_j a}(L)$

  If $dir < 0$:

  $T_{f,j}(out) = T_{f,j}(0)$; $T_{f,j+n_j a}(in) = T_{f,j+n_j a}(0)$

  If fluid flows into the PHE from the left side (Figure 4.1):

  $n_j = +1$ and $T_{f,z}(in) = T_{f,in}$

  If fluid flows into the PHE from the right side (Figure 4.1):

  $n_j = -1$ and $T_{f,z}(in) = T_{f,in}$

  Here, $T_{f,in}$ is the inlet fluid temperature and z is the channel number that fluid flows into the PHE. These values are set based on the experimental conditions.

  Single-pass PHEs:

$$T_{f,z}(in) = T_{f,in} \qquad \forall\, z \in [1, P] \qquad (5.4)$$

  Here, if $dir > 0$, $T_{f,z}(in) = T_{f,j}(0)$; otherwise, $T_{f,z}(in) = T_{f,j}(L)$.

- Adiabatic conditions are assumed for both end plates of the PHE (Figure 4.1 and Figure 4.4). Therefore, following two boundary conditions were imposed to the system:

$$q^{L}_{w,1}(x, y^{L}_{w}) = 0 \;\;\&\;\; q^{R}_{w,P}(x, y^{R}_{w}) = 0 \qquad (5.5) - (5.6)$$

Fouling model

Two cases (multiple-pass and single-pass PHEs) are considered for the concentration of different β-Lg protein species (Native, unfolded and aggregated):

Multiple-pass PHEs:

$$C_{protein,j}(out) = C_{protein,j+n_j a}(in) \qquad \forall\, j \in [1, P] \qquad (5.7)$$

$$C^{i}_{protein,j}(out) = C^{i}_{protein,j+n_j a}(in) \qquad \forall\, j \in [1,P],\ \forall\, i \in \{L,R\} \qquad (5.8)$$

Like the temperature continuity, a is a positive integer, whose value depends on the number of pass and the number of total channels (P) within the PHE.

Based on the configurations used, these inlet and outlet protein concentrations within the bulk and thermal boundary layer can be found using the following equations:

When $dir > 0$:

$C_{protein,j}(out) = C_{protein,j}(L)$; $C^{i}_{protein,j}(out) = C^{i}_{protein,j}(L)$

$C_{protein,j+n_j a}(in) = C_{protein,j+n_j a}(L)$; $C^{i}_{protein,j+n_j a}(in) = C^{i}_{protein,j+n_j a}(L)$

When $dir < 0$:

$C_{protein,j}(out) = C_{protein,j}(0)$; $C^{i}_{protein,j}(out) = C^{i}_{protein,j}(0)$

$C_{protein,j+n_j a}(in) = C_{protein,j+n_j a}(0)$; $C^{i}_{protein,j+n_j a}(in) = C^{i}_{protein,j+n_j a}(0)$

If fluid flows into the PHE from the left side (Figure 4.1):

$n_j = +1$; $C_{protein,z}(in) = C_{protein,in}$; $C^{i}_{protein,z}(in) = C^{i}_{protein,in}$

If fluid flows into the PHE from the right side (Figure 4.1):

$n_j = -1$; $C_{protein,z}(in) = C_{protein,in}$; $C^{i}_{protein,z}(in) = C^{i}_{protein,in}$

Here, $C_{protein,in}$ and $C^{i}_{protein,in}$ is the concentration of each protein species in the inlet flow (bulk flow and thermal boundary layer) and z is the channel number that fluid flows into the PHE.

Single-pass PHEs:

$$C_{protein,z}(in) = C_{protein,in} \qquad \forall\, z \in [1,P] \qquad (5.9)$$

$$C^{i}_{protein,z}(in) = C^{i}_{protein,in} \qquad \forall\, z \in [1,P],\ \forall\, i \in \{L,R\} \qquad (5.10)$$

When $dir > 0$:

$C_{protein,z}(in) = C_{protein,j}(0)$ and $C^{i}_{protein,z}(in) = C^{i}_{protein,j}(0)$

When $dir < 0$:

$C_{protein,z}(in) = C_{protein,j}(L)$ and $C^{i}_{protein,z}(in) = C^{i}_{protein,j}(L)$;

5.2 Model comparison

The main differences between the current and previous models are summarized in Table 5.1. For the current model, the fluid physical properties are assumed to be constant and calculated based on the average temperature in the combined PHE section using the updated

correlations from literature (section 4.2.3). While for the previous model, the correlations are integrated in the model and fluid physical properties are updated when the fluid temperature changes. By doing so, the fluid dynamics within the PHE are better represented. One the other hand, using constant physical properties reduces the model complexity and therefore scales down the size of the problem. This can effectively shorten the simulation time. However, if there is no prior information about the simulation, it is hard to select a proper average temperature for the calculation of constant physical properties. As a result, for small size problems, using correlations is recommended; while for large size problems, using constant values could be a better option.

Table 5.1. Comparisons between the current and previous model for the PHE.

Changes	**Current model**	**Previous model**[18]
Fluid physical properties	Constant	Vary with temperature
Channel gap	Vary with the deposit thickness	Constant
Fluid representation	Clearly identified in both thermal and fouling models	Only updated in the main thermal model
Proportionality constant (β)	Re-estimated based on the current model	Value estimated from the previous model

The calculation for the channel gap (e_x) is another change from the previous model. Previously, same value as the channel gap under clean condition is used in the calculation. In the current model, the deposit thickness is considered when calculate the channel gap at different locations within the PHE (Equation (4.11) & (4.17)). In this way, the flow conditions could be better described and thus enhance the model performance.

Additionally, different from the previous model, for which two fluids within the PHE are only distinguished in the main thermal model, the current one clearly identifies the two fluids in both thermal and fouling models. Therefore, it provides a more reasonable virtual representation of the actual setting and reduces the confusions for model users.

Based on all the changes, the proportionality constant (β) used in the fouling model for the prediction of deposition thickness also needs to be re-estimated. Analysis for the model performance comparison between the current and previous models are discussed in the later section in this chapter.

5.3 Thermal model validation

To validate the thermal model of the combined PHE, two different PHE configurations were simulated and the temperature profiles from the simulated results were compared with the values presented in the literature. Since milk fouling is not considered during thermal model validation, the rate of deposition is set to zero when perform the simulations.

5.3.1 Simulation description

Two PHE configurations (Figure 5.2 and Figure 5.3) have been studied extensively in previous work[12,18,24,56]. In the figures, colour blue and red are used to indicate cold and hot fluid streams respectively. Both configurations consist of twelve channels constructed from thirteen plates. The cold fluid (pre-heated milk) enters the PHE from the left side and the hot fluid (heating medium) enters the PHE from the right side. For both configurations, heating medium is configured as single inlet and six passes. As for the cold milk, it is configured as six inlets and single pass for configuration 1 and as one inlet and six passes for configuration 2. For both configurations, the same PHE plates are used, whose specifications are shown in Table 5.2. The operating conditions (inlet fluid temperature, volumetric flowrate and protein concentration) used for configuration 1 and 2 are presented in Table 5.3.

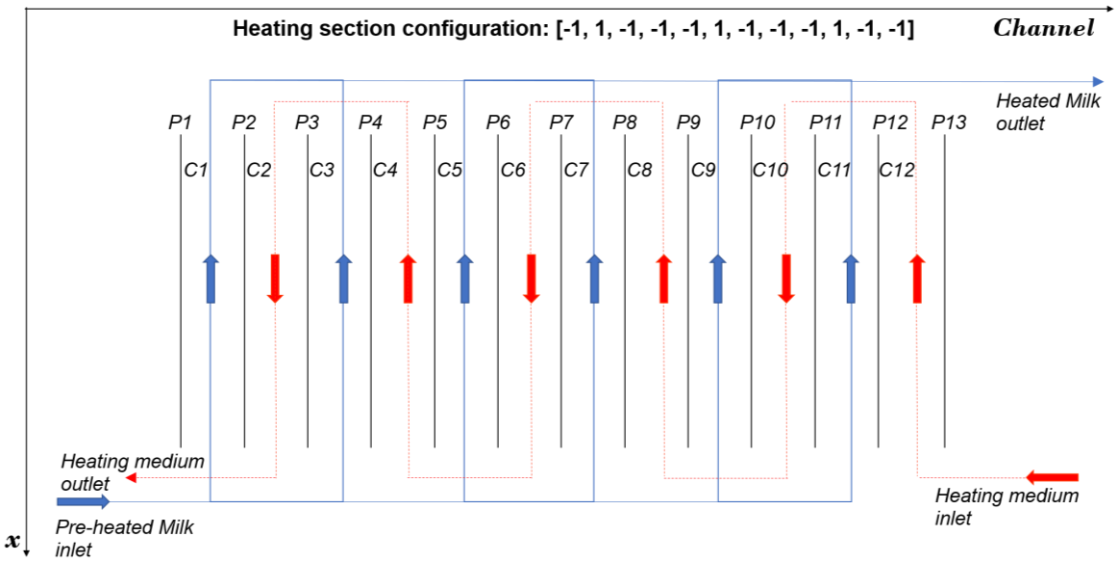

Figure 5.2. Schematic diagram of PHE configuration 1 (Pi: Plate i; Ci: Channel i).

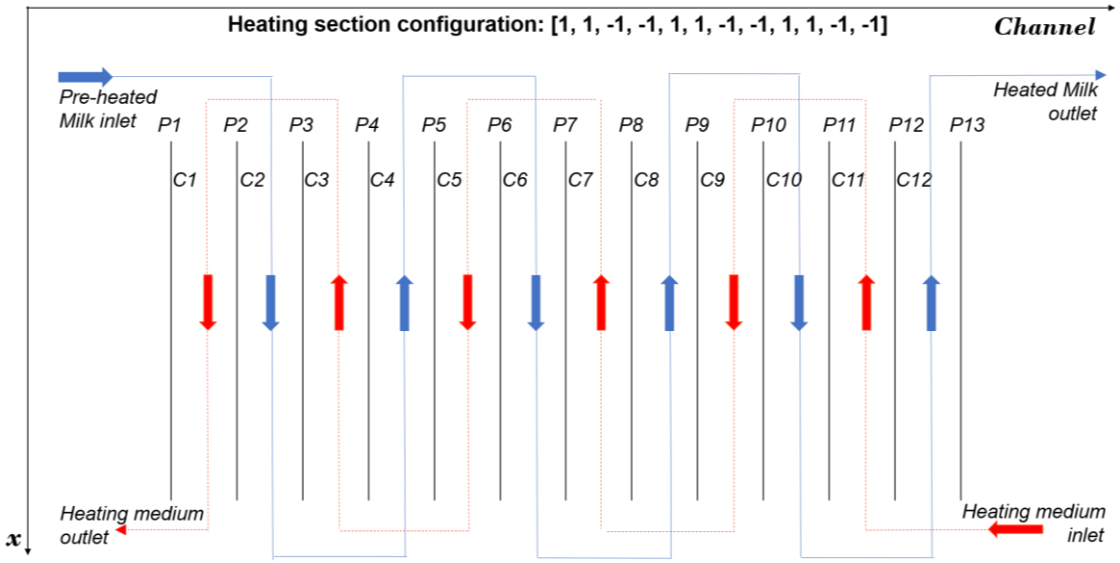

Figure 5.3. Schematic diagram of PHE configuration 2(Pi: Plate i; Ci: Channel i).

Table 5.2. Plate dimensions used in configuration 1 and 2[12,27].

Dimension	Value
Plate length - L (m)	0.75
Plate width - W (m)	0.25
Plate thickness - PT (mm)	0.745
Channel gap - e_j (mm)	4.0

Table 5.3. Fluid operation conditions used in configuration 1 and 2[12,27].

Processing Fluid	Config.	Inlet Temp (℃)	Inlet volumetric Flowrate (m^3/s)	Inlet protein concentration (kg/m^3)
Inlet Milk	1	60.0	1.388E-05	5.0 (Native protein only)
	2	60.0	0.833E-04	5.0 (Native protein only)
Heating Water	1	110.0	0.92E-04	0.0
	2	97.0	2.4E-04	0.0

Table 5.4. Physical properties of the fluid.

Physical properties	Configuration 1		Configuration 2	
	Milk ($T_{avg} = 70$℃)	Water ($T_{avg} = 85$℃)	Milk ($T_{avg} = 90$℃)	Water ($T_{avg} = 94$℃)
C_p (J/kg.K)	4023	4199	4023	4207
ρ (kg/m^3)	1011	969	998	963
λ (W/m.K)	0.677	0.672	0.720	0.677
μ (Pa.S)	6.00E-04	3.33E-04	4.71E-04	3.02E-04

5.3.2 Initial conditions

For both configurations, the experimental test starts from steady state. Therefore, following initial conditions were used in the simulations:

Thermal model:

$$\frac{\partial T_j}{\partial t} = 0 \qquad \forall\, j \in \{j |\, if\ dir > 0\},\ \forall\, x \in (0, L] \tag{5.11}$$

$$\frac{\partial T_j}{\partial t} = 0 \qquad \forall\, j \in \{j |\, if\ dir < 0\},\ \forall\, x \in [0, L) \tag{5.12}$$

$$\frac{\partial T_{w,j}^{L}}{\partial t} = 0 \qquad \forall\, j \in [1, P],\ \forall\, x \in [0, L],\ \forall\, y \in (-t_w, -t_l) \tag{5.13}$$

$$\frac{\partial T_{w,j}^{R}}{\partial t} = 0 \qquad \forall\, j \in [1, P],\ \forall\, x \in [0, L],\ \forall\, y \in (t_l, t_w) \tag{5.14}$$

$$\frac{\partial T_{l,j}^{i}}{\partial t} = 0 \qquad \forall\, j \in [1, P],\ \forall\, x \in [0, L],\ \forall\, \tilde{y} \in (0,1),\ \forall\, i \in \{L, R\} \tag{5.15}$$

It is noted that the initial condition equations vary with the boundary conditions used for the variables since the boundary conditions have been specified through continuity equations discussed previously (Section 5.1).

Fouling model:

For thermal model validation, the PHE starts under clean condition, i.e., the deposit mass and thickness were set to zero. Also, no fouling type was selected and therefore the concentration of proteins, the deposit mass and the deposit thickness are assumed to be constant throughout the simulation. Following conditions are used for initial protein concentrations. As noted in Table 5.3, only native protein was present in the milk inlet flow and no protein was present in the water flow.

$$C_{protein,j} = C_{protein,j}(0) \qquad \forall\, j \in \{j|\, if\ dir > 0\},\ \forall\, x\ \in (0, L] \tag{5.16}$$

$$C^{i}_{protein,j} = C^{i}_{protein,j}(0) \qquad \forall\, j \in \{j|\, if\ dir > 0\},\ \forall\, x\ \in (0, L],\ \forall\, i \in \{L, R\} \tag{5.17}$$

$$C_{protein,j} = C_{protein,j}(L) \qquad \forall\, j \in \{j|\, if\ dir < 0\},\ \forall\, x\ \in [0, L) \tag{5.18}$$

$$C^{i}_{protein,j} = C^{i}_{protein,j}(L) \qquad \forall\, j \in \{j|\, if\ dir < 0\},\ \forall\, x\ \in [0, L),\ \forall\, i \in \{L, R\} \tag{5.19}$$

Like the thermal model, the initial condition equations depend on the boundary conditions specified. Here, the value of $C_{protein,j}(0)$ and $C^{i}_{protein,j}(L)$ are determined through boundary conditions discussed in the continuity equation part (Section 5.1).

5.3.3 Solution method

The overall section model for the combined PHE (Figure 5.1) was implemented and solved in gPROMS ModelBuilder (version 5.1.1)[57]. The embedded PHE channel model in the overall section model (Chapter 0) is a partial differential algebraic equation (PDAE) system. It includes a set of algebraic, differential and partial differential equations. The partial differential equations (PDEs) are reduced to algebraic equations through discretization in the x- and y-axises. The performance of the reduced system depends on the discretization method and the size of discretization step selected (discretization grid). In the case of thermal model validation, based on the boundary conditions, different discretization methods were used for different domains. For instance, the differential variables along x-axis in all three domains (Figure 4.2) were discretized according to the flow direction (dir). When dir was positive, i.e., the fluid flows from top of the channel to the bottom, a second order backward finite difference method (BFDM) was used. When dir was negative, a second order forward finite difference method (FFDM) was used. Also, to obtain a good profile of the differential variables along x-axis, the domain is evenly divided into 20 segments. The differential variables in the wall domain (Ω_w^L & Ω_w^R) along y-axis (Figure 4.2) were discretized along the positive direction of the y-axis. For differential variables along y-axis in the deposit layer domain (Ω_l^L & Ω_l^R) (Figure 4.2), the direction of the dimensionless y coordinate ($\tilde{y}_l$) was used for discretization. For all the differential variables along y-axis, a second order central finite difference method (CFDM)

was used with 10 evenly spaced differential elements. Additionally, to solve the simulation, the index of the system needs to be reduced to 1, which can be performed automatically by gPROMS. After discretization, the system was solved using standard DAE solvers in gPROMS.

5.3.4 Results and discussion

Temperature profiles of milk in different channels were obtained from the simulated results. As shown in Figure 5.4, for configuration 1, the milk was heated from the inlet temperature (60℃) to various outlet temperatures depend on the channel it was located. Since the heating medium (hot water) entered the combined PHE from the right-hand side, the milk in the channels close to the right side was heated to a higher temperature comparing to the ones near the left-hand side. For configuration 2, since it is a single-inlet and six-pass arrangement, the milk was continuously heated along different channels. The continuity of temperature was correctly represented by the model as shown in the figure.

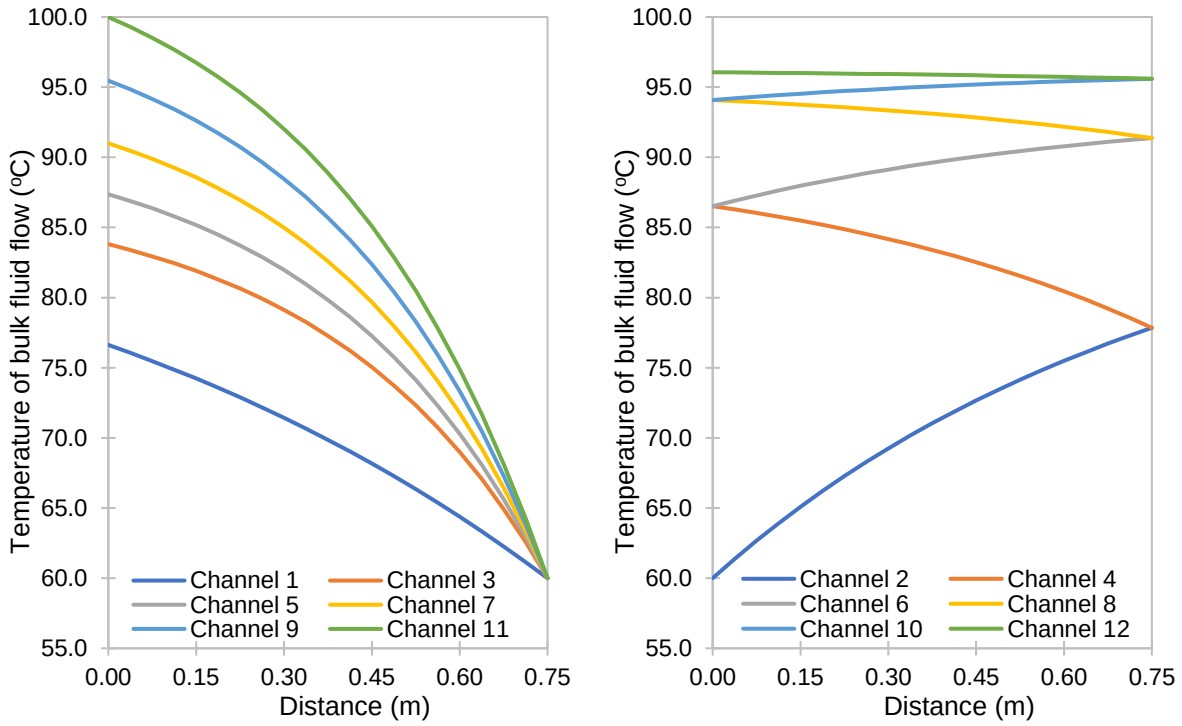

Figure 5.4. Temperature profile of milk (Left: configuration 1; Right: configuration 2).

To validate the simulation results, the outlet temperatures from different channels for both configurations were compared with the values in the literature[58–60]. For configuration 1, the simulated results from the current model are consistently higher than the experimental data and the differences are in the range of 0.2 to 4.5℃ (Table 5.5). The percent deviation of simulated results from the experimental value varies from 0.19% to 5.43%. This could be attributed to the overestimation of the effective heat transfer area in the model because the port opening area of plate was not excluded from the heat transfer area. Also, adiabatic

conditions were assumed for both end plates of the PHE, which could lead to underestimation of heat losses. Different from configuration1, for configuration 2, underestimation is noted for the outlet temperature (Table 5.6). However, for configuration 2, simulated results from Delplace et al[59] is used as reference value since experimental data is not available in literature. In this case, the deviations between the current model values and the simulated reference values are in the range of 0.6 to 4.9℃. Like the simulated results for configuration1 in the current model, Delplace et al[58] and Rene et al[60] also reported that the numerical predictions from their model were always higher than the measured ones and the deviations could be up to 3℃. Therefore, taking this into consideration, the results from current model for configuration 2 agrees with the reference value in a reasonable range.

Table 5.5. Channel outlet temperature comparison for configuration 1.

Channel	**1**	**3**	**5**	**7**	**9**	**11**
Simulated results – as[18] (℃)	76.9	85.8	88.9	92.1	95.9	99.8
Simulated results – mz (℃)	76.6	83.8	87.4	91.0	95.5	100.0
Experimental data (℃)[58]	73.7	79.5	82.9	87.7	93.5	99.8
% Deviation (as & Exp.)	4.41	7.90	7.26	5.06	2.61	-0.05
% Deviation (mz & Exp.)	3.97	5.43	5.38	3.76	2.10	0.19

Table 5.6. Channel outlet temperature comparison for configuration 2.

Channel	**2**	**4**	**6**	**8**	**10**	**12**
Simulated results – as[18] (℃)	75.6	84.8	90.3	93.4	95.2	95.8
Simulated results – mz (℃)	77.8	86.5	91.4	94.1	95.6	96.1
Simulated results - reference (℃)[59,60]	82.7	90.7	94.4	96.0	96.6	96.7
% Deviation (as & Exp.)	-8.63	-6.53	-4.38	-2.68	-1.42	-0.95
% Deviation (mz & Exp.)	-5.87	-4.62	-3.21	-2.00	-1.04	-0.66

For both configurations, the current model has better agreements with the values reported in the literature comparing to the previous model[18] (Table 5.5 & Table 5.6), which indicates that the modifications of the model (Table 5.1) lead to some improvements of the PHE section model.

In conclusion, the numerical results of the selected two configurations (single-pass and multiple-pass) demonstrate that the thermal model is capable capturing the main features of different configurations with reasonable experimental agreements.

5.4 Fouling model validation

Parameter estimation in used to determine the optimal value of the proportionality constant, β, in the two PHE configurations. Dep_A (fouling due to aggregated protein only) fouling mechanism was selected for the preliminary estimation, since it is the most common one used in the literature. The results of the parameter estimation are assessed through two aspects: (1) parameter statistical significance; (2) model adequacy. For parameter statistical significance, the 95% confidence interval was analysed; and for model adequacy, a chi-squared test was used. The results of parameter estimation are reported in Table 5.7. The predicted and experimental values of the deposition mass for both configurations are also shown in Table 5.8 and Table 5.9.

Table 5.7. Estimation of proportionality constant (β) (fouling due to aggregated protein).

Configuration	β	95% confidence interval	chi-squared value	
			Calculated	Critical
1	2.78	[2.50, 3.06]	6.41	11.1
2	24.1	[23.5, 24.7]	3788	21.0

Table 5.8. Deposition mass for configuration 1 (fouling due to aggregated protein).

Channel #	Experimental Value[15,58] (g)	Predicted Value (g)	Deviation (g)
1	0.0	0.08	0.08
3	1.5	1.46	-0.04
5	4.0	3.45	-0.55
7	7.0	6.22	-0.78
9	8.5	9.32	0.82
11	12.0	11.94	-0.06

Table 5.9. Deposition mass for configuration 2 (fouling due to aggregated protein).

Plate #	Experimental Value[15,59] (g)	Predicted Value (g)	Deviation (g)
2	6.0	0.0	-6.00
3	7.5	0.0	-7.50
4	12.3	0.4	-11.9
5	14.0	0.6	-13.4
6	18.8	5.5	-13.3
7	20.0	7.1	-12.9
8	20.0	13.5	-6.50
9	19.5	15.5	-4.01
10	18.5	17.5	-1.02
11	17.0	19.2	2.21
12	13.0	19.5	6.47
13	11.8	21.0	9.21

The newly estimated β values for configuration 1 and 2 are 2.78 and 24.1, respectively. The 95% confidence intervals of β for both configurations are narrow (Table 5.7), which indicate a high confidence of the estimated values being close to the true values. For configuration 1, the calculated chi-squared value is lower than the critical value, suggesting a good fit between the experimental and simulated results, which is also confirmed from the small deviations between experimental and predicted values (Table 5.8). As for configuration 2, the calculated

chi-squared value is significantly higher than the critical value and large differences between the predicted and experimental values are observed (Table 5.9), which implies that the current model is not accurate enough to describe the experimental data. It is noted that for experimental data, the deposition mass on the plate firstly increased and then deceased as the location of the plate gets closer to the right side of the PHE (higher temperature); while for predicted values, the deposition mass always increased. This mismatch could due to the fouling mechanism selected. Thus, another reaction scheme (Dep_U, i.e., fouling due to unfolded protein) was implemented. The newly estimated value for β is shown in Table 5.10 and the predicted values for the deposition mass are presented in Table 5.11. Using Dep_U reaction scheme, the trend of deposition mass on different plates is now correct and the deviations from the experimental values narrowed. However, the chi-squared test still failed. This suggests that instead of assuming only one type of protein is deposited onto the surface at a time, the reaction scheme for β-Lg protein might be a combination of both Dep_A and Dep_U. A new deposition model is required to test this hypothesis, which is beyond the scope of this project. Nevertheless, this is a positive direction to explore for fouling model improvements.

Table 5.10. Estimation of proportionality constant (β) (fouling due to unfolded protein).

Configuration	β	95% confidence interval	chi-squared value	
			Calculated	Critical
2	15.1	[14.8, 15.4]	556	21.0

Table 5.11. Deposition mass for configuration 2 (fouling due to unfolded protein).

Plate #	Experimental Value (g)	Predicted Value (g)	Deviation (g)
2	6.0	1.3	4.7
3	7.5	2.0	5.5
4	12.3	12.6	-0.3
5	14.0	15.5	-1.5
6	18.8	23.3	-4.5
7	20.0	24.2	-4.2
8	20.0	18.5	1.5
9	19.5	18.6	0.9
10	18.5	13.6	4.9
11	17.0	13.8	3.2
12	13.0	10.5	2.5
13	11.8	10.0	1.8

Overall, through both parameter confidence and model adequacy analysis, current model can accurately describe the fouling phenomena within PHE for configuration1 using the Dep_A mechanism; while for configuration 2, sufficient data is available for precise estimation of the parameter, but the model is not accurate enough to fit the experimental behaviour. Thus, for configuration 2, it is suggested to use a combined β-Lg reaction scheme for future improvements.

6 Model for a tube

This chapter covers the dynamic and distributed model of a tube undergoing milk fouling. The holding tube is an important section in the unit, which is used to hold the heated milk for at least the specified time above certain temperature. For HTST process and skimmed milk, the requirement is to hold milk for at least 15 seconds at or above 72 ℃ according to FDA regulations[10]. And for UHT process, it is required to hold milk for 2 to 5 seconds within the temperature range of 135 to 140℃ [10]. In this chapter, a non-isothermal tube is modelled using the moving boundary model developed previously[3,4]. The governing equations and major assumptions used for the thermal and fouling models are discussed along with their boundary conditions.

6.1 Overall thermal model description

The distributed moving boundary model of the tube is adapted from Coletti[3], Diaz-Bejarano and Macchietto[4] to account for milk deposition within the tube. A schematic diagram is shown in Figure 6.1. Major assumptions for the overall thermal model of the tube are listed below[61]:

- Radial symmetry is assumed for the tube with $r = 0$ defined at the center of the tube.
- Radial heat transfer of the bulk fluid is ignored.
- No heat or mass transfer in the axial direction for both wall and deposit regions.
- The milk deposit is assumed to be a solid material, which could attach or detach from the wall surface but cannot flow or displaced by the bulk fluid.

The governing equations and specific assumptions used for the heat transfer across different regions of the tube (wall, layer and flow) are discuss in the following paragraphs.

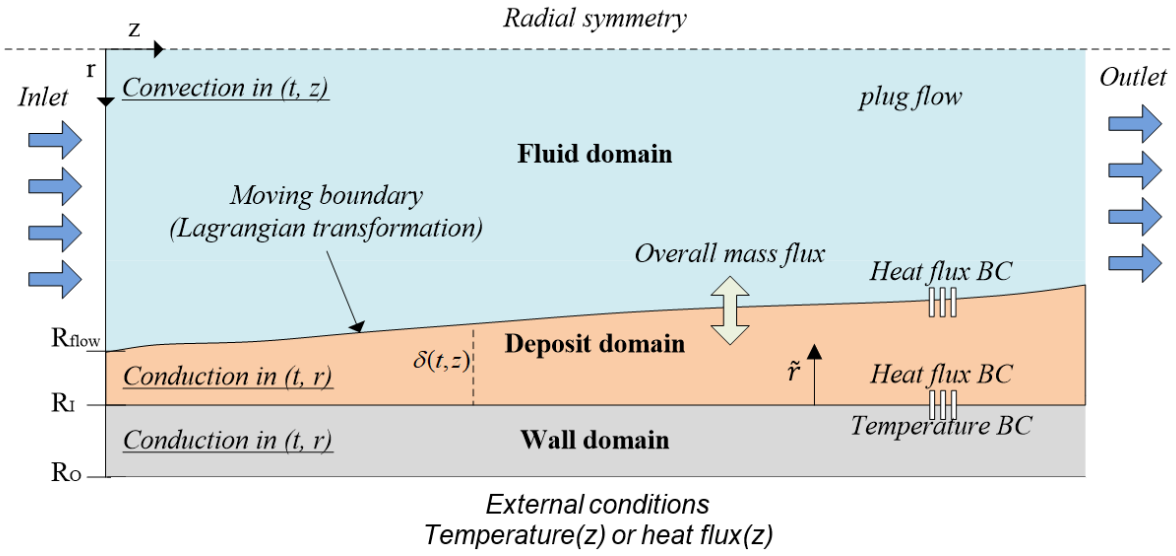

Figure 6.1. Cross-sectional diagram of the moving boundary model for a tube with Lagrangian transformation. BC stands for boundary condition[61].

6.1.1 Wall region

For the tube wall domain, similar heat transfer equations as the one used for the PHE channels are used with cylindrical coordinate:

$$\rho_{w,TB}\, C_{p,w_{TB}} \frac{\partial T_{w,TB}}{\partial t} = -\frac{1}{r}\frac{\partial\left(r q_{w,TB}\right)}{\partial r} \tag{6.1}$$

And the heat flux ($q_{w,TB}$) through the tube wall is calculated from Fourier's law:

$$q_{w,TB} = -\lambda_{w,TB}\frac{\partial T_{w,TB}}{\partial r} \tag{6.2}$$

Here, r is the radial coordinate of the wall position. In this model, the physical properties of the wall ($\rho_{w,TB}$, $C_{p,w_{TB}}$ and $\lambda_{w,TB}$) are assumed to be constant across the tube.

6.1.2 Milk deposit layer region

For the deposit layer region, the modified heat transfer and heat flux equations after Lagrangian transformation[3,24,61] is shown below:

$$\rho_{l,TB}\, C_{p,l_{TB}}\left(\frac{\partial T_{l,TB}}{\partial t} - \frac{\tilde{r}}{\delta}\frac{\partial \delta}{\partial t}\frac{\partial T_{l,TB}}{\partial t}\right) = -\frac{1}{(R_I - \tilde{r}\delta_{TB})\delta_{TB}}\frac{\partial\left((R_I - \tilde{r}\delta_{TB})\, q_{l,TB}\right)}{\partial \tilde{r}} \tag{6.3}$$

$$q_{l,TB} = \frac{\lambda_{l,TB}}{\delta_{TB}}\frac{\partial T_l}{\partial \tilde{r}} \tag{6.4}$$

Here, δ_{TB} is the deposit thickness in the tube, and $q_{l,TB}$ is the heat flux through the deposit layer. Also, $\tilde{r}$ is the dimensionless radial coordinate of the deposit position, which is defined as $\tilde{r} = \frac{R_I - r}{\delta_{TB}}$. It equals to 0 at wall-layer interface and equals to 1 at layer-fluid interface. Like the wall region, the physical properties of the deposit layer ($\rho_{l,TB}$, $C_{p,l_{TB}}$ and $\lambda_{l,TB}$) are assumed to be constant.

6.1.3 Flow region

For the flow region, constant mass flow rate is assumed through the tube. Heat transfer equation is obtained based on the shell balance:

$$\frac{\partial\left(A_{flow,TB}\rho_{f,TB}\, H_{f,TB}\right)}{\partial t} = -dir\, \frac{\partial\left(A_{flow,TB} v_{f,TB}\, \rho_{f,TB}\, H_{f,TB}\right)}{\partial z} - \frac{\partial\left(q^Z_{f,TB}\, A_{flow,TB}\right)}{\partial z} + q^r_{f,TB}(\pi\, R_{flow}) \tag{6.5}$$

Where, $q^Z_{f,TB}$ and $q^r_{f,TB}$ are axial conductive and radial convective heat flux, respectively, which can be calculated by the following equations:

$$q_{f,TB}^{z} = -\lambda_{f,TB} \frac{\partial T_{f,TB}}{\partial z} \tag{6.6}$$

$$q_{f,TB}^{r} = h_{f,TB}(T_{l,TB}|_{\tilde{r}=1} - T_{f,TB}) \tag{6.7}$$

Here, dir is used to indicate the direction of the flow along z-axis, which equals to +1 for fluid flows from left to right and equals to -1 if it flows from right to left (Figure 6.1). R_{flow} is the r-coordinate of the layer-fluid interface, which will vary with deposit thickness as time goes:

$$R_{flow} = R_I - \delta_{TB} \tag{6.8}$$

And $v_{f,TB}$ is the magnitude of the velocity for the processing fluid, which can be calculated as:

$$v_{f,TB} = \frac{Q_{f,TB,in}}{A_{flow,TB}} \tag{6.9}$$

Here, the cross-sectional area of the tube changes at different axial locations since R_{flow} varies along the axial direction:

$$A_{flow,TB} = \pi R_{flow}^2 \tag{6.10}$$

The convective heat transfer coefficient ($h_{f,TB}$) can be approximated using different equations depend on the flow regime. In this model, the flow in the tube is assumed to be fully developed. For internal convection in horizontal tubes, if the flow is in laminar regime, local Nusselt number (Nu) remains constant. For constant surface temperature boundary conditions, Nu = 3.66; and for constant surface heat flux, Nu = 4.36. From the Nu number, $h_{f,TB}$ can be found by the following equation:

$$Nu(z) = \frac{h_{f,TB}(z) D_{h,TB}(z)}{\lambda_{f,TB}(z)} \tag{6.11}$$

Where $D_{h,TB}$ is the hydraulic/equivalent diameter, which is approximated as the actual diameter of the fluid region to account for the deposit layer thickness:

$$D_{h,TB}(z) = 2R_{flow}(z) \tag{6.12}$$

If the flow is in the turbulent flow regime ($Re > 10000$), Nu can be approximated by the empirical correlations based on dimensionless numbers, for instance, the Dittus-Boelter equation:

$$Nu(z) = 0.023\, Re(z)^{0.8}\, Pr(z)^{0.4} \tag{6.13}$$

Where Re, Pr and Nu are calculated from the following equations:

$$Re(z) = \frac{D_{h,TB}(z)\rho_{f,TB}(z)v_{f,TB}(z)}{\mu_{f,TB}(z)} \tag{6.14}$$

$$Pr(z) = \frac{C_{pf_{TB}}(z)\mu_{f,TB}(z)}{\lambda_{f,TB}(z)} \tag{6.15}$$

$$Nu(z) = \frac{h_{f,TB}(z) D_{h,TB}(z)}{\lambda_{f,TB}(z)} \tag{6.16}$$

Based on preliminary simulation results, under experimental conditions interested[7], the flow is mainly found in the laminar flow regime.

Temperature drop across the tube length is relatively small since the tube in the pasteurizer unit is designed to transfer the fluid or hold it at certain temperature for a specified time period. Therefore, the constant physical properties assumption for the processing fluid ($\rho_{f,TB}$, $C_{pf_{TB}}$, $\lambda_{w,TB}$ and $\mu_{f,TB}$) used for the PHE channel section should still hold for the tube section.

6.1.4 Boundary conditions

Boundary conditions need to be specified to ensure thermal continuity at both wall-layer and layer-flow interfaces.

- For the wall-layer interface, equal temperature and equal heat flux conditions need to be satisfied (Figure 6.1).

$$T_{w,TB}(z, R_I) = T_{l,TB}(z, 0) \tag{6.17}$$

$$q_{w,TB}(z, R_I) = q_{l,TB}(z, 0) \tag{6.18}$$

- For the layer-flow interface, conductive heat flux from layer to flow has same magnitude as convective heat flux from flow to layer. Here negative sign is used since the increasing direction of dimensionless $\tilde{r}$-coordinate is defined from the wall-layer interface ($\tilde{r} = 0$) to layer-fluid interface ($\tilde{r} = 1$), which is opposite to the main dimensional r-coordinate (Figure 6.1).

$$q_{l,TB}(z, 1) = -q^r_{f,TB}(z) \tag{6.19}$$

Also, for the wall domain, either outer surface temperature of the tube wall or the outer heat flux through the tube wall need to be specified.

- For isothermal condition, the outer surface temperature is assumed to be uniform and equals to the constant temperature of the surrounding environment.

$$T_{w,TB}\,(z, R_o) = T_{surrounding} \tag{6.20}$$

- For constant heat flux condition, the outer heat flux is assumed to be same as the specified external heat flux.

$$q_{w,TB}\,(z, R_o) = q_{external} \tag{6.21}$$

As noted previously, large heat transfer between surrounding and the tube is undesired as the holding temperature (often much greater than the surrounding temperature) needs to remain high enough to eliminate bacteria in the milk. As a result, constant heat flux condition is used in this model.

6.2 model and material balance

Only a few models developed for pasteurization process considers holding tube (Table 2.2). Among these models, none of them considers fouling within the tubes as a relatively large diameter to length ratio are often used for holding tube and therefore it was often assumed that no significant fouling takes place due to large shear stress. Also, no experimental data regarding fouling in the tube has been reported in literature. However, to generalize the model and expand its applications, fouling model is still integrated with the main thermal model to set up the framework. In this way, when more experimental data is available, the model could easily be adapted to reflect the fouling mechanism within the tubes, especially for the comparison between the deposition and re-entrainment rates. This information could be useful for cleaning scheduling and product safety monitoring.

Here, the same kinetic and deposition model as the ones used for the PHE channels are adopted (Section 4.3.1 and 4.3.2)., For the tubes, only one side needs to be modelled since radial symmetry is assumed.

The mass flow rate of the processing fluid is assumed to be constant throughout the tube. With this assumption, material balance for different protein species within the fluid as well as the thermal boundary layer were derived with cylindrical coordinates and presented in Appendix E.

6.3 External heat flux determination

Previously, models developed for the holding tube in the pasteurization process either assumed an isothermal condition or a constant temperature drop based on the experimental data[7,47,48]. In this model, non-isothermal condition was used and an average external heat flux ($q_{external}$) for the process was determined using experimental data to account for the convective heat transfer of air around the holding tube/ tubular connections.

The experimental data is taken from Aguiar and Gut[48] and the experimental apparatus in the reference is same as the one depicted in Figure 1.1. For parameter estimation, the segments of the apparatus from T_3 to T_6 (TCH, holding tube (HT) and TCR) was modelled. Following continuity equations were used to connect the tubes:

$$T_4 = T_{f,TCH}(tube\ length) \tag{6.22}$$

$$T_{f,HT}(0) = T_4 \tag{6.23}$$

$$T_5 = T_{f,HT}(tube\ length) \tag{6.24}$$

$$T_{f,TCR}(0) = T_5 \tag{6.25}$$

$$T_6 = T_{f,TCR}(tube\ length) \tag{6.26}$$

Here, T_f is the fluid temperature within the tubes (TCH/HT/TCR).

Fouling is not included in this case. As noted by Aguiar and Gut[48], an average of 2℃ temperature drop was observed from T_3 to T_6. Therefore, T_6 was used as the objective function. Parameter estimation was then implemented in gPROMS. The average $q_{external}$ is found to be 467 W/m^2. Key temperatures in the process is shown in Table 6.1. Based on the estimated value of $q_{external}$, accurate temperature predictions were obtained.

Table 6.1. Experimental and predicted temperatures for tube parameter estimation.

	Temp (ºC)		
	Experimental[48]	**Predicted (reference model)**[48]	**Predicted (current model)**
$\boldsymbol{T_3}$	73.1 $\pm$ 0.5	73.4	73.1
$\boldsymbol{T_4}$	72.8 $\pm$ 0.4	73.4	72.8
$\boldsymbol{T_5}$	72.3 $\pm$ 0.3	71.4	72.0
$\boldsymbol{T_6}$	71.3 $\pm$ 0.1	71.4	71.3

Note: for the reference model[48], isothermal conditions were assumed for tubular connections and a constant temperature drop (2℃) was used for holding tube.

In conclusion, comparing to other models in the literature, using an average $q_{external}$ for tubes in the pasteurization process is a better way to describe heat transfer between the tube and the surroundings. This estimated value can be used for future simulations to enhance model performance.

7 Model for a full milk pasteurizer unit

This chapter focus on the dynamic and distributed model of a complete milk pasteurizer unit (Figure 1.1) subject to milk fouling. First, the general description of the model is discussed. Then, the thermal model is validated against experimental data in the literature. Following that, a start-up test is conducted to assess the model adequacy for dynamic changes. Lastly, fouling test is simulated to check fouling severity for the HTST process.

7.1 Model description

The pasteurizer unit consists of three PHEs (heating, regeneration and cooling), a non-isothermal holding tube, and two non-isothermal tubular connections. As illustrated in Figure 3.1, the section models of PHEs and tubes (Chapter 5 and 6) are connected in the main pasteurizer unit model. The overall unit model defines initial conditions (temperature of the fluid/wall/deposit layer, fluid flowrate), equipment specifications and equipment configurations for each PHE and tube section model. Then the overall model passes on this information to all PHEs and tubes. Between sequential section models (PHE/tube), fluid mass flowrate, fluid temperature and different β-lg protein concentrations within the fluid are linked via proper continuity equations.

The general PHE section model discussed in Chapter 5 is used for all three PHE sections in the pasteurizer unit. The β-Lg protein fouling normally occurs when the temperature is higher than 70℃ (Table 4.1), therefore fouling is considered in the milk channels for the heating section. The temperature range within the regeneration section depends on the heat treatment implemented (e.g. HTST, UHT). To increase the generality of the model, fouling is included in the analysis for both raw and regenerated milk channels. On the other hand, as the temperature is relatively low (normally below 35℃) in the cooling section, the effects of fouling are excluded from analysis.

For both holding tube and tubular connections, the section model discussed in Chapter 6 is adopted. Milk deposition is considered for all three tubes because the inlet fluid of the tubes exits from the heating section (Figure 1.1).

7.2 Model connection

In order to use the PHE and tube section models discussed previously, the inlet fluid temperatures and inlet β-Lg protein concentrations need to be specified. Previously, for each individual section model, these values were set based on the simulation/experimental conditions. In this case, the inlet and outlet fluid conditions between sequential models need to be matched because the models are connected. This is achieved via proper continuity equations.

Thermal & Fouling model – temperature & protein concentration continuity

Here a set, X_{in}, is used to represent the continuity equations, where $X_{in} = \{T_{f,in}, C_{protein,in}\}$. $T_{f,in}$ and $C_{protein,in}$ are the inlet temperature and inlet protein concentrations (native, unfolded and aggregated) for each section model, respectively. X_i is also used to denote fluid conditions at different locations in the pasteurizer unit (Figure 1.1), where $X_i = \{T_i, C_i | \forall i \in [1,8]\}$.

Continuity between regeneration and heating sections (cold fluid)

For regeneration section, the $X_{milk_{raw},in}$ for the raw milk equals to the condition of the unprocessed milk:

$$X_{milk_{raw},in} = X_1 \quad (7.1)$$

And the milk outlet condition in the regeneration section equals to the inlet milk condition in the heating section:

$$X_{milk_{heat},in} = X_2 \quad (7.2)$$

To determine the milk outlet condition in the regeneration section (location 2 in Figure 1.1), a logic variable $IsHot$ is introduced, which equals to $+1$ if the fluid in channel j is hot (to be cooled/heating medium); otherwise, it equals to -1 (to be heated/cooling medium). For the simulation, the PHE frame is set as following: the cold fluid enters the PHE from the left side; while the hot fluid enters the PHE from the right side (Figure 1.1). The experimental/simulation configurations differ from the pre-defined PHE frame can always be transferred into the desired configurations via rotation or minor image. In the regeneration section, because X_2 is the outlet condition of the cold fluid (raw milk), it can be determined using following equations:

If $IsHot < 0$ for the last channel (Channel P), i.e., the last channel is milk channel, then

$$X_2 = X_{f,P}(0) \quad \text{If } dir < 0 \quad (7.3)$$

$$X_2 = X_{f,P}(L) \quad \text{If } dir > 0 \quad (7.4)$$

If $IsHot > 0$ for Channel P, i.e., the second last channel is milk channel, then

$$X_2 = X_{f,P-1}(0) \quad \text{If } dir < 0 \quad (7.5)$$

$$X_2 = X_{f,P-1}(L) \quad \text{If } dir > 0 \quad (7.6)$$

Here, $X_{f,j}$ and dir are the condition (temperature or protein concentration) and the direction of the fluid in channel j, respectively.

Continuity between heating section and TCH

The inlet fluid condition of the connecting tube with heating section (TCH) (Figure 1.1) equals to the outlet fluid condition of the heating section (X_3). X_3 can be identified using same method as the one used for X_2 in equation (7.7) to (7.8) because, in the heating section, X_3 is also the outlet condition of the cold fluid (milk).

Continuity between TCH and holding tube (HT)

$$X_4 = X_{f,TCH}(tube\ length) \tag{7.9}$$

$$X_{f,HT}(0) = X_4 \tag{7.10}$$

Here, X_f is the fluid condition within the tubes (TCH/HT).

Continuity between HT and TCR

$$X_5 = X_{f,HT}(tube\ length) \tag{7.11}$$

$$X_{f,TCR}(0) = X_5 \tag{7.12}$$

Here, TCR stands for the tubular connection with regeneration section (Figure 1.1).

Continuity between TCR and regeneration section (hot fluid)

$$X_{f,TCR}(tube\ length) = X_6 \tag{7.13}$$

$$X_{milk_{reg},in} = X_6 \tag{7.14}$$

Here $X_{milk_{reg},in}$ is the inlet hot fluid condition in the regeneration section.

Continuity between regeneration and cooling section (hot fluid)

The hot fluid outlet condition in the regeneration section equals to the inlet milk condition in the cooling section.

$$X_{milk_{cool},in} = X_7 \tag{7.15}$$

Different determination method other than the one used for X_2 needs to be applied since X_7 is the outlet condition of the hot fluid.

If $IsHot > 0$ for Channel 1, i.e., the first channel is regenerated milk channel, then

$$X_7 = X_{f,1}(0) \quad \text{If } dir < 0 \tag{7.16}$$

$$X_7 = X_{f,1}(L) \quad \text{If } dir > 0 \tag{7.17}$$

If $IsHot < 0$ for Channel 1, i.e., the second channel is regenerated milk channel, then

$$X_2 = X_{f,2}(0) \quad \text{If } dir < 0 \tag{7.18}$$

$$X_2 = X_{f,2}(L) \quad \text{If } dir > 0 \tag{7.19}$$

For the cooling section, the outlet condition of the final pasteurized product (X_8) can also be identified using equation (7.20) to (7.21).

7.3 Steady-state thermal model validation

To validate the thermal model of the whole pasteurizer unit, a steady state experimental case for HTST process was simulated and the temperature profiles from the simulate results were compared with the ones presented in the literature[7,62]. Fouling was not considered in this simulation.

7.3.1 Simulation description

The experimental apparatus is depicted in Figure 1.1. The configurations of the PHEs used are shown in Figure B.4 to Figure B.6 (Appendix B). The heating, regeneration and cooling sections consists 12, 20 and 8 PHE channels, respectively. For all three sections, single-inlet-multiple-pass configurations were used. The dimensions of PHEs and tubes used in the apparatus is shown in Table 7.1 and Table 7.2. It is noted that the length of outer diameters (ODs) for the tubes are not available in the literature. Therefore, it was assumed to be 2 mm longer than the inner diameter (ID). The fluid operating conditions are presented in Table 7.3. In this simulation, water instead of milk was used as the working fluid[7,62]. As discussed previously, physical properties of the fluid are assumed to be constant within each section model and their values are calculated based on the average temperature within that section. The values used in this simulation as well as the temperature used for the calculation are displayed in Table 7.4 and Table 7.5. For the tubes, the estimated $q_{external}$ value (467 W/m^2) from section 6.3 was used to better describe the heat transfer.

Table 7.1. Plate dimensions of PHEs (Armfield F-43 plate)[62]

Dimension	Value
Plate length - L (mm)	90
Plate width - W (mm)	60
Plate thickness - PT (mm)	1.0
Channel gap - e_j (mm)	1.5

Table 7.2. Dimensions of the tubes (HTST)[7]

	Length (m)	Inner diameter (ID) (mm)	Outer diameter (OD) (mm)
Holding Tube	0.99	10.7	12.7
TCH	0.42	9.5	11.5
TCR	1.06	8.0	10.0

Note: OD information is not available in paper. In the simulation, it is assumed that OD = ID + 2mm

Table 7.3. Fluid operation conditions (HTST)[7,62].

Processing Fluid	Inlet Temp (℃)	Inlet volumetric Flowrate (L/h)	Inlet protein concentration (kg/m^3)
Cold Water	19.4	20	0.0
Heating Water	76.3	60	0.0
Cooling Water	10.1	60	0.0

Table 7.4. Physical properties of working fluid (water) in different sections of pasteurizer unit (HTST).

	Cooling ($T_{avg} = 15$℃)	Heating ($T_{avg} = 70$℃)	Regeneration		Tube ($T_{avg} = 72$℃)
			($T_{avg} = 50$℃)	($T_{avg} = 35$℃)	
C_p (J/kg.K)	4023	4023	4023	4023	4199
ρ (kg/m^3)	1036	1011	1021	1028	969
λ (W/m.K)	0.560	0.677	0.635	0.603	0.672
μ (Pa.S)	2.05E-03	6.00E-04	8.52E-04	1.19E-03	3.33E-04

Table 7.5. Physical properties of heating/cooling water in different sections of pasteurizer unit (HTST).

Physical properties	Cooling ($T_{avg} = 7$℃)	Heating ($T_{avg} = 85$℃)
C_p (J/kg.K)	4185	4199
ρ (kg/m^3)	1002	969
λ (W/m.K)	0.583	0.672
μ (Pa.S)	1.33E-03	3.33E-04

7.3.2 Solution method

As discussed in section 5.3.3, discretization is used to transfer the PDAE system into the DAE system. For the PHEs, same discretization methods were implemented (section 5.3.3). For the tubes, the first order BFDM discretization method was selected for the axial domain (z) with 10 evenly spaced discretization elements. For the radial domain (r), a second order CFDM was used with 20 evenly spaced elements. As for the transformed radial domain ($\tilde{r}$), a second order CFDM was applied with 20 elements and an exponential distribution of the points were used to help with the accuracy of the integration.

7.3.3 Results and discussion

Steady state initial conditions were used, and the simulation was solved using a standard DAE solver in gPROMS. The key temperatures for model validation are presented in Figure 7.1. From the simulation results, it is noted that the continuity of temperature between and within different sections was correctly represented by the model. Also, good agreements between the experimental data and simulated values were observed. This indicates that, for steady state operation, the thermal model of the whole pasteurizer unit can describe the actual experimental conditions well.

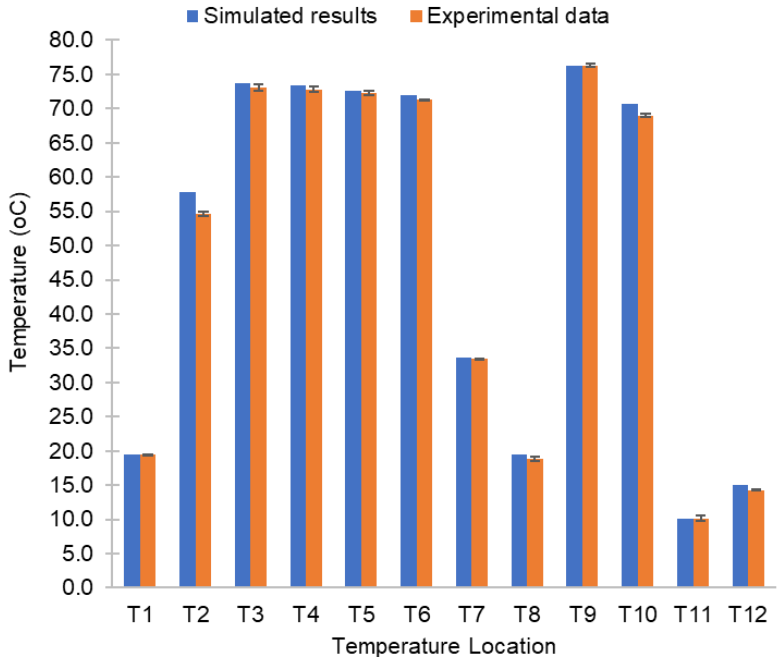

Figure 7.1. Key temperatures for model validation (Exp. Data taken from Aguiar&Gut[48])

7.4 Start-up test and validation

7.4.1 Simulation description

To assess the model performance under dynamic conditions, a start-up test was implemented. Like the steady-state test, water was used as the processing fluid and fouling was not considered. The experimental settings and the fluid properties were same as the ones in the steady-state test. However, different initial conditions were used in this case. The whole pasteurizer unit was first fed with water at ambient temperature (20℃) at a volumetric flowrate of 20 L/h. Once the steady state of ambient condition was achieved in the experiment (after about 95 seconds), the hot- and cold- water circuits were connected to the equipment, whose volumetric flowrate was all adjected to 60 L/h. Also, for the hot water, the temperature was changed to 90℃. No information about the inlet cold water temperature was given by Gutierrez, Diniz and Gut[7] in the paper; thus, the value used in another paper from the same group[48] was applied in this simulation. As for the working fluid (water), it still enters the equipment at the same volumetric flowrate (20 L/h) and temperature (20℃). The simulation was then continued for another 655 seconds.

7.4.2 Results and discussion

Same solution methods as the one used for steady-state simulation was implemented. Temperatures at different locations of the pasteurizer unit (Figure 1.1) were plotted, whose values were then compared with both experimental and simulated results in the literature[7]. As shown in Figure 7.2, similar trends for the dynamic behaviour during start-up were captured in the simulated results. However, in the transition region (regions between two steady states), the experimental value responded slower comparing to the simulated results. It can be attributed to the fact that the thermal inertia was not considered in the models[7]. The average absolute error of the temperature predictions during steady-state and dynamic situations were quantified and reported in Table 7.6.

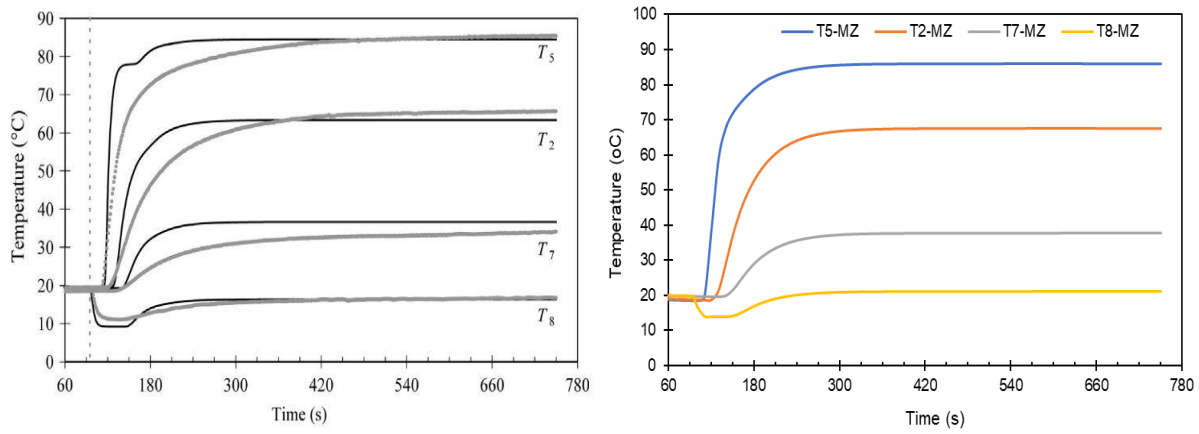

Figure 7.2.Temperature profile at different locations in the pasteurizer unit (Left: reference - grey dots: experimental data; solid black line: simulated results-GCC[7]; Right: MZ).

Table 7.6. Error analysis for temperature prediction during steady-state and dynamic conditions.

Temperature	Steady state average absolute error (℃)		Dynamic average absolute error (℃)	
	MZ	GCC[7]	MZ	GCC[7]
T_2	2.16	1.55	4.70	3.03
T_5	1.03	0.04	4.39	5.53
T_7	3.91	3.01	4.49	4.77
T_8	4.14	0.11	4.28	0.60

Note: steady state is defined for $60 \leq t < 95$s and $440 \leq t \leq 750$s; dynamic is defined for $95 \leq t \leq 440$s.

From Table 7.6, it is observed that, for both simulated results, errors during steady state are always lower than the errors involved in dynamic conditions. It is because that, for dynamic conditions, the effects of the simplified assumptions (e.g. negligible thermal inertia, negligible heat loss to the surroundings) became more significant. Overall, the model developed by Gutierrez et al[7] agrees with experimental value better during steady state conditions while during dynamic conditions, current model has comparable performance as the reference model. For the temperature profile of T_5, less oscillation is observed in results from current model during transitions. As for the temperature profile of T_7, similar trend is observed among the experimental and simulated values, but both simulated results (GCC[7] & MZ) overestimate the final steady state value. This might due to the use of constant physical properties in both models. For the heating fluid, large temperature drop across the PHE channels was observed in the regeneration section, therefore it might be better to use correlations for physical properties. For T_8, it is noted that the predicted value from current model has relatively large deviations from experimental data. It can be attributed to the inlet cold water temperature assumed (value from another paper).

Above all, during start-up process, current model can capture the main trend of temperature evolution at different locations. And the deviations from experimental values were within an acceptable range.

7.5 Fouling model test

A fouling model test for the whole unit was conducted to check the fouling severity during the HTST pasteurization process. Same experimental apparatus as the steady-state test was used while the working fluid was switched from water to milk to account for fouling effects. Based on the fouling test in section 5.4, the Dep_U (fouling due to unfolded protein) fouling mechanism was selected for the simulation because all three PHEs used were configured as single inlet and multiple passes (Figure B.4 to Figure B.6 in the Appendix B). The fluid operation conditions and the physical properties of milk used are presented in Table 7.7 and Table 7.8, respectively. The model was solved using the same solution method as the steady-state simulation case.

Table 7.7. Fluid operation conditions (HTST)[7,62].

Processing Fluid	Inlet Temp (℃)	Inlet volumetric Flowrate (L/h)	Inlet protein concentration (kg/m^3)
Cold Milk	19.4	20	5.0 (Native protein only)
Heating Water	76.3	60	0.0
Cooling Water	10.1	60	0.0

Table 7.8. Physical properties of milk in different sections of pasteurizer unit (HTST).

	Cooling ($\boldsymbol{T_{avg} = 15}$℃)	**Heating** ($\boldsymbol{T_{avg} = 70}$℃)	**Regeneration**		**Tube** ($\boldsymbol{T_{avg} = 72}$℃)
			($\boldsymbol{T_{avg} = 50}$℃)	($\boldsymbol{T_{avg} = 35}$℃)	
C_p (J/kg.K)	4023	4023	4023	4023	4199
ρ (kg/m^3)	1036	1011	1021	1028	969
λ (W/m.K)	0.560	0.677	0.635	0.603	0.672
μ (Pa.S)	2.05E-03	6.00E-04	8.52E-04	1.19E-03	3.33E-04

From the simulated results, it is found that deposition mass for the HTST process was not significant (less than 1.0g in each PHE channel) for the first 2.1 days. The temperature of milk was above 70℃ (the temperature threshold for fouling to occur) in the following locations: channel 9 and 11 in heating section, tubes (both holding tube and tubular connections) and channel 20 in regeneration section. The fluid temperature in majority of the pasteurizer unit was under the threshold that would trigger the fouling reactions. This led to negligible deposition mass for a long period. Also, the effect of fouling on the heat transfer is not significant. From the simulated result, T_5, the outlet temperature from the holding tube, only dropped by 0.03 ℃ after 2.1 days. As a result, to reduce the fouling effects, HTST pasteurization process is always recommended for milk treatment if extended shelf-life, i.e., the elimination of thermal resistant bacteria (e.g. B. licheniformis and B. subtilis), is not required for the milk product.

8 Model applications: cleaning scheduling

As discussed previously, fouling could reduce the heat transfer efficiency of the PHEs. Thus, periodic cleanings are required to restore the performance of the pasteurization unit and safeguard the process operation. The complete pasteurizer unit model developed (Chapter 7) is used to identify the cleaning strategies and schedules. To achieve this purpose, a proper CIP model needs to be integrated with the existing model. For this project, the two-stage CIP model developed by Bird and Fryer[40] are used. In this chapter, firstly, the CIP model used is introduced. Then the integration method of the CIP model is discussed. Lastly, two heating-CIP tests conducted are analysed.

8.1 CIP model description

The two-stage empirical CIP model developed by Bird and Fryer[40] is based on alkali cleaning using 1wt% NaOH solution. As noted in Figure 3.2, the CIP model needs initial deposit thickness and cleaning fluid temperature as inputs. In this model, the deposit is considered to have two forms (removable and non-removable). Initially, all the deposit is assumed to be in the non-removable form. In the first stage, the non-removable form is transferred to a removable form. Then, it is removed in the second stage by shear. Following model equations[18,40] are used for the rate of change of the deposit thickness initially:

$$\frac{\partial(\delta_{nr})}{\partial t} = -k_{nr} \tag{8.1}$$

$$\frac{\partial(\delta_{r})}{\partial t} = k_{nr} - k_r\delta_r \tag{8.2}$$

Here, δ is the deposit thickness and the subscripts r and nr are used to denote the removable and non-removable form of the deposit, respectively. The total deposit thickness (δ_T) is the sum of δ_{nr} and δ_r. The kinetic constants for the deposit removal rates are expressed by k_{nr} and k_r for two forms respectively, whose value can be estimated from the Arrhenius equations[37,40].

$$k_r = 1.0E\text{-}4\exp(0.0680\,T_f) \tag{8.3}$$

$$k_{nr} = 3.0E\text{-}8\exp(0.0497\,T_f) \tag{8.4}$$

Here, T_f is the temperature of the cleaning fluid.

Once all the non-removable deposit form has converted to the removable form, the equations for the rate of change of deposit thickness switches to:

$$\frac{\partial(\delta_{nr})}{\partial t} = 0 \tag{8.5}$$

$$\frac{\partial(\delta_{r})}{\partial t} = -k_r\delta_r \tag{8.6}$$

And the time for the switch is defined as t_s, whose value is calculated as $\frac{\delta_0}{k_{nr}}$. Here δ_0 is the initial deposit thickness.

Since only the removable form of the deposit is cleaned out through shear. The rate of cleaning (R_c) (removal of the deposit thickness) at any time is defined as

$$R_c = k_r \delta_r \tag{8.7}$$

The cleaning operation would end when the stopping condition is met. Based on different regulations or safety requirements, different stopping criteria could be used. For instance, maximum final deposition mass within the system after cleaning is a common criterion implemented.

It is also noted that this model is only suitable for fluid with Reynolds number (Re) less than 3000. Therefore, Re value is calculated[37,40] in the model to check if the model is valid. Here, the Reynolds number is estimated based on an empirical correlation[37,40]:

$$Re = 742.79 \exp\left(0.0173\, T_f\right) \tag{8.8}$$

8.2 CIP model integration

To integrate the CIP model with the existing model, different operation modes (heating, cleaning and rinsing) were defined. In the heating mode, the raw milk will be processed, and deposit will form on the equipment surface. In the current model, critical deposition mass density is used as the criteria for operation switch. When the $m_{critical} < m_{total\ deposit}$, rinsing mode will be triggered. In the rinsing mode, water is used to pass through the system for a fixed duration. For numerical reasons, rinsing water with same temperature and flowrate flows through all sections in the pasteurizer unit and therefore no heat transfer occurs during rinsing. Also, it is assumed that rinsing has no effect on the deposit. When rinsing is done, it will switch to the cleaning mode, where CIP model developed will be used. When the CIP operation stops, another rinsing cycle is performed to neutralize the remaining cleaning solution and pre-treat the equipment surface so that it is safe to be used for milk treatment. The fouling-cleaning cycles could be implemented continuously using this model.

It is noted that the model developed previously[18] integrated the CIP model by updating the deposit thickness and rate of removal to the main thermal model; while the temperature and other properties of the cleaning fluid are only defined in the CIP model. Therefore, the fluid within the main thermal model as well as the embedded fouling model is not updated. In the current model, fluid properties will be switched from the working fluid (milk in this case) to cleaning solution in the thermal model and this information will be passed on to the CIP as well as fouling model (Figure 3.2). In this way, the fluid within the whole system would also be updated.

8.3 Heating-CIP model test

Two cases were studied for the heating-CIP cycles: one for the heating section only, and the other for the complete pasteurizer unit. For the heating section, the configuration 2 from section 5.2 (Figure 5.3) was used with same experimental settings. As for the full pasteurizer unit, a realistic case for UHT was simulated[10]. The simulation descriptions and their corresponding results are discussed in the following sections.

8.3.1 Heating-CIP cycle of the heating section

The configuration 2 (Figure 5.3) was used for heating-CIP cycle study of the heating section. Same experimental settings were applied. And the simulation started from steady state and under clean condition for the equipment. As noted in section 5.4, Dep_U (fouling due to unfolded protein) is a better β-Lg reaction scheme for PHEs with single-inlet-multiple-pass configurations. Therefore, it was selected as the fouling type in the simulation. Two heating-CIP cycles were scheduled. In this case, the rinsing time was fixed to 3 minutes; the critical mass density[2,12] within the PHE was specified to be 16g/m^2, and the deposition mass on each plate was used as the stopping criteria for cleaning (m < 0.1g). An overview for the operation cycle is shown in Figure 8.1. The physical properties of water were utilized for the cleaning agent ($NaOH$ solution) and temperature for the cleaning and rinsing fluid was set to 50℃ (Table 8.1). The volumetric flowrate of the cleaning/rinsing fluid was assumed to be same as the flowrate of heating/cooling water (2.4E-4 m^3/s), whose mass flowrate was then calculated to be 0.237kg/s. This case was solved using the same solution method for the thermal model tests (section 7.3.2).

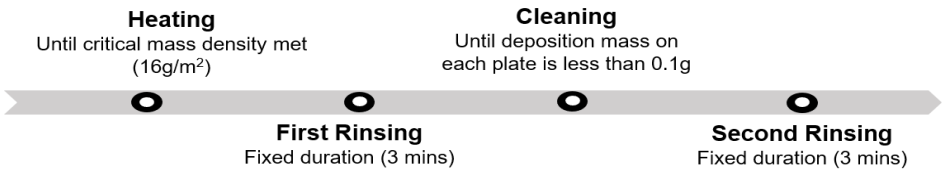

Figure 8.1.Heatin-CIP operation cycle.

Table 8.1. Physical properties of cleaning/rinsing water used

Physical properties	Cleaning ($T = 50$℃)
C_p (J/kg.K)	4179
ρ (kg/m^3)	988
λ (W/m.K)	0.642
μ (Pa.S)	5.49E-04

The predicted mass of the deposit during the heating-CIP cycles is depicted in Figure 8.2. For comparison, the simulated results from previous model developed by Sharma[18] is also shown in Figure 8.3. In the figures, the flat lines between heating and CIP operations were the rinsing

operations, during which the deposition mass remains unchanged. Similar to the trend of deposition mass for configuration 2 (section 5.4), the mass on the plates firstly increased and reached the peak at plate 7, and then decreased as the plate approaches to the right side of the PHE where the heating water entered. It is also observed that the predicted deposition mass was always higher in the current model than that of the previous model, and the CIP cycle was also longer comparing to the results from previous model[18]. This is attributed to the model differences presented in Table 5.1.

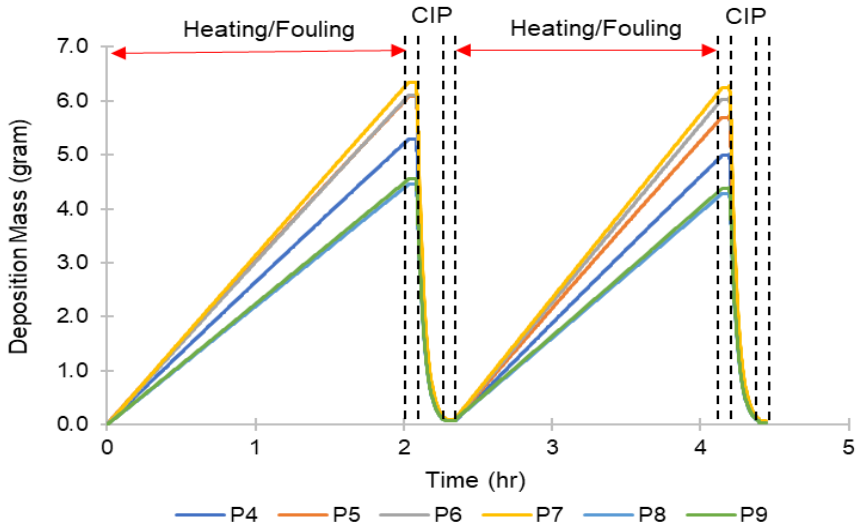

Figure 8.2. Deposition mass on different plates during heating-CIP cycles (configuration 2) estimated from current model (Pi: Plate i).

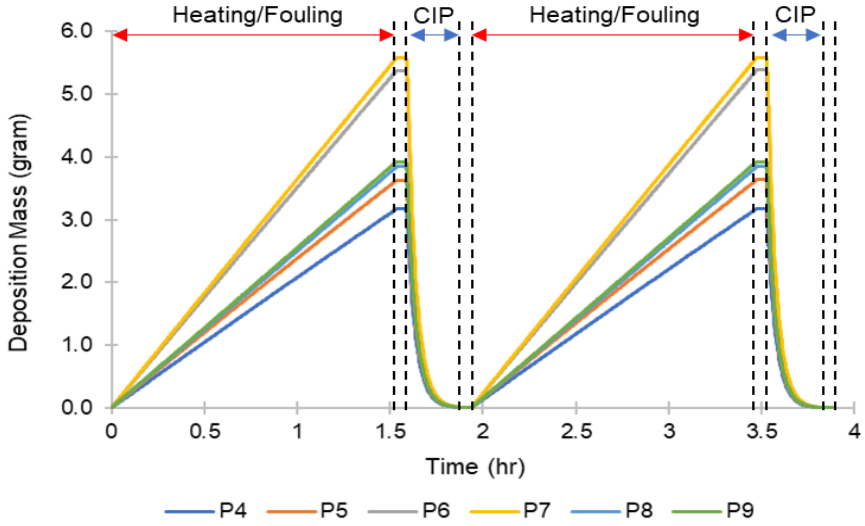

Figure 8.3. Deposition mass on different plates during heating-CIP cycles (configuration 2) estimated from previous[18] (Pi: Plate i).

The duration of the heating, cleaning and rinsing operations in heating-CIP cycles for the current and previous model are also shown in Table 8.2. It is noted that, for the previous model, the CIP cycle time for the first and second cycle was almost identical with a difference of 3.78

seconds; while for the current model, a deviation of 13.45 minutes was observed. Additionally, in the current model, the 2nd cycle had higher deposit mass comparing to the 1st cycle during a fixed period. These deviations between the current and previous model could due to the different CIP model integration method used. As noted in section 8.2, for the previous model, only values for deposit mass, deposit removal rate and deposit thickness were updated to the main model during cleaning/rinsing period. The temperature as well as other properties of the cleaning fluid was defined in the CIP model but not updated to the main thermal model and therefore also not passed on the embedded fouling model (Figure 3.2). Thus, during cleaning/rinsing period, the concentration of proteins in the embedded fouling model was still changing/reacting assuming milk was continuously passing through. As a result, when the 2rd cycle started, even though the initial deposit mass of cycle 2 was higher than cycle 1 (which started from clean state), the initial concentration of the proteins in cycle 2 was lower than that of cycle 1. In this case, the two effects cancelled each other, resulting in a similar deposit mass profile over time for the two cycles. On the other hand, for the current model, the information (temperature and other properties) of the cleaning fluid was passed on to the CIP model through the thermal model (Figure 3.2). Therefore, the processing fluid would switch from milk to cleaning agent or rinsing water during cleaning/rinsing period for all the models involved. When the new cycle started, fresh milk would enter the PHE. Due to the remaining deposit from last cycle, for a fixed period, the deposition mass in the new cycle would be higher than that of the old one and result in shorter cycle time, which is reasonable.

Table 8.2. Comparisons of duration of different operations within the heating-CIP cycles

Description	**Current model**		**Previous model**[18]	
	1st cycle	**2rd cycle**	**1st cycle**	**2rd cycle**
Total cycle time (hr)	2.34	2.11	1.94	1.94
Heating time (hr)	2.03	1.81	1.54	1.53
Cleaning time (hr)	0.202	0.202	0.304	0.304
Total rinsing time (min)	6	6	6	6

Moreover, even though the deposition mass predicted by current model was higher than the ones from previous model, the CIP duration was shorter in the current simulation. It is because, for the previous model, 0.01g instead of 0.1g was used as the stopping criterion for cleaning operation. Hence, longer cleaning time was required to further reduce the mass deposit on each plate of the PHE.

In this case, the effects of fouling are significant. For the outlet temperature of channel 12 (Figure 5.3), a drop of 8.3℃ was observed throughout the heating operation. Also, the amount of cleaning and rinsing fluid required in the cycles was estimated based on the mass flowrate as well as the cleaning and rinsing time (Table 8.3). From the values, it is noted that large amount of waste water was generated during cleaning and rinsing operations for the PHEs. Consequently, optimization of the cleaning operation is necessary.

Table 8.3. Information of cleaning and rinsing fluid used in the cycles - MZ

Description	1st cycle	2rd cycle
Mass flowrate (cleaning fluid) (kg/s)	0.237	0.237
Total amount required (kg)	172	172
Mass flowrate (rinsing fluid) (kg/s)	0.237	0.237
Total amount required (kg)	85.3	85.3

Above all, current model was used to simulate different heating-CIP cycles for the PHE heater. And with the modified CIP model integration method, the current model provides a better representation of the experimental conditions and demonstrated an improved performance over the previous model[18]. Additionally, from the simulated results, a need for the optimization of the cleaning operation was identified to minimize the generation of waste water during operations.

8.3.2 Complete pasteurizer unit

A heating-CIP cycle of the UHT process was simulated for the whole pasteurizer unit. It is noted that for the UHT process, no experimental data on a configuration or measured performance of the unit was available in literature, so a realistic case was used based on the requirements for the UHT process[6,10].

For the experimental apparatus, same plates used in section 5.2 was adopted (Table 5.2) for all three sections of PHEs. And the configurations of three PHE sections are shown in Figure B.7 to Figure B.9 (Appendix B). The heating, regeneration and cooling sections consists 12, 8 and 12 PHE channels, respectively. As for the tubes, the dimensions were calculated based on the holding time required[6,10] (Table 8.4). The fluid operating conditions (inlet temperature, volumetric flowrate and protein concentrations) are presented in Table 8.5. And the physical properties used for the fluids within different sections are shown in Table 8.6 and Table 8.7. The physical properties of milk and cooling water were calculated based on the average temperature within that section using equation (4.18) to (4.25). As for the heating water, since the average temperature (137℃) was high, the correlations used previously is not applicable. It is because that the correlations were formed based on the thermodynamic data of water at 1 atm; while water would be in gas state at the operation temperature (137℃) in this condition (1 atm). Therefore, the values were acquired from NIST[53] with pressure set to 10 atm to ensure water is in fluid state.

Table 8.4. Dimensions of the tubes for UHT process.

	Length (m)	Inner diameter (ID) (mm)	Outer diameter (OD) (mm)
Holding Tube	1.0	40.0	44.0
TCH	0.42	30.0	33.0
TCR	1.06	30.0	33.0

Note: OD is calculated based on ID, OD = ID + 2mm.

Table 8.5. Fluid operation conditions (UHT).

Processing Fluid	Inlet Temp (℃)	Inlet volumetric Flowrate (m^3/s)	Inlet protein concentration (kg/m^3)
Cold Milk	4.0	0.833E04	5.0 (Native protein only)
Heating Water	140	2.4E-4	0.0
Cooling Water	4.0	2.4E-4	0.0

Table 8.6. Physical properties of milk in different sections of pasteurizer unit (UHT).

	Cooling ($T_{avg} = 15$℃)	Heating ($T_{avg} = 120$℃)	Regeneration		Tube ($T_{avg} = 137$℃)
			($T_{avg} = 95$℃)	($T_{avg} = 40$℃)	
C_p (J/kg.K)	4023	4023	4023	4023	4023
ρ (kg/m^3)	1036	975	994	1026	961
λ (W/m.K)	0.560	0.784	0.730	0.613	0.820
μ (Pa.S)	2.05E-03	4.02E-04	4.51E-04	1.06E-03	4.09E-04

Table 8.7. Physical properties of heating/cooling water in different sections of pasteurizer unit (UHT).

Physical properties	Cooling ($T_{avg} = 7$℃)	Heating ($T_{avg} = 140$℃)	Cleaning ($T = 50$℃)
C_p (J/kg.K)	4185	4199	4179
ρ (kg/m^3)	1002	926	988
λ (W/m.K)	0.583	0.684	0.642
μ (Pa.S)	1.33E-03	1.97E-04	5.49E-04

As discussed in section 4.3, for UHT process, both protein and mineral fouling would occur at different temperature ranges, but for the scope of this project, only protein fouling was modelled. Consequently, underestimation of deposition mass is expected. Moreover, Dep_U fouling mechanism was used since single-inlet-multiple-pass configurations were applied for all three PHE sections. Also, the same proportionality constant (β) estimated in section 5.4 was used because no sufficient deposit information was available in literature for another parameter estimation.

Same critical mass density, cleaning mass threshold, rinsing time and cleaning fluid properties used for the PHE heater (section 8.3.1) were applied for the whole pasteurizer unit. As for the operation switch from heating to the first rinsing, a combined local stopping criterion is used, which means that the operation switch for the whole unit will occur when the critical mass density in one of the sections gets above the critical mass density. Here, two scenarios were considered: (1) account for deposition mass in the tubes for all operation switches; (2) only account for tube deposition mass for operation switch from cleaning to second rinsing.

8.3.2.1 Results and discussion

Both simulations started from steady state and under clean conditions, which were then solved with the same solution method used for steady-state thermal model simulations (section 7.3.2). The predicted deposition mass at different sections of the pasteurizer unit are depicted in Figure 8.4 to Figure 8.9 for both scenarios. The duration of the heating, cleaning and rinsing operations in heating-CIP cycle for both scenarios are also shown in Table 8.8.

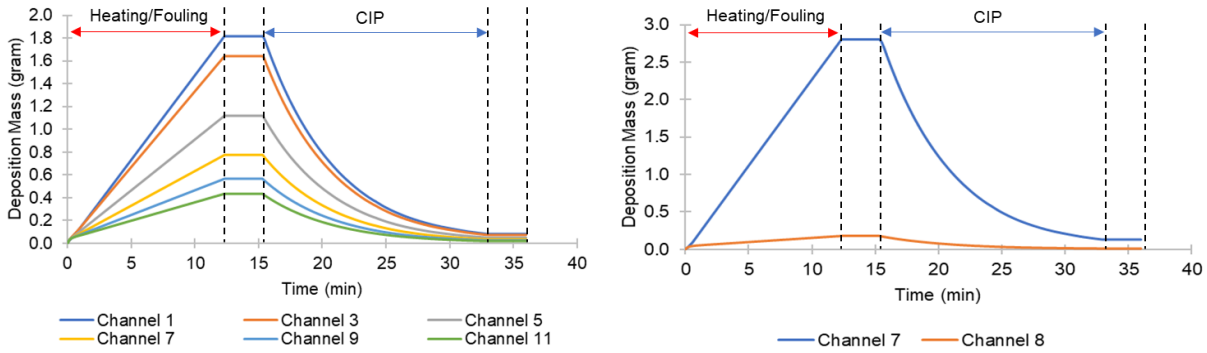

Figure 8.4. Deposition mass in different channels during heating-CIP cycle (UHT) for scenario 1 (Left: heating section; Right: regeneration section).

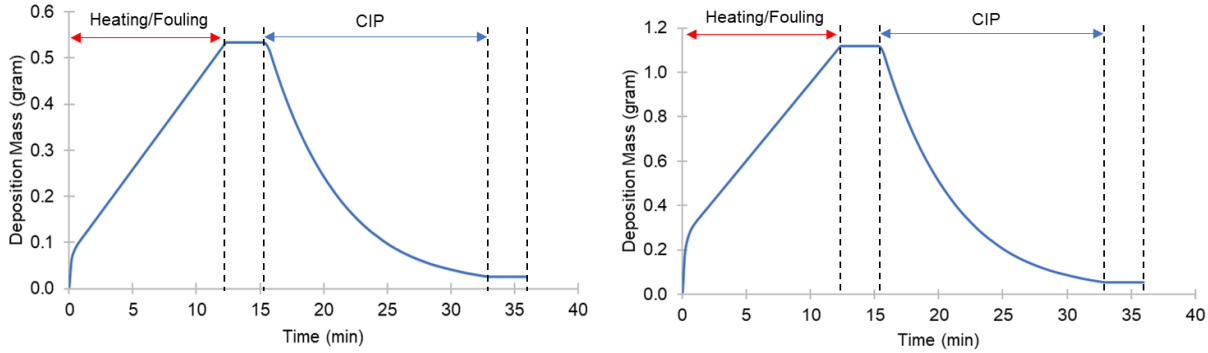

Figure 8.5. Deposition mass in tubular connections during heating-CIP cycle (UHT) for scenario 1 (Left: TCH; Right: TCR).

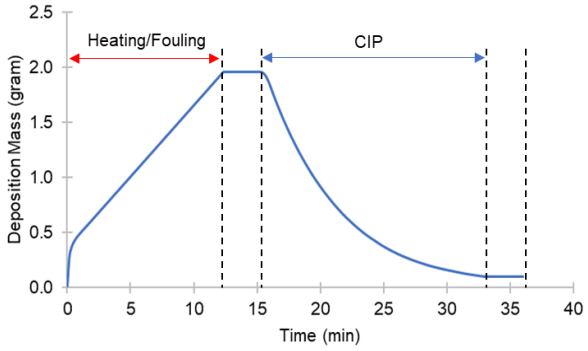

Figure 8.6. Deposition mass in holding tube during heating-CIP cycle (UHT) for scenario 1.

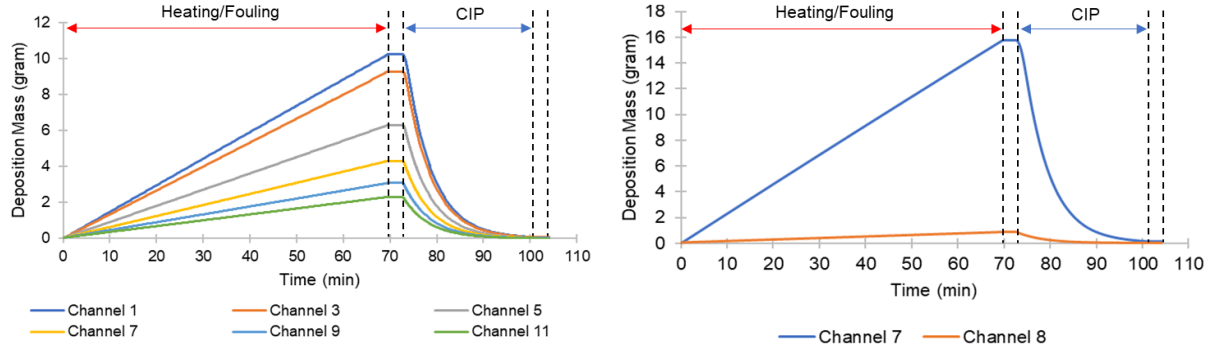

Figure 8.7. Deposition mass in different channels during heating-CIP cycle (UHT) for scenario 2 (Left: heating section; Right: regeneration section).

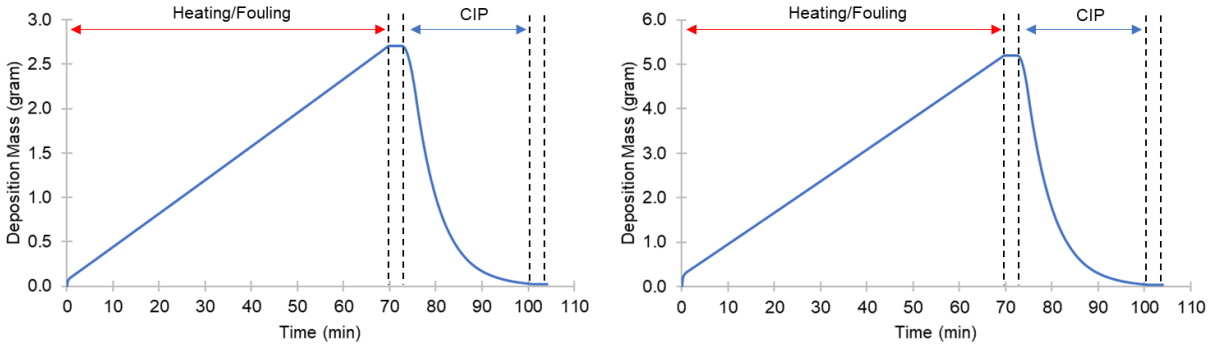

Figure 8.8. Deposition mass in tubular connections during heating-CIP cycle (UHT) for scenario 2 (Left: TCH; Right: TCR).

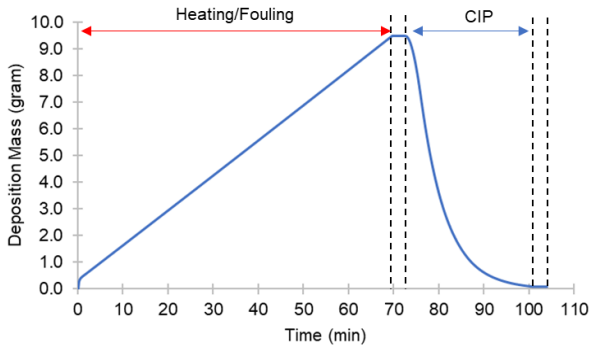

Figure 8.9. Deposition mass in holding tube during heating-CIP cycle (UHT) for scenario 2.

Table 8.8. Duration of different operations within the heating-CIP cycle for both scenarios (UHT).

Description	Scenario one	Scenario two
Total cycle time (min)	36.0	104.1
Heating time (min)	12.3	69.7
Cleaning time (min)	17.7	28.4
Total rinsing time (min)	6	6

From the simulated results, it is noted that, comparing to the HTST process (section 7.5), much more severe fouling was found in the main PHE heater and tubes for the UHT process. On the other hand, no significant deposit was observed in most of the regeneration PHE channels and all cooling PHE channels since the temperature was lower than the one that can trigger the fouling process (70℃). For numerical reasons, a small initial deposit thickness (1.0E-7 m) was applied to all tubes; while for PHEs, zero initial deposit thickness was used. This explains the initial jump of the deposition mass in the tubes (Figure 8.5, 8.7, 8.9 & 8.10). It is also noted that, for scenario one, the operation switch from heating to the first rising was triggered by the deposition mass in the holding tube; while for scenario two, it was triggered by the deposition mass in the heating section. Also, the operation cycle for scenario two was significantly longer than the cycle for scenario one (Table 8.8). This is due to the operation switch condition used. In the current model, same stopping criteria ($m_{section} > m_{critical}$) was applied to both PHEs and tubes for operation switch from heating to first rinsing; while as

noted in section 6, fouling effects could be less significant on tubes because of the relatively large diameter to length ratio. Therefore, using same stopping criteria for both PHEs and tubes can underestimate the cycle time that the process could actually reach. That's why when the tube deposition mass was not considered during operation switch for scenario two, its heating period increased significantly comparing to scenario one.

For both cases, short cycle time were determined from simulation results and the cleaning operation started before significant temperature drop in the process occurs. This shows that, when the overall interactions between different sections of the pasteurizer unit are accounted, fouling effects from one section would have limited impact on the overall processing temperature. This suggests that a more reasonable global stopping criteria other than the combined local criteria should be used for operation switch.

The amount of cleaning and rinsing fluid required in the cycle for two scenarios was shown in Table 8.9. Large amount of waste water was generated during operations so optimization of the operation is necessary. In the simulation, the full pasteurizer unit was cleaned at the same time when one of the sections reached the critical mass density. However, as noted previously, fouling in most of the regenerator and cooling channels were not severe and therefore cleaning was not necessary. A parallel set of equipment can be installed and instead of cleaning the whole unit together, smart switching between parallel PHEs/tubes can be used to clean one part of the unit at a time. If so, less cleaning agent and rinsing water would be required. Additionally, operational downtime due to cleaning could be reduced.

Table 8.9. Information of cleaning and rinsing fluid used in the cycles - MZ

Description	**Scenario one**	**Scenario two**
Mass flowrate (cleaning fluid) (kg/s)	0.237	0.237
Total amount required (kg)	252	404
Mass flowrate (rinsing fluid) (kg/s)	0.237	0.237
Total amount required (kg)	85.3	85.3

In conclusion, current model can be used to simulate heating-CIP cycles for the whole pasteurizer unit based on user-defined operation switching conditions. It can test different operating conditions as well as identify cleaning strategies and schedules. However, it is also noted that becasue no experimental data is currently available in literature, the simulation was run based on the proportionality constant value (β) estimated from another configuration. Additionally, only protein fouling was considered in the simulations. Thus, experimental validation is still needed to confirm the prediction of deposition mass. Moreover, for operation switches of the whole unit, instead of applying a combined local criterion based on deposition mass, it would be better to use a more reasonable one (e.g. pressure/temperature drop, effects on mass flowrate). Otherwise, cleaning would be performed too frequently based on the simulated results

9 Model applications: controller implementation

For different pasteurization processes, the milk needs to be heated to a certain temperature and hold at that temperature for a specified time period (Table C. 1). Also, for food safety and shelf-life requirements, the pasteurized product needs to be stored at certain temperature. As a result, a controller within the process could be useful to make sure the desired temperature is met. Controller models could be integrated with the pasteurizer unit model developed (Chapter 7). In this way, different operation conditions can be tested with disturbance and preliminary tuning of the controller can be done before implementing it on the actual setting, which could be a more effective and resource saving approach. Also, the model performance under dynamic conditions can be assessed through the tuning process.

In this chapter, firstly, the general description of the controller model is introduced. Then the methods used for controller parameter identification are discussed. Lastly, a case study for HTST process is conducted to test the performance of the controller, for which the results are analysed and discussed.

9.1 General description

For pasteurization process, T_5 and T_8 (Figure 9.1) are two main temperatures that need to be controlled. In this project, two standard parallel PI controllers were implemented (Figure 9.1). In the heating section, the controller is used to assure the required pasteurization temperature (T_5) is met. Additionally, it could help prevent overheating and therefore save energy. In the cooling section, the controller is used to ensure the required storage/end temperature is met and prevent subcooling.

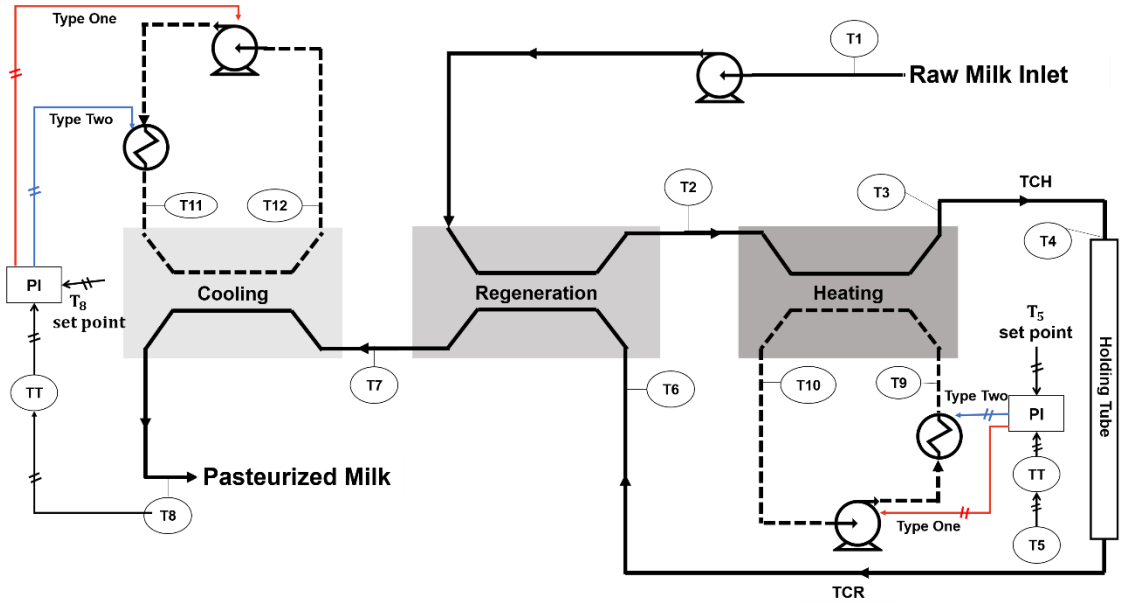

Figure 9.1. Schematic of a pasteurizer unit with two types of controller schemes (Type one: mass flowrate; Type two: temperature) (modified from Fig. 1.1[7]) (TCH: tubular connection with heating section; TCR: tubular connection with regeneration section).

For each controller, two types of manipulated variables were selected: mass flowrate (type one) and temperature (type two), which are indicted by red and blue lines, respectively in the figure. Here, pump is used to alter the mass flowrate in response to the controller signal and heat exchanger can be used to change the inlet cooling/heating medium temperature based on the controller signal.

9.2 Controller parameter identification

To ensure proper heat transfer and avoid non-physical values (<0) in the simulation, saturation is imposed to set a lower bound for each manipulated variable (MV) (Figure 9.2); while no upper bound is applied:

$$MV_{implemented} = \begin{cases} MV_{calculated} & if\ MV > MV_{min} \\ MV_{min} & if\ MV \leq MV_{min} \end{cases} \quad (9.1)$$

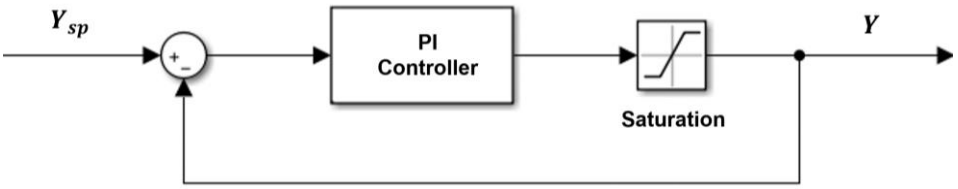

Figure 9.2. Block diagram of the PI controller.

To identify and tune the controller parameters, the process transfer function needs to be estimated. Firstly, a dynamic simulation was performed with step changes in each manipulated variable. Then, from the profile of the process variable (variable to be controlled), K_p and τ_P were estimated. Lastly, the controller parameter K_c and τ_I were calculated using internal model control (IMC) tuning relations. The estimated values for K_p and τ_P are shown in Table 9.1 and detailed information about the estimation process can be found in Appendix G. It is noted that due to the nonlinearities involved in the process, the process variables in the transfer function were not constant and an average values was used. Also, both controllers were tuned independently, and their interactions were not considered.

Table 9.1. Process parameters estimated from dynamic simulations.

Process parameter	Type one (Mass flowrate)		Type two (Temperature)	
	T_5	T_8	T_5	T_8
K_p	163.7 $\left(\frac{℃\,s}{kg}\right)$	-151.0 $\left(\frac{℃\,s}{kg}\right)$	0.955	0.563
τ_P	41.67 (s)	6.67 (s)	32.5 (s)	7.5 (s)

For moderate tuning, τ_c was set to the same value as τ_P since the deadtime for both controller is negligible (Figure G. 1 to G.4 in Appendix G), Thus, the IMC tuning correlation was reduced to Equation (9.2) and the tuned controller parameters are present in Table 9.2.

$$K_c = \frac{1}{K_P} \;\&\; \tau_I = \tau_P \tag{9.2}$$

Table 9.2. Controller parameters identified through IMC tuning relations.

Process parameter	Type one (Mass flowrate)		Type two (Temperature)	
	T_5	T_8	T_5	T_8
K_C	6.11E-03 $\left(\frac{kg}{°C\ s}\right)$	-6.62E-03 $\left(\frac{kg}{°C\ s}\right)$	1.047	1.775
τ_I	41.67 (s)	6.67 (s)	32.5 (s)	7.5 (s)

9.3 Case study: HTST process with disturbance

A dynamic test for the HTST process was used to assess the performance of the controllers. The simulation started from the nominal steady state condition as the one noted in section 7.3. Then, changes of T_1 as depicted in Figure 9.3 were implemented. Three simulations were carried out: one uncontrolled case, and two controlled case with type one and two controllers, respectively.

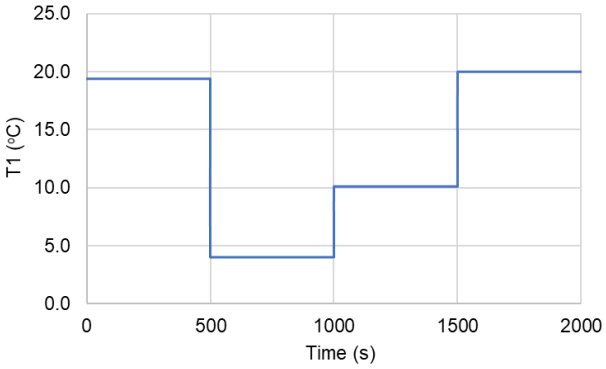

Figure 9.3. Temperature profile of inlet milk (T_1) through the controller test.

9.3.1 Results and discussion

Temperature comparison of T_5 and T_8 among three tests are shown in Figure 9.4 and Figure 9.5 along with their corresponding manipulated variable profiles. It is observed that both control types can help meet the set points of T_5 and T_8 to some extend within relatively short period of time. For T_5, almost identical performances of the controllers were obtained from the two types. And some oscillations were observed due to the integral part of the controller. Obviously, larger step change resulted in longer response time, but overall, the new steady state could be reached within relative short period of time. As for T_8, the performance of Type two (temperature) controller was better compared to the performance of Type one (mass flowrate) controller. For Type one controller, relatively large offset is observed from 527 to1622 seconds. It is because that the controller was saturated and therefore the minimum mass flowrate was implemented instead of the calculated mass flowrate from the controller (Figure 9.4).

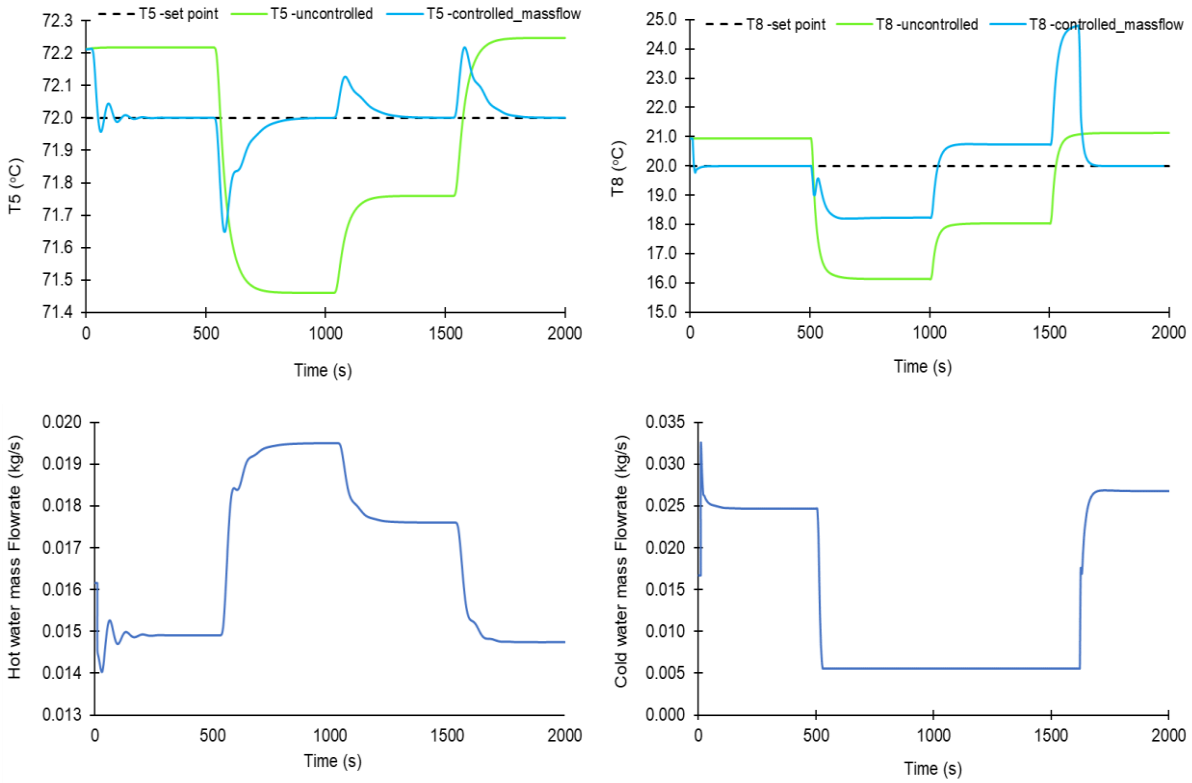

Figure 9.4. Profiles of the controlled and manipulated variables for type one controller (Top left: controller variable T_5; Top right: controller variable T_8; Bottom left: manipulated variable $\dot{m}_{hot}$; Bottom right: manipulated variable $\dot{m}_{cold}$).

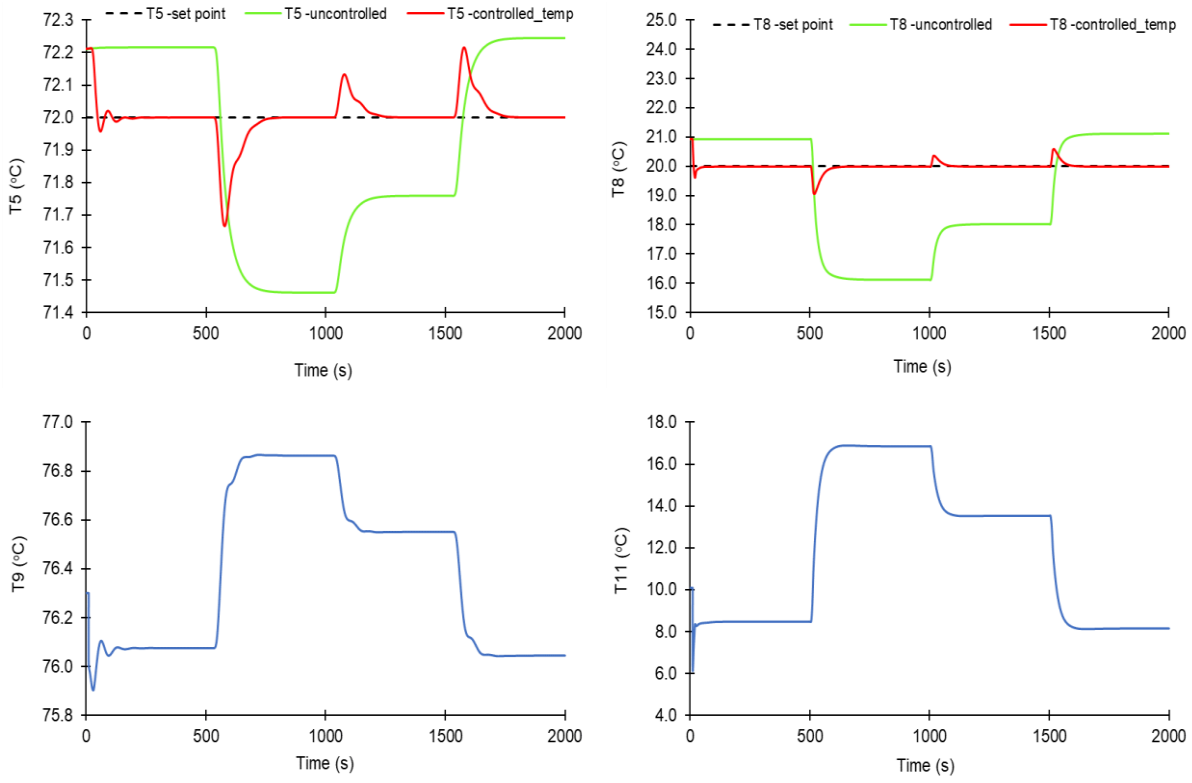

Figure 9.5. Profiles of the controlled and manipulated variables for type two controller (Top left: controller variable T_5; Top right: controller variable T_8; Bottom left: manipulated variable T_9; Bottom right: manipulated variable T_{11}).

In conclusion, both controllers can help achieve the required pasteurization and storage/end temperature. And depend on the equipment setting, it might be easier to implement one or the other type of controller. From the simulation point of view, temperature variation of the heating/cooling fluid introduces less dynamics/noise into the system comparing to flowrate changes. It is because that flowrate step change would not only influence the heat transfer between the fluids but also the fluid dynamics. It would bring more disturbance into the system comparing to the temperature change, which often results in simulation failure. Additionally, based on the analysis for the tests performed (Figure 9.4 and Figure 9.5), saturation of the manipulated variable for Type one controller is a main problem that hinders the performance. Nevertheless, from the practical point of view, flowrate variation would be relatively easier and cheaper to implement since flowrate can be altered through pump or valves with sample mechanisms. On the other hand, due to complex thermodynamics involved, targeting a specific temperature within short response time could be challenging.

10 Conclusions and future works

This thesis extended the 2D distributed thermal model of the milk heater (PHE) developed by Guan, Sharma and Macchietto[1,2] to a complete pasteurizer unit. The unit comprises three PHEs (heating, cooling and regeneration), one holding tube and two tubular connections.

First, the PHE section model developed previously[1,2] was modified, and its performance was validated against experimental and simulation results in the literature, where better agreements were observed comparing to the results of the previous model. Then, the tube section model was adopted and modified from the distributed model by Coletti[3], Diaz-Bejarano and Macchietto[4]. Lastly, the entire pasteurizer unit was modelled by joining the component section models of PHE and tube via proper boundary and continuity equations. The thermal model of the unit has been validated with the experimental results reported by Gutierrez, Diniz and Gut[7] for a HTST process.

A semi-mechanistic fouling model and an empirical CIP model was also integrated with the main thermal model for all sections of the pasteurizer unit. The fouling model was first verified through two configurations of the PHE heater. For configuraiton1, good agreements with the experimental data was observed; while for configuration 2, a better β-Lg reaction scheme might be needed to model the fouling phenomena accurately. As for the CIP model, a new model integration method was introduced, and more realistic simulation results of deposition mass over the heating-CIP cycles were obtained comparing to that of the previous model. With the combined pasteurizer unit model, a heating-CIP cycle was simulated for a realistic UHT case of the whole unit. The simulation results suggest an attenuated fouling effects of a single section on the overall process, which led to a need for the use of a more reasonable operation switch criteria other than the combined local critical mass density criteria currently being used. Additionally, large amount of cleaning and rinsing water was required during the heating-CIP cycle, indicating a need for operation optimization.

Two PI controller models were also added to the main unit model, which was used to assess the dynamic performance of the model as well as pre-tune the PI controllers. The simulation results indicate that the model can describe the dynamic conditions well and the tuned controller can be used to ensure the required pasteurization and storage/outlet temperature are met.

10.1 Future works

Based on the analysis in this work, several future works are suggested for model improvements and model applications.

Model improvements

1. ***Experimental validations:*** for the fouling model, limited deposition mass data is available in literature, which can greater hinders the model adequacy. It is because a semi-mechanistic fouling model is currently being used, for which sufficient data is needed to accurately estimate the value of the proportionality constant (β) and therefore better represent the deposition growth rate.
2. ***Explore different β-Lg reaction schemes:*** As noted for configuration 2, none of the reaction schemes (Dep_U and Dep_A) currently being implemented can describe the fouling phenomena well. In the current reaction scheme, only one protein species is allowed to deposit onto the surface at a time. For future exploration, an advanced reaction scheme that combines both Dep_U and Dep_A could be developed.
3. ***Include mineral fouling (type B) in the fouling model:*** In this work, only protein fouling (type A) is included, while, for the UHT case, significant mineral fouling is expected to occur. Therefore, to better estimate the deposition mass in the UHT process, it is essential to include a model for mineral fouling.
4. ***Physical properties of the fluid:*** In this work, constant physical properties of the processing fluid are assumed to reduce the model complexity and problem size. This assumption can introduce some misrepresentations of the experiential conditions. As an alternative, correlations can be implemented for the physical properties that have large impact on the outlet temperature (identified through sensitivity analysis) and constant values can be used for the ones that have minor influence.
5. ***Develop a more general CIP models:*** the CIP model implemented in this work is taken from Bird & Fryer[40], which was developed specifically for cleaning with 1wt% $NaOH$ soltuion. A more general CIP model (e.g. the one proposed by Lanchas-Fuentes *et al*[42]) can be used to reduce the limitations of this empirical model.

Model applications

1. ***Expand to other types of milk:*** this work focus on the analysis for the skimmed milk, while fouling is expected to have larger impact for the processing of the whole and concentrated milk due to higher fat content. By integrating parameters such as fat, protein and mineral contents in the model, it can be adapted to simulate heating-CIP cycles for different types of milk.
2. ***Automation of heating-CIP cycles:*** the operational downtime can be reduced through automation of heating-CIP cycles. Two alternative options can be used: (1) include a separate set of spared PHEs to form a heat exchanger network (HEN) and schedule the PHEs so that while one set of the PHEs are being cleaned, the other could continuously be in operation[63]; (2) change the configuration of the existing PHEs

to include additional channels and install valves that control and alter the flow directions along the PHEs. By doing so, portions of the PHEs could remain in operation while others being cleaned simultaneously. The pasteurizer unit model developed in this work can be modified and then implemented to test these two options and identity the optimal operation policies.

References

1. Guan, S. & Macchietto, S. A novel dynamic model of Plate Heat Exchangers subject to fouling. in *28th European Symposium on Computer Aided Process Engineering* (2018).

2. Sharma, A. & Macchietto, S. Fouling and cleaning of Plate Heat Exchangers for Milk Pasteurisation: a moving boundary model. in *29th European Symposium on Computer Aided Process Engineering* (2018).

3. Coletti, F. & Macchietto, S. A Dynamic, Distributed Model of Shell-and-Tube Heat Exchangers Undergoing Crude Oil Fouling. *Ind. Eng. Chem. Res.* **50**, 4515–4533 (2011).

4. Diaz-Bejarano, E., Coletti, F. & Macchietto, S. A new dynamic model of crude oil fouling deposits and its application to the simulation of fouling-cleaning cycles. *AIChE J.* **62**, 90–107 (2016).

5. Wang, L. (Lieke), Sundén, B. & Manglik, R. M. *Plate heat exchangers : design, applications and performance*. (WIT Press, 2007).

6. Tetra-Pak. *Dairy Processing Handbook*. *Lund: Tetra Pak Processing Systems AB* (2015).

7. Gutierrez, C. G. C. C., Diniz, G. N. & Gut, J. A. W. Dynamic simulation of a plate pasteurizer unit: Mathematical modeling and experimental validation. *J. Food Eng.* **131**, 124–134 (2014).

8. Alfa-Laval. Alfa Laval – plate technology. (2018). Available at: https://www.alfalaval.com/globalassets/documents/industries/chemicals/petrochemicals/brochure_alfa_laval_plate_technology_ppm00063en.pdf.

9. Bon, J., Clemente, G., Vaquiro, H. & Mulet, A. Simulation and optimization of milk pasteurization processes using a general process simulator (ProSimPlus). *Comput. Chem. Eng.* **34**, 414–420 (2010).

10. U.S. Food and Drug Administration. CFR - Code of Federal Regulations Title 21. (2018). Available at: https://www.accessdata.fda.gov/scripts/cdrh/cfdocs/cfcfr/CFRSearch.cfm?fr=1240.61. (Accessed: 9th September 2019)

11. Towler, G. P. *Chemical engineering design*. (Oxford, 2009).

12. Georgiadis, M. C. & Macchietto, S. Dynamic modelling and simulation of plate heat exchangers under milk fouling. *Chem. Eng. Sci.* **55**, 1605–1619 (2000).

13. De Jong, P., Te Giffel, M. C., Straatsma, H. & Vissers, M. M. M. Reduction of fouling and contamination by predictive kinetic models. *Int. Dairy J.* **12**, 285–292 (2002).

14. Wilson, D. I. Fouling during food processing – progress in tackling this inconvenient truth. *Curr. Opin. Food Sci.* **23**, 105–112 (2018).

15. Georgiadis, M. C., Rotstein, G. E. & Macchietto, S. Modelling and simulation of complex plate heat exchanger arrangements under milk fouling. *Comput. Chem. Eng.* **22**, S331–S338 (1998).

16. Van Asselt, A. J., Vissers, M. M. M., Smit, F. & De Jong, P. In-line control of fouling. in *Proceddings of heat exchanger fouling and cleaning-challenges and opportunities* (Engineering Conferences International, 2005).

17. Bansal, B. & Chen, X. A Critical Review of Milk Fouling in Heat Exchangers. *Compr. Rev. Food Sci. Food Saf.* **33**, 273–277 (2006).

18. Sharma, A. A computational study on fouling and cleaning operation in milk pasteruisation using a moving boundary model. (Imperial College London, 2018).

19. Bennett, H. A. E. Aspects of fouling in dairy processing. (2007).

20. Alharthi, M. Fouling and cleaning studies of protein fouling at pasteurization temperatures. (The University of Birmingham, 2013).

21. Burton, H. Section G. Deposits from whole milk in heat treatment plant—a review and discussion.

J. Dairy Res. **35**, 317 (1968).

22. Burton, H. *Ultra-High-Temperature Processing of Milk and Milk Products*. (Springer US, 1994). doi:10.1007/978-1-4615-2157-0

23. Blanpain-Avet, P. *et al.* Predicting the distribution of whey protein fouling in a plate heat exchanger using the kinetic parameters of the thermal denaturation reaction of β-lactoglobulin and the bulk temperature profiles. *J. Dairy Sci.* **99**, 9611–9630 (2016).

24. Guan, S. Modelling , Operation and Fouling of Plate Heat Exchangers. (Imperial College London, 2017).

25. Sadeghinezhad, E. *et al.* A Comprehensive Review of Milk Fouling on Heated Surfaces. *Crit. Rev. Food Sci. Nutr.* **55**, 1724–1743 (2015).

26. Tolkach, A. & Kulozik, U. Reaction kinetic pathway of reversible and irreversible thermal denaturation of β-lactoglobulin. *Lait* **87**, 301–315 (2007).

27. Jun, S. & Puri, V. M. A 2D dynamic model for fouling performance of plate heat exchangers. *J. Food Eng.* **75**, 364–374 (2006).

28. Gut, J. A. W. & Pinto, J. M. Modeling of plate heat exchangers with generalized configurations. *Int. J. Heat Mass Transf.* **46**, 2571–2585 (2003).

29. Aouanouk, A. S., Mouheb, A. & Absi, R. NUMERICAL STUDY OF MILK FOULING THICKNESS IN THE CHANNEL OF PLATE HEAT EXCHANGER. *J. Therm. Eng.* **4**, 2464–2470 (2018).

30. Jun, S. & Puri, V. M. 3D milk-fouling model of plate heat exchangers using computational fluid dynamics. *Int. J. Dairy Technol.* **58**, 214–224 (2005).

31. Grijspeerdt, K., Hazarika, B. & Vucinic, D. Application of computational fluid dynamics to model the hydrodynamics of plate heat exchangers for milk processing. *J. Food Eng.* **57**, 237–242 (2003).

32. Wang, Y. N. *et al.* A Study on 3D Numerical Model for Plate Heat Exchanger. *Procedia Eng.* **174**, 188–194 (2017).

33. Bouvier, L. *et al.* A CFD model as a tool to simulate β-lactoglobulin heat-induced denaturation and aggregation in a plate heat exchanger. *J. Food Eng.* **136**, 56–63 (2014).

34. De Bonis, M. V. & Ruocco, G. Conjugate fluid flow and kinetics modeling for heat exchanger fouling simulation. *Int. J. Therm. Sci.* **48**, 2006–2012 (2009).

35. Memisi, N., Moracanin, S. V., Milijasevic, M., Babic, J. & Djukic, D. CIP Cleaning Processes in the Dairy Industry. *Procedia Food Sci.* **5**, 184–186 (2015).

36. Müller-Steinhagen, H. *Heat Exchanger Fouling: Mitigation and Cleaning Technologies*. (Institution of Chemical Engineers, 2000).

37. Chandrakash, S. A new risk analysis of Clean-In-Place milk processing. (The University of Adelaide, 2012).

38. Davey, K. R., Chandrakash, S. & O'Neill, B. K. A new risk analysis of Clean-In-Place milk processing. *Food Control* **29**, 248–253 (2013).

39. Tetra-Pak. *Cleaning in place Handbook: A guid to cleaning technology in the food processing industry*. (Lund: Tetra Pak Processing Systems AB, 2015).

40. Bird, M. R. & Fryer, P. J. An analytical model for cleaning of food process plant. *Food Eng. a Comput. Clim. ICHEME Symp. Ser.* 325–330 (1992).

41. Xin, H., Chen, X. D. & Özkan, N. A Mathematical Model of the Removal of Milk Protein Deposit Hong. in *Heat Exchanger Fouling and Cleaning: Fundamentals and Applications* (ECI Digital Archives, 2003).

42. Lanchas-Fuentes, L., Diaz-Bejarano, E., Coletti, F. & Macchietto, S. Condition-based chemical cleaning of crude oil deposits – a conceptual model. in *Proceedings of the 26th European*

Symposium on Computer Aided Process Engineering - ESCAPE 26 (eds. Zdravko, K. & Miloš, B.) 1905–1910 (Elsevier, 2016). doi:10.1016/B978-0-444-63428-3.50322-2

43. Wallhäußer, E., Hussein, M. A. & Becker, T. Detection methods of fouling in heat exchangers in the food industry. *Food Control* **27**, 1–10 (2012).

44. Piepiórka-Stepuk, J., Mierzejewska, S. & Jakubowski, M. Application of Nephelometry to Automatic Control of Cleaning Time during Cleaning Process in Clean in Place System. *Int. J. Food Eng.* **13**, 1–10 (2017).

45. Mahdi, Y., Mouheb, A. & Oufer, L. A dynamic model for milk fouling in a plate heat exchanger. *Appl. Math. Model.* **33**, 648–662 (2009).

46. Boloorchi, A. S. & Jafari Nasr, M. R. A model for fouling of plate-and-frame heat exchangers in food industry. *Asia-Pacific J. Chem. Eng.* **7**, 427–433 (2012).

47. Grijspeerdt, K., Mortier, L., De Block, J. & Van Renterghem, R. Applications of modelling to optimise ultra high temperature milk heat exchangers with respect to fouling. *Food Control* **15**, 117–130 (2004).

48. Aguiar, H. F. & Gut, J. A. W. Continuous HTST pasteurization of liquid foods with plate heat exchangers: Mathematical modeling and experimental validation using a time-temperature integrator. *J. Food Eng.* **123**, 78–86 (2014).

49. Kessler, H. G. *Food and bio process engineering: dairy technology*. (Verlag A. Kessler, 2002).

50. Minim, L. A., Coimbra, J. S. R., Minim, V. P. R. & Telis-Romero, J. Influence of Temperature and Water and Fat Contents on the Thermophysical Properties of Milk. *J. Chem. Eng. Data* **47**, 1488–1491 (2002).

51. Fernández-Martín, F. Influence of temperature and composition on some physical properties of milk and milk concentrates. II. Viscosity. *J. Dairy Res.* **39**, 75–82 (1972).

52. Munir, M. T., Zhang, Y., Yu, W., Wilson, D. I. & Young, B. R. Virtual milk for modelling and simulation of dairy processes. *J. Dairy Sci.* **99**, 3380–3395 (2016).

53. *NIST Chemistry WebBook, NIST Standard Reference Database Number 69*. *National Institute of Standards and Technology* (Gaithersburg MD, 20899). doi:10.18434/T4D303

54. Choi, Y. & Okos, M. R. Effects of temperature and composition on thermal properties of foods. *J. Food Process Appl.* **1**, 93–101 (1986).

55. De Jong, P. Modelling and optimization of thermal processes in the dairy industry. (TU Delft, 1996).

56. Delplace, F. & Leutiet, J. C. Modeling fouling of a plate heat exchanger with different flow arrangements by whey protein solutions. *Trans. IChemE, Food Bioprod. Process.* **73**, 112–120 (1995).

57. Process System Enterprise Limited. gPROMS. (2018).

58. Delplace, F., Leutiet, J. C. & Levieux, D. A reaction engineering approach to the analysis of fouling by whey proteins of a six-channels-per-pass plate heat exchanger. *J. Food Eng.* **34**, 91–108 (1997).

59. Delplace, F., Leuliet, J. & Tissier, J. Fouling experiments of a plate heat exchanger by whey protein solution. *Inst. Chem. Eng.* **72**, 163–169 (1994).

60. Rene, F., Leuliet, J. C. & Lalande, M. Heat transfer to newtonian and non-newtonian food fluid in plate heat exchangers: experimental and numerical approaches. *Trans. IChemE* **69**, 115–126 (1991).

61. Lozano Santamaria, F. *Two phase heat exchanger modelling*. (2019).

62. Gut, J. A. W. & Pinto, J. M. Optimal configuration design for plate heat exchangers. *Int. J. Heat Mass Transf.* **47**, 4833–4848 (2004).

63. Deka, D. & Datta, D. Multi-objective optimization of the scheduling of a heat exchanger network under milk fouling. *Knowledge-Based Syst.* **121**, 71–82 (2017).

64. Al-Dawery, S. K., Alrahawi, A. M. & Al-Zobai, K. M. Dynamic modeling and control of plate heat exchanger. *Int. J. Heat Mass Transf.* **55**, 6873–6880 (2012).

65. Loyola-Fuentes, J., Jobson, M. & Smith, R. Fouling modelling and mitigation for crude oil heat exchanger networks using reconciled operating data. *Chem. Eng. Trans.* **70**, 193–198 (2018).

66. Lozano Santamaria, F. & Macchietto, S. Integration of Optimal Cleaning Scheduling and Control of Heat Exchanger Networks Undergoing Fouling: Model and Formulation. *Ind. Eng. Chem. Res.* **57**, 12842–12860 (2018).

67. Davey, K. R., Chandrakash, S. & O'Neill, B. K. A Friday 13th failure assessment of clean-in-place removal of whey protein deposits from metal surfaces with auto-set cleaning times. *Chem. Eng. Sci.* **126**, 106–115 (2015).

68. Fryer, P. J. & Slater, N. K. H. A direct simulation procedure for chemical reaction fouling in heat exchangers. *Chem. Eng. J.* **31**, 97–107 (1985).

Appendix A. Summary tables for models developed

Table A.1. Summary of PHE models.

Reference	Model Type	Remarks/Advantages	Limitations/Simplifications
[28]	- 1D - Steady-state - Plug-flow	- Algorithmic model for gasketed PHE with generalized configurations. - The assumption of constant overall heat transfer coefficient was tested and validated.	- Hard to be used for optimization due to the nature of algorithmic feature embedded in the model. - Simplified plate geometry. - Plate topology was not considered.
[31]	- 2D & 3D - CFD - Steady-state	- Considered detailed geometry of the plate (corrugation) - Experiments were conducted to compare the simulation results	- Single plate simulation - Computational heavy - The 2D model has limited predictive ability
[62]	- 1D - Steady-state - Plug-flow	- Algorithmic model - Optimized PHE configuration by minimizing the heat transfer area	- Simplified plate geometry. - Plate topology was not considered, which could significant affect the heat transfer area and therefore influence the optimization results.
[64]	- Dynamic - Linear process	- Predicted transient responses of PHE - Considered control strategies and verified model with temperature controllers	- Empirical model - Plate topology was not considered.
[32]	- 3D - CFD - Steady-state	- Considered and analysed three corrugation parameters (angle, depth and pitch) of plates	- Computational heavy - A single plate analysis

Table A.2. Summary of other models that could be adapted for milk pasteurization.

Reference	Model Type	Fluid	Remarks/Advantages	Limitations/Simplifications
[3]	- Dynamic - Distributed - STHE	Crude oil	- Considered local deposit growth and aging - Moving boundary - Parameter estimation using refinery data	Only considered fouling on tube-side, could underpredict fouling on shell-side
[4]	- Dynamic - Distributed - STHE	Crude oil	- Could be used to simulate fouling-cleaning cycles in one deposit model - Overcome several assumptions that were commonly used in previous models	Only considered fouling on tube-side, could underpredict fouling on shell-side
[65]	- HEN (Preheat train) - Fouling rate model	Crude oil	- Included data reconciliation (redundancy analysis and variable classification), which included measurement and instrument (systematic) errors	Semi-empirical model (rely on operating data)
[66]	- MILP/MINLP (cleaning schedule) - NLP (control)	Crude oil	- Considered optimal cleaning scheduling and control with versatile formulation	- Validation of the results against plant data needs to be done - Limited ability for large-scale optimization

Table A.3. Summary of combined models (PHE & Fouling) for milk pasteurization.

Reference	Model Type	Fouling Type	Remarks	Limitations/Simplifications
[12,15]	- 1D - Dynamic - Plug-flow	β-Lg reaction scheme	- Distributed model - Consider axial convection and radial continuity	- Plate topology was not considered. - Plug-flow
[47]	- 1D - Dynamic - Plug-flow	β-Lg reaction scheme	- Considered the bacteriological quality and lactulose and hydroxymethylfurfural formation of UHT process - Considered homogenisation and holding tube sections - Optimization of UHT process was performed	- Plate topology was not considered. - Plug-flow - Used β-Lg reaction scheme (Type A) to model fouling of UHT process, which is often dominated by Type B fouling (minerals)
[30]	- 3D - CFD	β-Lg reaction scheme	- Considered the corrugation (both shape and orientation) of plates - Simulated a full PHE system	- Computational heavy - The chemical reaction scheme used can not fully capture the fouling phenomena
[27]	- 2D - Dynamic - Navier-Stokes	β-Lg reaction scheme	- Simulated results were validated against both empirical data and previous simulated results in the literature	- Plate topology was not considered.
[34]	- 3D - CFD - Dynamic - Navier-Stokes	β-Lg reaction scheme	- Considered milk fouling and plate corrugation - Considered conjugate framework, which solved the mass and heat transfer in solid and fluid phase simultaneously	- Single-channel analysis - Computational heavy
[45]	- 2D - Dynamic -	- β-Lg reaction scheme - Minearl deposition	- Considered mineral deposition - Simulated deposition rate was compared with literature data and simulated temperature profile was compared with an industrial heating plant.	- Plate topology was not considered. - The comparison results were not shown or discussed in paper.
[46]	- 2D - Dynamic	Empirical fouling threshold model	- Considered mass deposit change (both deposition and removal)	- Based on empirical data, which limits its application to other configurations/topology
[33]	- 2D - CFD	β-Lg reaction scheme	- Simulated a full PHE system to study the denaturation and aggregation of β-Lg on PHE - Considered the corrugation	- Computational heavy -
[29]	- 2D - Dynamic	β-Lg reaction scheme	- Relationship between fouling thickness and wall temperature were studied	- Plate topology was not considered. - The milk fouling model is not generalized
[1]	- 2D - Dynamic - Distributed	β-Lg reaction scheme	- Detailed 2D distributed model - Moving boundary used to account deposit layer growth	- Single-channel analysis
[2]	- 2D - Dynamic - Distributed	β-Lg reaction scheme	- Full PHE system analysis - Simulated different configurations with two deposition mechanism (aggregation and denaturation of protein)	- Different models need to be used for different configurations

Table A.4. Summary of CIP models.

Reference	Model Type	Remarks	Limitations/Simplifications
[40]	- Simplified 1D model - Dynamic - Chemical cleaning	- For dairy processing (whey and whole milk) - Used to determine temperature and velocity effects on cleaning - Verified against experimental data	- The chemistry involved in cleaning was not analysed/included in the model - Included several oversimplified assumptions
[41]	- Dynamic - Chemical cleaning based on polymer dissolution	- For dairy processing (milk protein deposit) - Considered and included several processes (e.g. reputation, disengagement, mass transfer) through the boundary layer - Considered surface area change during decay cleaning stage - Verified against experimental data over a wide range	- Deposits removed by shear force was not considered
[38, 67]	- Risk assessment - Monte Carlo - Latin Hypercube sampling	- Integrated milk CIP models[40,41] with a risk factor to account for potential failures of CIP operation - Model could be extended to any unit-operations	- Extensive experimental data or expert knowledge is required to accurately predict the risk factor - The model used for the unit-operation need to be relatively accurate
[42]	- Chemical cleaning - Dynamic - Conceptual	- For crude oil fouling - Considered deposit conditions, effectiveness of the chemical cleaning agent and duration - Conditional-based cleaning (differ from the fixed-duration cleaning that are commonly used) - Could be adapted for other fluids	- General “functional form” - Parameters used need to be adjusted/verified against experimental data
[2]	Same model proposed by Bird & Fryer[40]	- Integrated CIP model[40] with the fouling model and simulated heating-CIP cycles	Same limitations as the one proposed by by Bird & Fryer[40]

Appendix B. Complementary figures

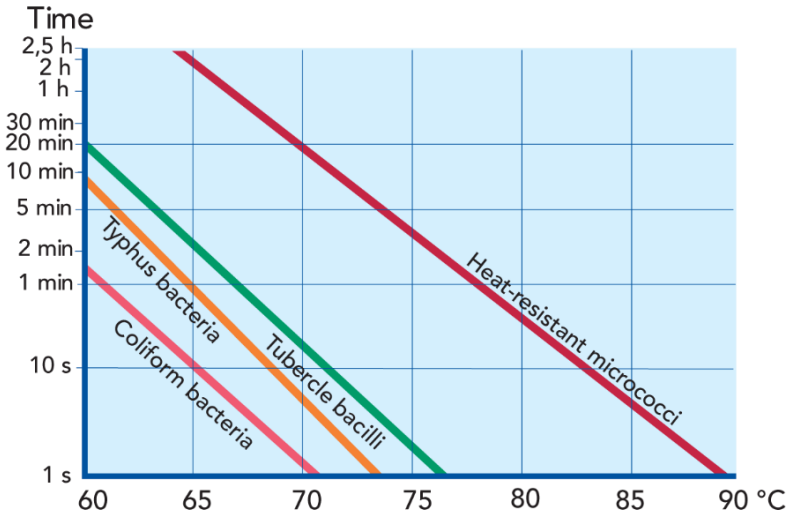

Figure B.1. Lethal effect on common bacteria presented in raw milk[6].

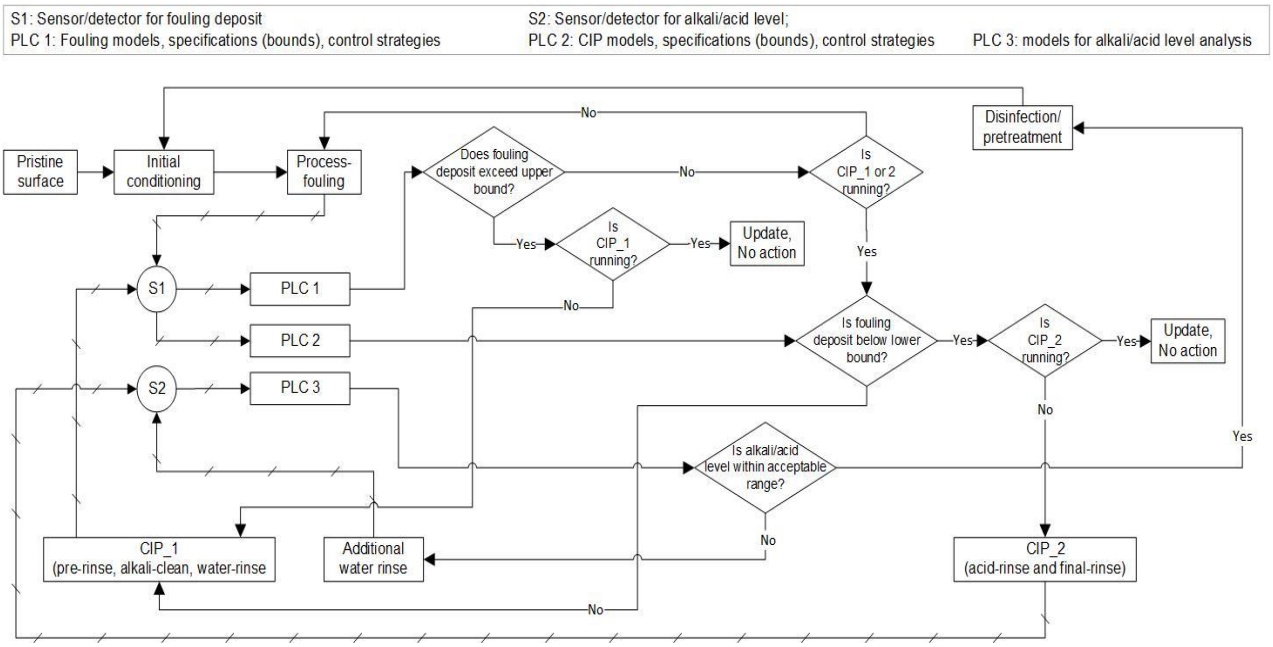

Figure B.2. Stages for heating-CIP cycles with monitoring

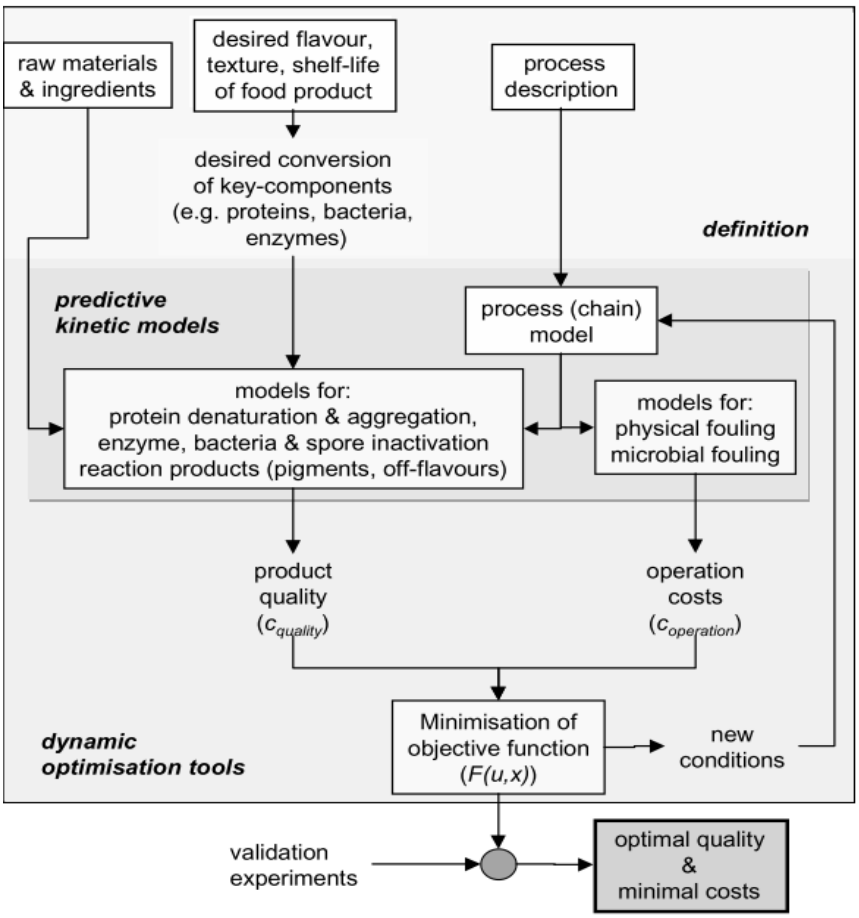

Figure B.3. The use of kinetic models for process development[13].

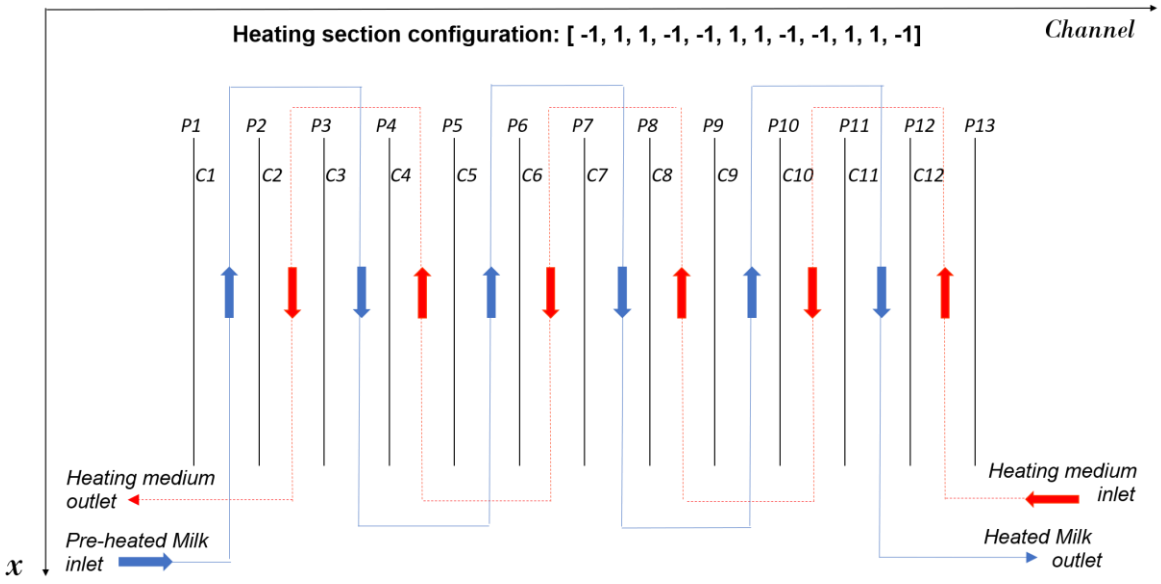

Figure B.4. Schematic of PHE for heating section for HTST process (Pi: Plate I; Ci: Channel i).

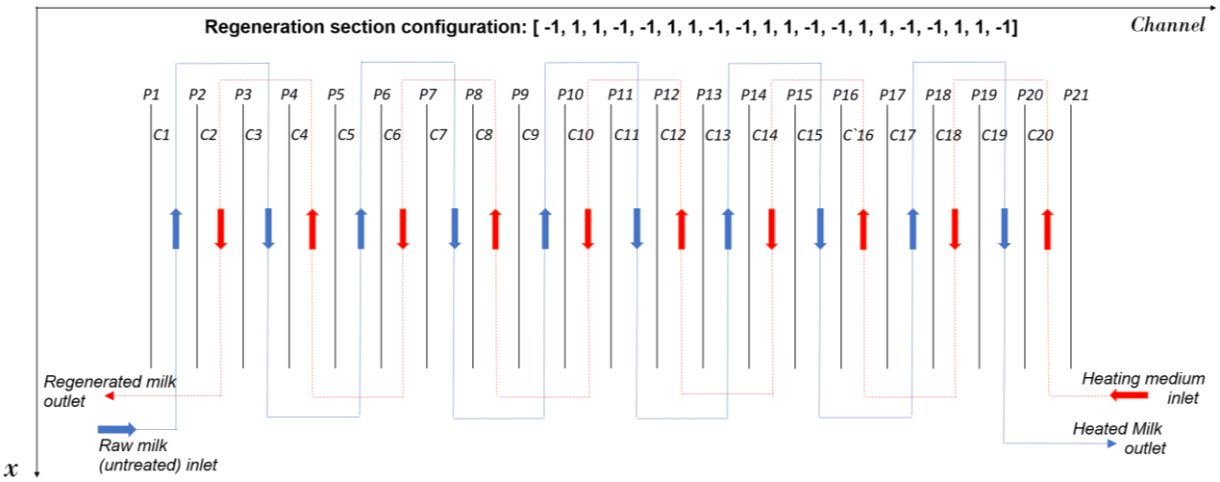

Figure B.5. Schematic of PHE for regeneration section for HTST process (Pi: Plate I; Ci: Channel i).

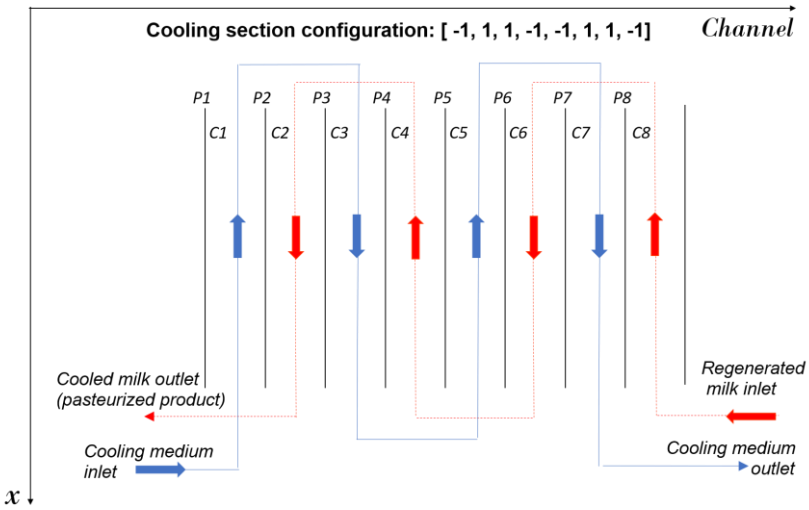

Figure B.6. Schematic of PHE for cooling section for HTST process (Pi: Plate I; Ci: Channel i).

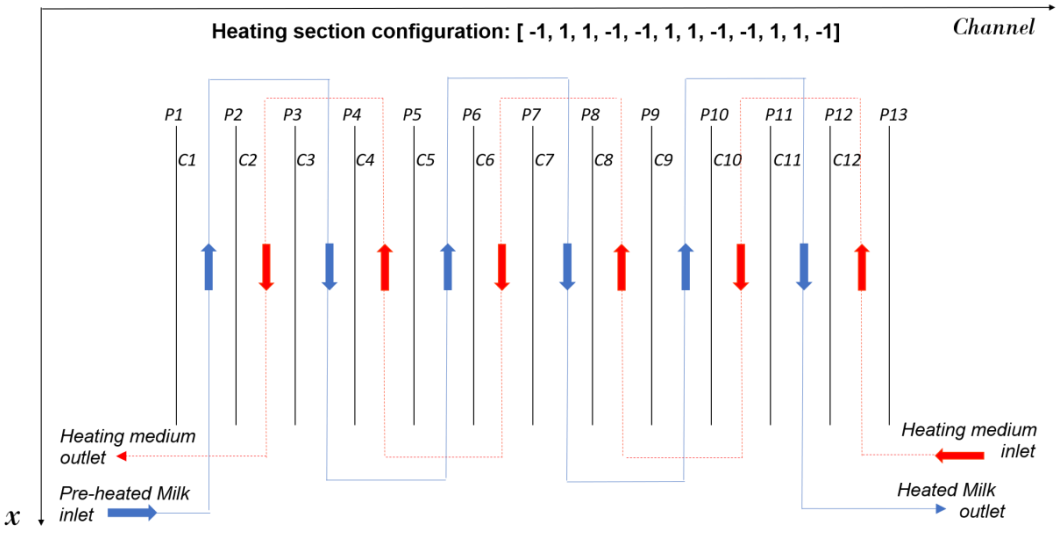

Figure B.7. Schematic of PHE for heating section for UHT process (Pi: Plate I; Ci: Channel i).

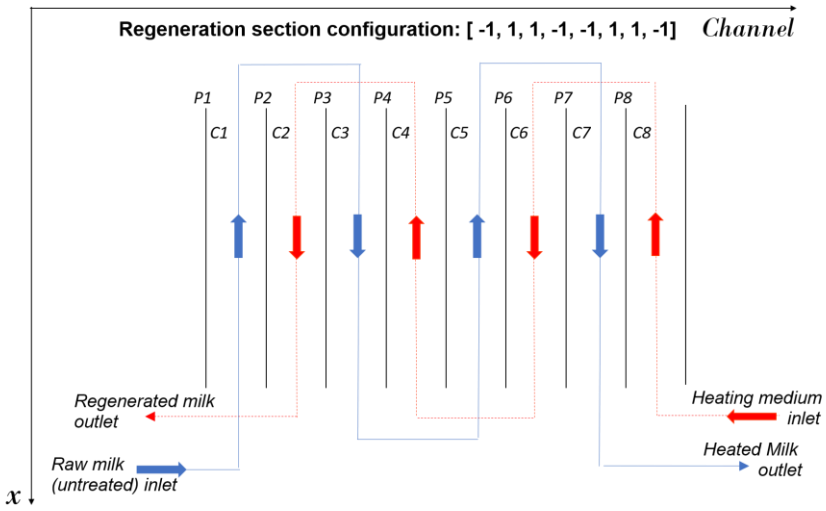

Figure B.8. Schematic of PHE for regeneration section for UHT process (Pi: Plate I; Ci: Channel i).

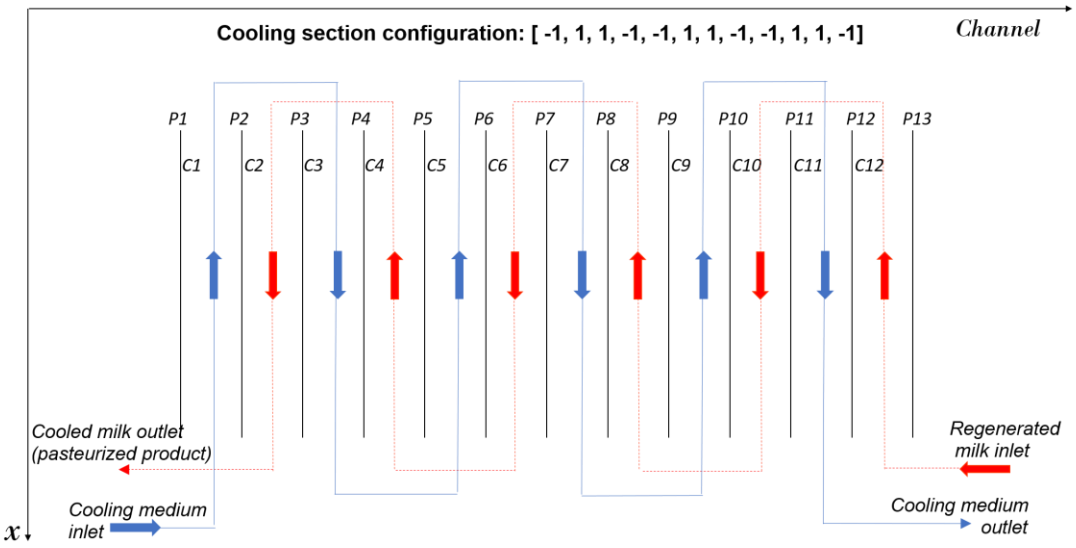

Figure B.9. Schematic of PHE for cooling section for UHT process (Pi: Plate I; Ci: Channel i).

Appendix C. Complementary tables

Table C. 1. Typical heat treatments used in the dairy industry[6].

Process	Temperature, ºC	Time
Thermization	/	/
LTLT pasteurization of milk	63	30 min
HTST pasteurization of milk	72 – 75	15 – 20 s
HTST pasteurization of cream, etc.	> 80	1 – 5 s
Ultra pasteurization	125 – 138	2 – 4 s
UHT (flow sterilization) normally	135 – 140	a few seconds
Sterilization in container	115 – 120	20 – 30 min

Note: LTLT: low temperature long time; HTST: high temperature short time; UHT: ultra-high temperature

Table C. 2. Aspects of type A fouling mechanisms in the literature[17].

Aspects	References
Protein denaturation is reversible	de Wit and Swinkles (1980), Anema and McKenna (1996), Changani and others (1997), Chen and others (1998a)
Protein denaturation is irreversible	Ruegg and others (1977), Lalande and others (1985), Arnebrat and others (1987), Gotham and others (1992), Roef and de Kruif (1994), Karlsson and others (1996)
Protein aggregation is irreversible	Mulvihill and Donovan (1987), Anema and McKenna (1996), Changani and others (1997), Chen and others (1998a)
Protein denaturation is the governing reaction	Lalande and others (1985), Hege and Kessler (1986), Arnebrant and others (1987), Kessler and Beyer (1991), de Jong and others (1992)
Protein aggregation is the governing reaction	Lalande and René (1988), Gotham and others (1992), Delplace and others (1997)
Formation of protein aggregates enable to reduce fouling	de Jong and others (1992), Delplace and others (1997), van Asselt and others (2005)
Only protein aggregates cause fouling	Toyoda and others (1994)
Fouling is considered to depend on protein reactions only	de Jong and van del Linden (1992), de Jong and others (1992), Belmar-Beiny and others (1993), Delplace and others (1994, 1997), Schreier and Fryer (1995), Grijspeerdt and others (2004), Sahoo and others (2005), Nema and Datta (2005)
Fouling is considered to depend on protein reactions as well as mass transfer	Toyoda and others (1994), Georgiadis and others (1998), Georgiadis and Macchietto (2000), Chen and others (1998a, 2000, 2001), Bansal and Chen (2005), Bansal and others (2005)

Appendix D. Fouling model mass balance equations for PHEs

The mass balance equations for different β-lg protein species are adapted with minor modifications from previous researches[12,18,24].

Native proteins (N) in bulk fluid:

$$\frac{\partial C_N}{dt} = -dir\frac{\partial}{\partial x}\left(u_f C_N\right) + D_N\frac{\partial^2 C_N}{\partial x^2} - r_{fU} - \frac{k_{mN}^L}{\delta_T^L}(C_N - C_N^L) - \frac{k_{mN}^R}{\delta_T^R}(C_N - C_N^R) \quad \text{(D.1)}$$

Unfolded proteins (U) in bulk fluid:

$$\frac{\partial C_U}{dt} = -dir\frac{\partial}{\partial x}\left(u_f C_U\right) + D_U\frac{\partial^2 C_U}{\partial x^2} + r_{fU} - r_{fA} - \frac{k_{mD}^L}{\delta_T^L}(C_U - C_U^L) - \frac{k_{mU}^R}{\delta_T^R}(C_U - C_U^R) \quad \text{(D.2)}$$

Aggregated proteins (A) in bulk fluid:

$$\frac{\partial C_A}{dt} = -dir\frac{\partial}{\partial x}\left(u_f C_A\right) + D_A\frac{\partial^2 C_A}{\partial x^2} + r_{fA} - \frac{k_{mA}^L}{\delta_T^L}(C_A - C_A^L) - \frac{k_{mA}^R}{\delta_T^R}(C_A - C_A^R) \quad \text{(D.3)}$$

Native protein (N) in thermal boundary layer:

$$\frac{\partial C_N^i}{dt} = -dir\frac{\partial}{\partial x}\left(u_f C_N^i\right) + D_N\frac{\partial^2 C_N^i}{\partial x^2} - r_{TU}^i + \frac{k_{mN}^i}{\delta_T^i}\left(C_N - C_N^i\right) \qquad \forall\, i \in \{L, R\} \quad \text{(D.4)}$$

Unfolded protein (U) in thermal boundary layer:

$$\frac{\partial C_U^i}{dt} = -dir\frac{\partial}{\partial x}\left(u_f C_U^i\right) + D_D\frac{\partial^2 C_U^i}{\partial x^2} + r_{TU}^i - r_{TA}^i + \frac{k_{mU}^i}{\delta_T^i}\left(C_U - C_U^i\right) - \frac{Dep_U + 1}{2}r_{dU}^i + \frac{Ent_U + 1}{2}r_{eU}^i \qquad \forall\, i \in \{L, R\} \quad \text{(D.5)}$$

Aggregated protein (A) in thermal boundary layer:

$$\frac{\partial C_A^i}{dt} = -dir\frac{\partial}{\partial x}\left(u_f C_A^i\right) + D_A\frac{\partial^2 C_A^i}{\partial x^2} + r_{TA}^i + \frac{k_{mA}^i}{\delta_T^i}\left(C_A - C_A^i\right) - \frac{Dep_A + 1}{2}r_{dA}^i + \frac{Ent_A + 1}{2}r_{eA}^i \qquad \forall\, i \in \{L, R\} \quad \text{(D.6)}$$

Here, $r_{f_{protein}}$ and $r_{T_{protein}}^i$ can be calculated from equation (4.29) and (4.30), respectively. $k_{m_{protein}}^i$ is the mass transfer coefficient of different protein species; $D_{protein}$ is the diffusivity of different protein species and δ_T^i is the thermal boundary layer thickness for left or right plate. Their value could be determined from the following equations[55]:

$$Sh(x) = 0.0902\, Re(x)^{0.663} Sc(x)^{0.333} \tag{D.7}$$

$$Sc(x) = \frac{\mu_f(x)}{\rho_f(x)\, D_N} \tag{D.8}$$

$$\delta_M(x) = \frac{D_h(x)}{Sh(x)} \tag{D.9}$$

$$\delta_T(x) = Pr(x)^{\frac{1}{3}}\, \delta_M(x) \tag{D.10}$$

$$D_{protein} = \frac{1.31 \times 10^{-17}\, T_f}{\mu_f \left(N_{av} \left(\frac{1}{6} \pi d_i^3 \right) \right)^{0.6}} \tag{D.11}$$

$$k_m^i = D_i\, \delta_M \tag{D.12}$$

Here, Sh and Sc are the dimensionless Sherwood and Schmidt number. δ_M is the mass boundary layer thickness. N_{av} is the Avogadro number (6.023×10^{23}) and d_i is the diameter of different protein species whose values[12,27] are shown in Table D.5.

Table D.5. Mean particle diameter of different protein species[12,27]

Protein species	**Mean particle diameter (m)**
Native (*N*)	9.92×10^{-11}
Unfolded (U)	9.12×10^{-11}
Aggregated (*A*)	5.0×10^{-10}

Also, r_{dA}^i and r_{dU}^i are the rate of deposition for Dep_A and Dep_U fouling models, which are calculated from the following equations:

$$r_{dA}^i = \frac{\rho_l}{\delta_T^i} \frac{d\delta_{dA}^i(x)}{dt} \qquad \forall\, i \in \{L, R\} \tag{D.13}$$

$$r_{dU}^i = \frac{\rho_l}{\delta_T^i} \frac{d\delta_{dU}^i(x)}{dt} \qquad \forall\, i \in \{L, R\} \tag{D.14}$$

Here, ρ_l is the deposit layer density. And $\frac{d\delta_{d_{protein}}^i(x)}{dt}$ is the rate of change for the deposit thickness, which can be determined from (4.37) and (4.38). When Dep_A fouling model is used, r_{dU}^i will be set to 0. And when Dep_U fouling model is used, r_{dA}^i will be set to 0. This can be achieved by using a logic parameter $Dep_{protein}$, whose value equals to -1 when the fouling model is not selected and equals to +1 when it is selected.

Additionally, entrainment due to shear stress could bring deposit protein back to the thermal boundary layer. It is take into account through the term r_{eA}^{i} and r_{eU}^{i} (the rate of entrainment for Dep_A and Dep_U fouling models), which are be calculated from the following equations[68]:

$$r_{eA}^{i} = \frac{\rho_l}{\delta_T^i}\ \delta_{dA}^{i}(x)\ k_\tau \qquad \forall\ i\ \in \{L, R\} \qquad \text{(D.15)}$$

$$r_{eU}^{i} = \frac{\rho_l}{\delta_T^i}\ \delta_{dU}^{i}(x)\ k_\tau \qquad \forall\ i\ \in \{L, R\} \qquad \text{(D.16)}$$

Here, k_τ is the pre-exponential factor of entrainment whose value[68] is determined to be $1.3 \times 10^{-3}\ s^{-1}$. Like the deposition model, a logic parameter $Ent_{protein}$ is used to indicate whether the entrainment term is included or not: it equals to -1 when it is not included in the model and equals to +1 when it is included.

Appendix E. Fouling model mass balance equations for tubes

The mass balance equations for different β-lg protein species in the tube are obtained by transferring the ones for PHEs (cartesian coordinates) into the cylindrical coordinates.

Native proteins (N) in bulk fluid:

$$\frac{\partial C_N}{dt} = -dir\frac{\partial}{\partial Z}\left(v_{f,TB}C_N\right) + D_N\frac{\partial^2 C_N}{\partial Z^2} - r_{fU} - \frac{k_{mN}^l}{\delta_T^l}\left(C_N - C_N^l\right) \quad \text{(E. 1)}$$

Unfolded proteins (U) in bulk fluid:

$$\frac{\partial C_U}{dt} = -dir\frac{\partial}{\partial z}\left(v_{f,TB}C_U\right) + D_U\frac{\partial^2 C_U}{\partial z^2} + r_{fU} - r_{fA} - \frac{k_{mD}^l}{\delta_T^l}\left(C_U - C_U^l\right) \quad \text{(E. 2)}$$

Aggregated proteins (A) in bulk fluid:

$$\frac{\partial C_A}{dt} = -dir\frac{\partial}{\partial z}\left(v_{f,TB}C_A\right) + D_A\frac{\partial^2 C_A}{\partial z^2} + r_{fA} - \frac{k_{mA}^l}{\delta_T^l}\left(C_A - C_A^l\right) \quad \text{(E. 3)}$$

Native protein (N) in thermal boundary layer:

$$\frac{\partial C_N^l}{dt} = -dir\frac{\partial}{\partial z}\left(v_{f,TB}C_N^l\right) + D_N\frac{\partial^2 C_N^l}{\partial z^2} - r_{TU}^i + \frac{k_{mN}^l}{\delta_T^l}\left(C_N - C_N^l\right) \quad \text{(E. 4)}$$

Unfolded protein (U) in thermal boundary layer:

$$\frac{\partial C_U^l}{dt} = -dir\frac{\partial}{\partial z}\left(v_{f,TB}C_U^l\right) + D_D\frac{\partial^2 C_U^l}{\partial z^2} + r_{TU}^l - r_{TA}^l + \frac{k_{mU}^l}{\delta_T^l}\left(C_U - C_U^l\right) \quad \text{(E. 5)}$$

$$-\frac{Dep_U+1}{2}r_{dU}^l + \frac{Ent_U+1}{2}r_{eU}^l$$

Aggregated protein (A) in thermal boundary layer:

$$\frac{\partial C_A^l}{dt} = -dir\frac{\partial}{\partial z}\left(v_{f,TB}C_A^l\right) + D_A\frac{\partial^2 C_A^l}{\partial z^2} + r_{TA}^i + \frac{k_{mA}^l}{\delta_T^l}\left(C_A - C_A^l\right) \quad \text{(E. 6)}$$

$$-\frac{Dep_A+1}{2}r_{dA}^l + \frac{Ent_A+1}{2}r_{eA}^l$$

Here, superscript l is used to denote variables in the layer domain of the holding tube. Other variable definitions are analogous to the ones used for the plate fouling model and can be calculated using equations discussed previously (Section 4.3.3).

Appendix F. Sensitivity analysis of fluid physical properties

For both configuration 1 and 2 (Figure 5.2 and Figure 5.3), a general sensitivity analysis of the physical properties for milk and heating water is conducted. Firstly, the temperature ranges for the sensitivity test of the fluid were selected (Table F. 1). Then, the physical properties of the fluid at the maximum and minimum temperatures were estimated using equation (4.18) to (4.25). The values are presented in Table F. 2. The percent variations of the physical properties over the temperature range are shown in Table F. 3. From the table, it is noted that when temperature increases, some of the physical properties (C_p & λ) would also increase, while others would decrease. Lastly, the sensitivity of each physical property was assessed by comparing to the baseline case. Here, only main-effect (1st order) sensitivity was assess, i.e., the interactions between different physical properties were not included.

Table F. 1. Temperature ranges of the fluid for sensitivity test.

	Milk	**Water**
Max. (℃)	110	110
Min. (℃)	60	80

Table F. 2. Physical properties of the fluid for sensitivity test.

Physical properties	**Min temperature**		**Max temperature**	
	Milk ($T_{min} = 60$℃)	**Water ($T_{min} = 80$℃)**	**Milk ($T_{max} = 110$℃)**	**Water ($T_{max} = 110$℃)**
C_p (J/kg.K)	4023	4197	4023	4226
ρ (kg/m^3)	1016	971	983	951
λ (W/m.K)	0.656	0.671	0.762	0.684
μ (Pa.S)	7.06E-04	3.41E-04	4.12E-04	2.62E-04

Table F. 3. Percent variations of physical properties over the temp range of interests.

	Milk	**Water**
C_p	0.0%	0.7%
ρ	-3.2%	-2.0%
λ	16.2%	1.9%
μ	-41.6%	-23.2%

The baseline of the sensitivity analysis was selected as the simulated outlet temperature based on the physical properties calculated from T_{min}. To check the effects of each physical properties on the outlet temperature, the simulation was performed by changing one of the physical properties of one fluid (milk or water) at a time. Then the newly obtained outlet temperature and the baseline outlet temperature were compared. And the sensitivity of each physical property is assessed using equation (F.17). Since the magnitude of these physical properties (C_p, ρ, λ and μ) are quite different, to compare the sensitivity of each properties, normalization is used (Equation (F.17)):

$$\frac{\partial T_{f,j}\widetilde{(out)}}{\partial \widetilde{PP}} = \frac{\partial T_{f,j}\,(out)}{\partial PP} \times \frac{PP_{nominal}}{T_{f,j,nominal}(out)} \qquad \forall\, j \in [1, P] \qquad \text{(F.17)}$$

Where $\frac{\partial T_{f,j}\,(out)}{\partial PP}$ is estimated using the following equations:

$$\frac{\partial T_{f,j}\,(out)}{\partial PP} \approx \frac{T_{f,j}(out) - T_{f,j,nominal}(out)}{PP - PP_{nominal}} \qquad \forall\, j \in [1, P] \qquad \text{(F.18)}$$

Here, PP is the physical properties of the processing fluid. $T_{f,j}(out)$ is the outlet temperature of milk at different channels. $T_{f,j}\widetilde{(out)}$ is the normalised outlet temperature of milk. $T_{f,j,nominal}(out)$ is the nominal outlet temperature of milk and $PP_{nominal}$ is the nominal value of the physical property.

The results for the sensitivity analysis for both configurations are depicted in Figure F. 1 and Figure F. 2. The maximum deviation from the baseline results for each channel are also presented in Table F. 6 and Table F. 7. For both configurations, the density of the milk has largest impact on the outlet temperature, followed by the density of water and the heat capacity of the water. All other physical properties have relatively minor effects on the outlet temperatures. It is also noted that change of physical properties has larger impact on configuration1 comparing to configuration 2. It is reasonable since configuration 1 is a single-pass PHE, when the physical property changes, it would directly affect the outlet temperature of each channel. And depend on the actual temperature within each channel, the effects would vary. On the other hand, the configuration 2 is a single-inlet-six-pass PHE, for which the fluid in sequential channels are linked and therefore the effects of changing physical properties reduced as the fluid flow along different channels (Table F. 7).

Table F. 4. Baseline channel outlet temperature for configuration 1.

Channel	**1**	**3**	**5**	**7**	**9**	**11**
Baseline outlet temp (℃)	76.2	83.6	87.0	90.5	94.8	99.2

Table F. 5. Baseline channel outlet temperature for configuration 2.

Channel	**2**	**4**	**6**	**8**	**10**	**12**
Baseline outlet temp (℃)	76.0	84.7	89.9	93.1	94.9	95.6

Table F. 6. Max deviations of channel outlet temperature from baseline values for configuration 1.

Channel	**1**	**3**	**5**	**7**	**9**	**11**	**Max**
% Deviation (+)	3.16	4.02	3.56	3.03	2.17	1.60	4.02
% Deviation (-)	-3.84	-4.34	-4.05	-3.67	-3.06	-2.41	-4.34

Table F. 7. Max deviations of channel outlet temperature from baseline values for configuration 2.

Channel	2	4	6	8	10	12	Max
% Deviation (+)	2.25	2.51	2.08	1.49	0.92	0.69	2.51
% Deviation (-)	-3.31	-3.55	-2.90	-2.06	-1.29	-0.98	-3.55

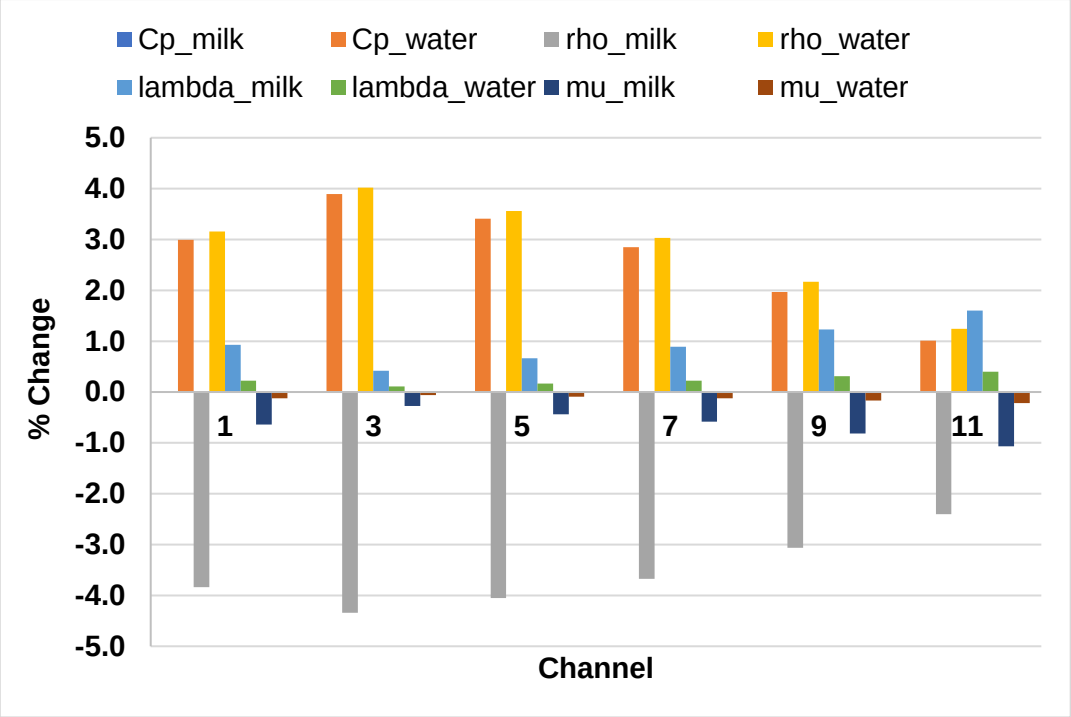

Figure F. 1. Sensitivity analysis of physical properties for configuration 1.

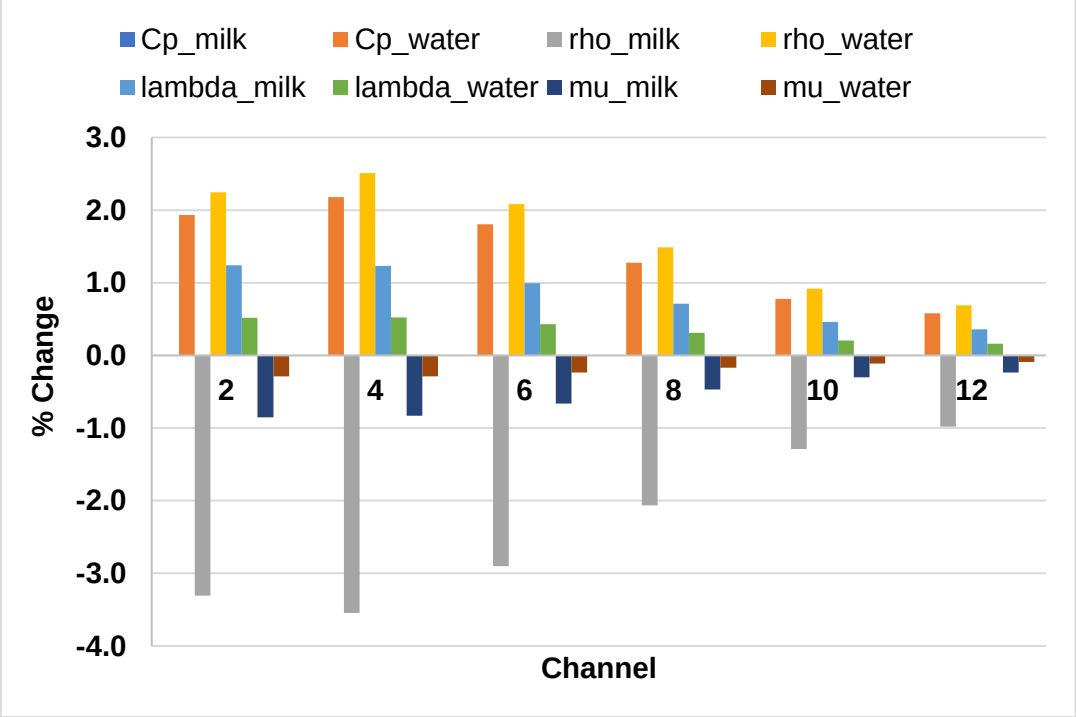

Figure F. 2. Sensitivity analysis of physical properties for configuration 2.

Overall, no significant difference of outlet temp is observed over the temp range of interests, especially for single-inlet-multiple-pass configurations. As a result, the assumption of constant physical properties is valid. If correlations instead of constant values of the physical properties are used, the values of the physical properties need to be updated at each location of the fluid when the fluid temperature changes, in this case, every discretized location along x-axis (information about discretization could be found in section 0). Using constant physical properties could reduce the model complexity and therefore scale down the size of the problem. This could effectively shorten the simulation time. However, if there is no prior information about the simulation, it is hard to select the average temperature for the calculation of constant physical properties in advance. Therefore, for small size problems, it is still recommended to use correlations to enhance the model performance. And for large size problems, when this assumption is used, a preliminary simulation could be conducted for better selection of average temperature to be used. As an alternative, correlations could be implemented for the physical properties that have large impact on the outlet temperature and constant values could be used for the ones that have minor influence.

Appendix G. PI controller transfer function estimation

Here, the process for PI controller transfer function estimation is presented. The nominal steady state HTST process operation are shown in Table 7.3 and the pasteurizer unit configurations are depicted in Figure B.4 to Figure B.6. For each step change of the manipulated variable, K_P is estimated from the value of $\frac{\Delta Y}{\Delta U}$. And τ_P is estimated from the time between the start of the step change and the time when it reaches 63.2% of the next steady state. Then the average value of K_P and τ_I from these three step changes are used for controller parameter tuning.

Controller for the heating section (Note: controller is used to control T5)

Type one (change heating water mass flowrate)

1. For the simulation, start from the nominal steady state
    a. Continued for 500 seconds
2. Reassigned the inlet mass flowrate of the heating water from 0.0162kg/s (60 L/h volumetric flowrate) to 0.0323kg/s (120 L/h volumetric flowrate)
    a. Continued for 500 seconds
3. Reassigned the inlet mass flowrate of the heating water from 0.0323kg/s (120 L/h volumetric flowrate) back to 0.0162kg/s (60 L/h volumetric flowrate)
    a. Continued for 500 seconds
4. Reassigned the inlet mass flowrate of the heating water from 0.0162kg/s (60 L/h volumetric flowrate) to 0.00808kg/s (30 L/h volumetric flowrate)
    a. Continued for 500 second.

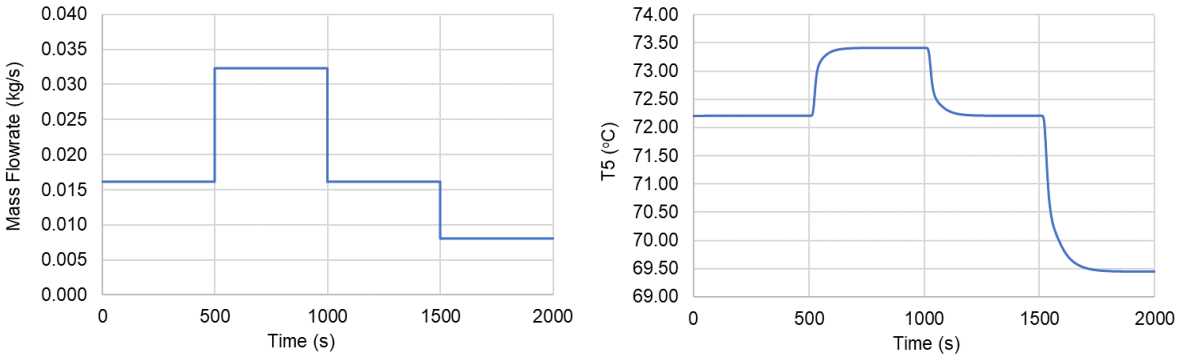

Figure G. 1. Left: Step changes of the inlet heating water mass flowrate (ΔU); Right: T5 temperature response to the step changes (ΔY).

Average K_P and τ_I calculated: K_P = 163.7 $\frac{℃\, s}{kg}$, τ_I = 41.67 s

Type two (change heating water temperature, T9)

1. For the simulation, start from the nominal steady state
    a. Continued for 500 seconds
2. Reassigned the inlet temperature of the heating water from 76.3 ℃ to 90 ℃
    a. Continued for 500 seconds
3. Reassigned the inlet temperature of the heating water from 90℃ back to 76.3℃
    a. Continued for 500 seconds
4. Reassigned the inlet temperature of the heating water from 76.3 ℃ to 60℃
    a. Continued for 500 seconds

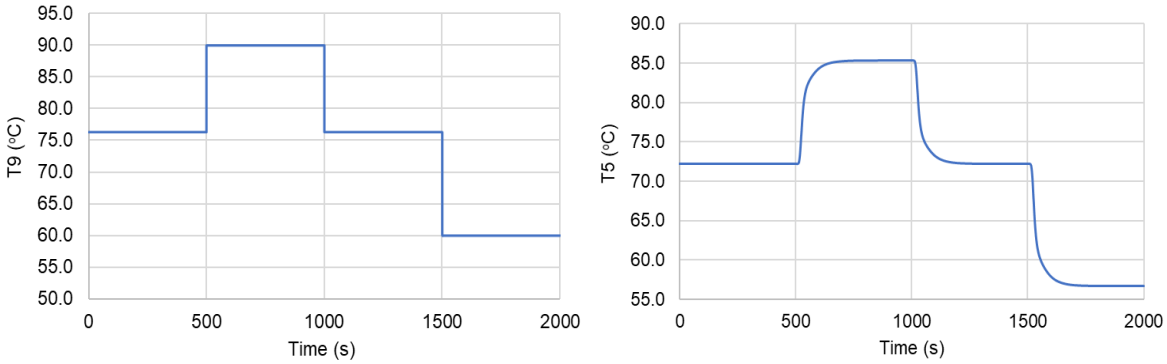

Figure G. 2. Left: Step changes of the inlet heating water temperature (ΔU); Right: T5 temperature response to the step changes (ΔY).

Average K_P and τ_I calculated: K_P = 0.955, τ_I = 32.5 s

Controller for the cooling section (Note: controller is used to control T8)

Type one (change heating water mass flowrate)

1. For the simulation, start from the nominal steady state
    a. Continued for 500 seconds
    b. (HTST process and pasteurizer unit configurations are described in detail in previous report – July 25th)
2. Reassigned the inlet mass flowrate of the cooling water from 0.0162kg/s (60 L/h volumetric flowrate) to 0.0323kg/s (120 L/h volumetric flowrate)
    a. Continued for 500 seconds
3. Reassigned the inlet mass flowrate of the cooling water from 0.0323kg/s (120 L/h volumetric flowrate) back to 0.0162kg/s (60 L/h volumetric flowrate)
    a. Continued for 500 seconds
4. Reassigned the inlet mass flowrate of the cooling water from 0.0162kg/s (60 L/h volumetric flowrate) to 0.00808kg/s (30 L/h volumetric flowrate)
    a. Continued for 500 seconds

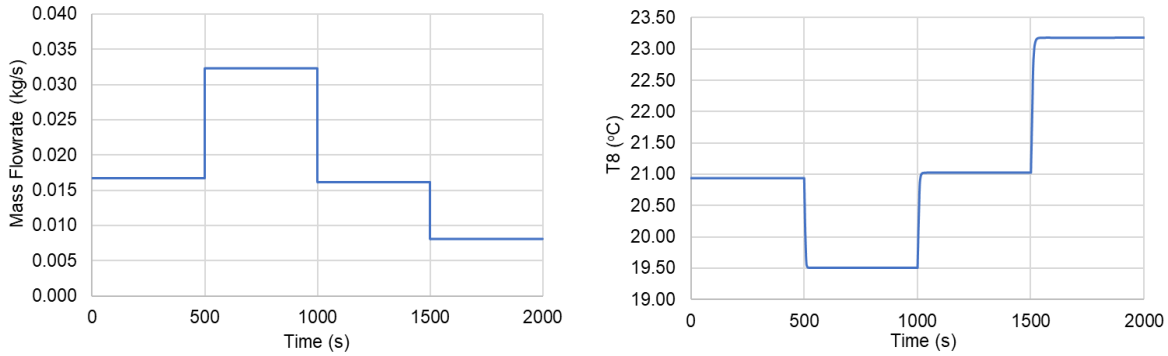

Figure G. 3. Left: Step changes of the inlet cooling water mass flowrate (ΔU); Right: T8 temperature response to the step changes (ΔY).

Average K_P and τ_I calculated: K_P = -151.0 $\frac{℃\,s}{kg}$, τ_I = 6.67 s

Type two (change heating water temperature, T11)

1. For the simulation, start from the nominal steady state
    a. Continued for 500 seconds
    b. (HTST process and pasteurizer unit configurations are described in detail in previous report – July 25th)
2. Reassigned the inlet temperature of the cooling water from 10.1 ℃ to 4 ℃
    a. Continued for 500 seconds
3. Reassigned the inlet temperature of the cooling water from 4℃ back to 10.1℃
    a. Continued for 500 seconds
4. Reassigned the inlet temperature of the cooling water from 10.1 ℃ to 15℃
    a. Continued for 500 seconds

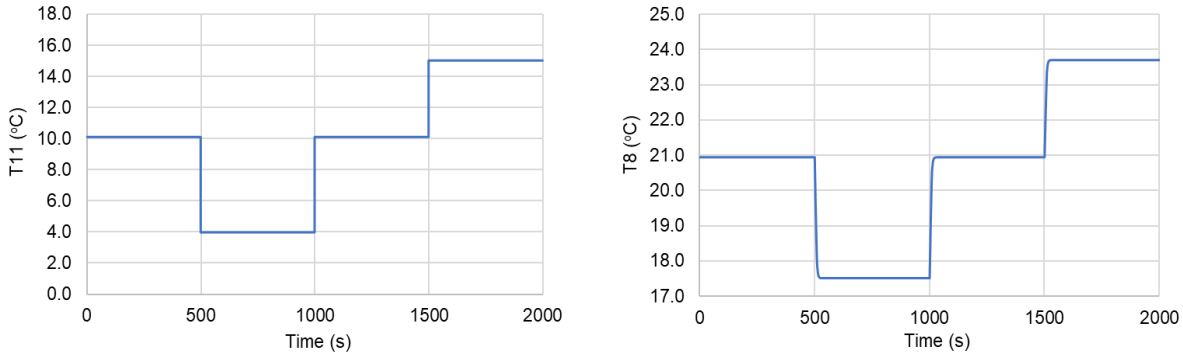

Figure G. 4. Left: Step changes of the inlet cooling water temperature (ΔU); Right: T8 temperature response to the step changes (ΔY).

Average K_P and τ_I calculated: K_P = 0.563, τ_I = 7.5 s